MASS TRANSFER ENHANCEMENT FOR TUBULAR REVERSE OSMOSIS SYSTEMS

by

Quentin Edward Hurt

A dissertation submitted in fulfilment of the requirements of the degree of Master of Science in Engineering in the Department of Chemical Engineering, University of Natal

Durban

March 1994

DECLARATION OF CANDIDATE

I, Quentin Edward Hurt, declare that unless otherwise indicated, this dissertation is my own work and that it has not been submitted for a degree at another University or Institution.

.....

March 1994

SUMMARY

Improving the performance of reverse osmosis by altering the hydrodynamics of the feed flow of sodium nitrate solution through cellulose acetate tubular membranes was examined. Pulsed flow, baffle placement and pulsed, baffled were assessed. Two baffle designs were compared: doughnut and angled, elliptical shape. Two membranes were used in series. The baffles were tested simultaneously under similar flow conditions. A novel pulsing pump design was used.

The membrane parameters (the pure water permeability parameters, A, and the solute transport parameters, $\frac{D_{AM}}{K\delta}$) were calculated. Mass transfer coefficients were calculated for each set of hydrodynamically similar feed flows examined.

The results for the conventional mode of operation formed the basis against which the effectiveness of the three modes were compared. In order to extenuate the effect of concentration polarisation, laminar and transition flow regimes were used. The mass transfer coefficient increased exponentially with Reynolds number across the range of flows.

A secondary pump, that bridged the outlets of the membrane holders, pulsed the flow. The frequency and amplitude of the pulses was varied and the pulse-action recorded digitally. Gains in mass transfer coefficient of up to 800 % were calculated for the largest amplitudes and highest frequencies.

Baffles enhanced mass transfer by up to 300 and 200 % for the elliptical and doughnut-shaped baffles respectively. However, baffle design superiority is inconclusive in this instance because of experimental error. Possible maximum baffle effectiveness was apparent around for superficial Reynolds number of 2 000, indicating that the baffles were both turbulence and convection promoters.

Pulsing the feed flow through a baffled tube produced gains up to 2 000 % in the mass transfer coefficient. Trends indicate that the elliptical baffles were most effective. Increasing the frequency of the pulses enhanced the mass transfer coefficient. There was an optimum amplitude for a given frequency, whose value appears to be related to baffle design.

ACKNOWLEDGEMENTS

Chris Brouckaert

for invaluable help throughout the project and especially for modifying his RO simulation program to allow me to calculate the mass transfer coefficients that proved so useful in understanding the results of this work : even working weekends over the Festive Season.

Chris Buckley

for persuading me to do the project, helping and advising me throughout it and, finally, for acting as supercourier to facilitate its completion. I am very grateful for the assistance, interest and advice throughout the project.

Ed Jacobs

who gave up time and Stellenbosch on a number of occasions to nudge me onto the right track and offer invaluable advice.

Loveena Kissoon

for doing the corrections to and for the superb formatting of the document.

My family

for accommodating me and leaving the door open to all hours in the interest of science.

The members of the Pollution Research Group

for their help, humour and spirit. It was a pleasure working with such dedicated individuals.

The Water Research Commission

for their partial sponsorship of the project and interest in the work.

The Foundation for Research Development

for their partial sponsorship of the project.

TABLE OF CONTENTS

LIST OF FIGURES

LIST OF TABLES

Chapter 1

INTRODUCTION

1.1 WHAT IS REVERSE OSMOSIS?

Reverse osmosis (RO) involves the separation of a solution into a more and a less concentrated stream. The mechanism of separation is based on the difference in sorption of the solute and solvent onto the membrane (a thin porous film). Some basic RO terminology is depicted in Figure 1.1.

Most often, the sorbed component is water and the retained component is a salt. Hence, RO has been applied mainly in the fields of sea- and brack-water desalination. RO is increasingly being used in applications where high quality water is required from streams where salt or low molecular mass contamination is present. Examples of such applications are to be found in the metal finishing, paint manufacture and effluent polishing sectors.

1.2 RO LIMITATIONS

RO applications have been limited by the costs involved. To overcome the osmotic pressure differences and allow for a reasonable driving force, high feed pressures are required. The retained species tend to accumulate adjacent to the membrane, forming a second barrier to permeation through the membrane. Where the RO configuration has allowed, high feed flow rates are used to aid fluid mixing adjacent to the membrane to restrict the build-up of the retained species. Further, the ratio of feed to permeate collected is often low, requiring the recycle of the treated fluid or increased membrane area to increase recovery.

All these factors lead to high operating costs. Reluctance to introduce RO plant has typically been associated with the high capital cost, the limited operating life of the RO membrane, the small operating window dictated by the membrane materials and the membranes' susceptibility to damage and degradation.

1.3 PERFORMANCE ENHANCEMENT

The key to improving RO economics lies in either decreasing the operating or the capital cost of the systems. One route to reducing the operating cost is to use a lower

feed flow rate without sacrificing the membrane product flux or ratio of mass transfer. This route is evaluated for the purposes of this work as viable alternatives to traditional RO operating methodologies.

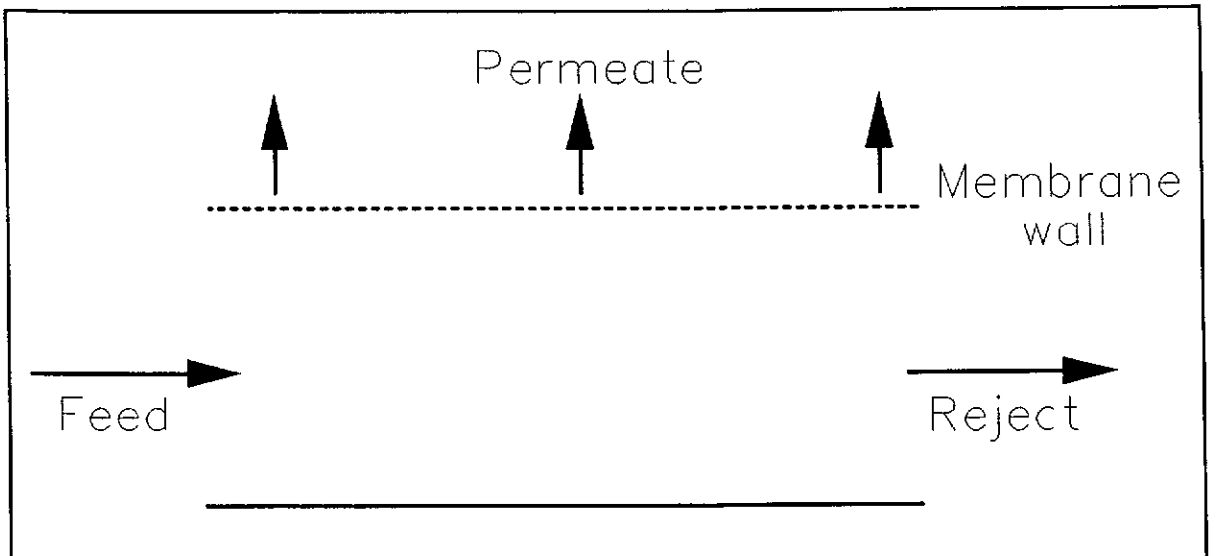

FIGURE 1.1 : *Pictorial representation of some basic RO terminology*

1.4 AIMS OF THIS THESIS

The aim of this thesis is to compare the effectiveness of strategies for mass transfer enhancement for tubular reverse osmosis. Three strategies are proposed that alter the hydrodynamic nature of the feed flow: (i) pulsed flow; (ii) baffled flow; and (iii) pulsed-baffled flow. The intention is to propose or compare mechanisms by which RO systems might be modified without altering the nature of the membrane. By these means it is hoped that the economics of RO might be improved.

In keeping with these aims, all the experiments are conducted with low linear feed flows in an attempt to obtain superior RO performance in the laminar and transition regimes that would be associated with low running cost and consequently low pumping costs.

The work of a number of authors in the field of mass and heat transfer enhancement (most notably Finnigan et al. (1989/90); Mackley et al. (1990); Pitera et al. (1973) and Thomas et al. (1968)) was evaluated to assess the effectiveness of various equipment configurations. As a result, novel pulsing pump and baffle designs are proposed. The pump design is simple and does not significantly increase the energy requirements of the system. The effectiveness of a diagonal baffle design, conceived to exploit the

hydrodynamic features that occur within the RO tube (both steady and pulsing flow) without increasing the energy requirements to the extent that conventional baffles do, will also be evaluated.

All comparisons are made on the basis of mass transfer coefficients calculated for each of the flow conditions on the basis of the experimental results obtained. The mass transfer coefficient describes RO membrane performance by condensing the dependent variables into a single value, the value of which is an indication of the effectiveness of the convection promotion of each of the strategies employed. Although not initially central to the work, the effectiveness of this strategy itself will also be evaluated.

1.5 STRUCTURE OF THE THESIS

The theory necessary to describe RO performance and used to generate the mass transfer coefficients is discussed in Chapter 2. It is shown how each membrane can be characterised by only two parameters. Using these and the experimental results, mass transfer coefficients can be calculated for each flow regime. Some of the problems encountered with RO are discussed and different RO systems are explained.

Chapter 3 deals with tubular RO, the membrane configuration system used throughout this thesis. The results of the base-line experiments (which characterise the membranes and represent the behaviour of a conventional RO system operated under conditions of laminar and transition flow regimes) are reported. The ability of the theoretical model used in the thesis to predict RO performance accurately is also discussed.

Chapters 4, 5 and 6 deal with the operation of RO with pulsed, baffled and pulsed-baffled flow superimposed on laminar and transition region feed flows respectively. Literature pertaining to other work in each of the areas studied is referenced and discussed. The results obtained with each of these techniques is compared to those shown in Chapter 2.

Chapter 7 presents the conclusions and recommendations of this work. The relative merits of each strategy are compared and some general remarks are made about the mathematical modelling along with recommendations for further research in these areas.

The most important appendices deal with factors that are common to most of the chapters to prevent repetition. For instance, Appendix A contains some RO terminology, Appendix B reports the experimental method which was used throughout the work and Appendix C discusses the analysis of the experimental error. While the latter two appendices are important to the understanding of the thesis, it was felt that they would detract from the main thrust of the argument if they were included as separate chapters, or repeated in each although they may augment the Introduction for the uninitiated reader as their implications are cross-referenced in each section.

Chapter 2

REVERSE OSMOSIS

2.1 INTRODUCTION

There are two major theories for transport through RO membranes reported in the literature : the solution diffusion model and the preferential sorption capillary flow model (Rautenbach and Albrecht, 1989). The latter model is largely due to the work of Sourirajan and co-workers since 1960 (Sourirajan and Matsuura, 1985). It has been shown (Muldowney and Punzi, 1988) that the predictions of the two models are virtually identical in practice. The modelling in this work is based exclusively on Sourirajan's theory.

It is not the aim of this thesis to reproduce all of his theory but rather to highlight some of it, particularly those areas pertaining to mass transfer and concentration polarisation.

Some basic terminology not referred to in this Chapter is given in **Appendix A** because there appear to be a number of terms used by different authors to describe the same process or phenomenon.

2.2 THE SOURIRAJAN THEORY

The term solute refers to that component of the feed which is retained at the membrane (denoted by subscript A) and the solvent is that component which is preferentially sorbed at the membranes (denoted by subscript B)

An idealised radial concentration profile of the feed is depicted along with some of the reverse osmosis symbols in Figure 2.1.

The water flux through the membrane, N_B, (as defined by Sourirajan, 1985) is related to the operating pressure and the stream concentrations as follows :

$$N_B = A[P - \pi(X_{A2}) + \pi(X_{A3})] \tag{2.1}$$

$$N_B = \left(\frac{D_{AM}}{K\delta}\right)\left(\frac{1 - X_{A3}}{X_{A3}}\right)(c_2 X_{A2} - c_3 X_{A3}) \tag{2.2}$$

where A = the pure water permeability constant, [kg-mol H_2O/m^2.s.Pa], defined in Eqn 2.3

P = the operating pressure, [Pa]

X = the mole fraction of solute at the radial positions indicated in the diagram.

c = the molar density of the solution [kg-mol/m^3]

$\left(\frac{D_{AM}}{K\delta}\right)$ = the solute transport parameter [m/s]

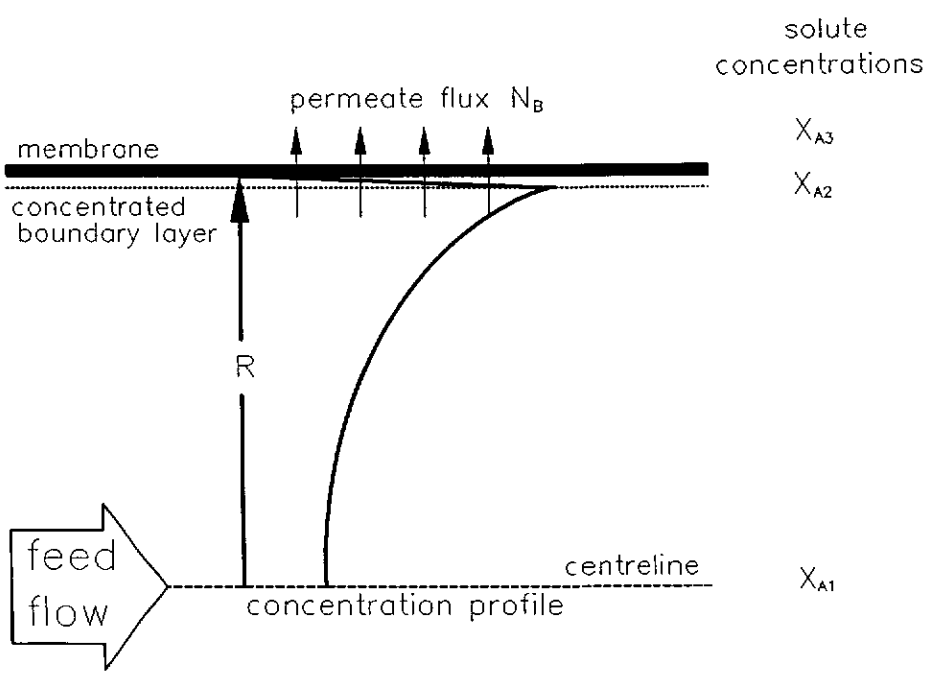

FIGURE 2.1 : *Idealised representation of the concentration profile within an RO tube. Also depicted is some of the RO terminology used.*

$$A = \frac{PWP}{M_b \; S \; P} \tag{2.3}$$

where PWP = the pure water permeation rate through a given membrane area [kg/s]

M_B = the molecular mass of the solvent

S = the operational membrane area [m^2]

The mass transfer coefficient (units of m/s) may be defined as :

$$k = \frac{N_A + N_B}{c_1} \left[\ln \frac{X_{A2} - X_{A3}}{X_{A1} - X_{A3}} \right]^{-1} \tag{2.4}$$

where N_A = is the solute flow through the membrane [k-mol/m^2s]

The equations 2.2 and 2.4 are commonly simplified by the assumption that :

$$c = c_1 = c_2 = c_3 \tag{2.5}$$

c = is the solution molar density [k-mol/m^3]

c_1 = is the feed molar density [k-mol/m^3]

c_2 = is the wall fluid molar density [k-mol/m^3]

c_3 = is the permeate molar density [k-mol/m^3].

This assumption may be justified on the basis that the molar density of the solution does not change significantly for a wide range of solute concentrations and may be assumed to be essentially constant. This assumption has been used during the course of this work and the fundamental RO equations modified accordingly.

2.2.1 The Significance of the Membrane Constants

Eqn 2.1 to 2.4 govern reverse osmosis transport : all four must be solved simultaneously to describe the membrane system. However, with the three constants A, $\left(\frac{D_{AM}}{Kb}\right)$ and (for a given feed flow) k, one can predict membrane performance over a range of pressures. Knowing these constants allows one to predict membrane behaviour.

Consider the pure water permeability constant, A, as described by Eqn 2.3. The value of A describes the membrane's porosity and thus its resistance to permeation. Permeate flow will be directly restricted by its value (Eqn 2.1).

Similarly, consider the value of the solute transport parameter, $\left(\frac{D_{AM}}{K\delta}\right)$ as defined by Eqn 2.2. It is a measure of the average pore size of the membrane and is dependent on the chemical nature of the solute and of the membrane material: hence the solute transport through the membrane.

Both of these parameters are functions only of the membrane, the solvent and the solute. A single set of primary RO data at known operating conditions is sufficient to predict A, $\left(\frac{D_{AM}}{K\delta}\right)$ and k. Naturally, the larger the set of data, the more accurate the prediction.

The third factor, k, is also dependent on the flow conditions in the tube. It is, however, independent of pressure (Sourirajan, 1985). The value of k directly affects on the permeate flow and quality. It is a measure of the disparity between the bulk solute concentration and the solute concentration adjacent to the membrane.

The philosophy of this thesis is that the cellulose acetate membrane performance on a sodium nitrate-water system is better described in terms of its mass transfer coefficients than in terms of permeate quality and flow. In so doing, any variation caused by the membrane itself is discounted and the basis for comparison becomes the hydrodynamic conditions adjacent to the membrane which directly affect the salt passage and permeate flow rate.

Hence the variables : operating temperature, feed concentration and flow, and permeate concentration and flow are reduced to the mass transfer coefficient. All results are reported and compared as such.

2.3 PROBLEMS ASSOCIATED WITH REVERSE OSMOSIS

RO performance is adversely affected by various phenomena, some of which are avoidable and, as this thesis will attempt to show, open to manipulation : other effects are permanent. A short description of the most common adverse phenomena follow.

2.3.1 Membrane Compaction

The high pressures used in reverse osmosis causes the compression of the membrane known as membrane compaction, characterised by an initial comparatively rapid decrease in permeate flow and salt passage. The membrane porosity is reduced (or is *densified*), increasing the resistance to flow through the membrane.

The plastic deformation of the pressurised membrane results in a progressively slower compaction rate, the characteristics of which are dependent on the membrane composition and structure, the operating temperature and the applied pressure. It is important to account for this process during the course of reverse osmosis experiments by allowing for any initial rapid compaction by pre-testing the membranes until assessed uniform results are achieved.

2.3.2 Concentration Polarisation

Within the membrane, two distinct mechanisms are at work that dictate the solute concentration profile (simply depicted in Figure 2.1). Convective transport, governed by the preferential sorption tendency of the membrane, the osmotic pressure difference driving force and, to a lesser extent, the replacement flow of fluid, draws solvent and solute towards the membrane surface. The solvent is preferentially sorbed out of the fluid adjacent to the membrane wall, causing a relative increase in the solute concentration in this region of the fluid (commonly referred to as the interfacial region). Diffusive transport then governs the flow of retained solute ions towards the bulk fluid away from the interfacial region.

The presence of the concentrated boundary solution on the high pressure side of the membrane is known as *concentration polarisation*. It is this effect that this work seeks to minimise by enhancing the diffusion of retained ions from the interfacial region to the bulk flow.

A study of the mechanisms governing concentration polarisation indicates that the higher the separation characteristics of the membrane and the higher the withdrawal rate of the permeate, the more pronounced the effect will be become. As Equation 2.2 indicates, the performance of the RO system is governed by the interfacial region solute concentration and is not strictly dependent on the solute concentration within the bulk flow. Although interrelated, both the permeate flux and the concentration of the solute in the permeate are described by this equation (as they are by the Equation 2.4).

Equation 2.4 also introduces the notion of the mass transfer coefficient governing the effectiveness of the diffusion mechanism. By increasing the degree of mass transfer, the differential between the interfacial region solute concentration and that in the bulk

fluid should be reduced. If this can be achieved while maintaining values of permeate flux and containing the solute concentration in the permeate, then by the definition of this work, membrane performance may be considered to be enhanced.

A common technique for reducing concentration polarisation is to increase the linear flow velocity of the feed to a create highly turbulent flow. The turbulence may improve the degree of fluid mixing within the tube and narrow the discrepancies between the solute concentration in the interfacial region and in the bulk of the fluid. This technique would be associated with increased pressure drop through the system, low overall solvent recovery and increased pumping costs. Ultimately, the perceived performance enhancement may not be economically warranted.

It is the intention of this work to reduce the degree of concentration polarisation by improving solute mass transfer from the concentrated boundary layer to the bulk flow under conditions of low linear feed flow. In this manner, full advantage may be taken of the potential for solvent recovery and low pumping costs. Improving the mass transfer characteristics is seen as the key to reducing concentration polarisation. This should be done while containing the operating energy requirements to effect real improvement in overall reverse osmosis performance.

2.3.3 Fouling and Scaling

If the feed solution to the membrane system is contaminated with particles, these may adhere to the membrane surface. This phenomenon is known in the broadest sense as fouling and may seriously impair membrane performance. Rautenbach and Albrecht (1989) define fouling as the deposition of suspended or colloidal material at the membrane surface. Scaling is defined as the crystalisation of dissolved water components (after exceeding the solubility limits) at the membrane surface.

The fouling layer presents an additional barrier to permeate flow by creating a layer of contaminants adjacent to the membrane surface. In extreme cases, the layer can cause physical membrane damage. Permeate flow would decrease and salt passage would increase as a result of fouling.

In this work, the fouling potential of the feed solution and the apparatus had to be kept at a minimum. Only RO permeate was used for feed solution base and make-up. The solute used was of an analytical grade. The feed tank and permeate collection trays were covered to prevent the ingress of particles to the system. The state of the equipment was monitored by using sacrificial membranes that were installed prior to any testing. These were run installed and their condition visually inspected after a week of operating the unit.

2.3.4 Membrane Damage

Membrane damage can be generally be divided into mechanical or physical damage.

The former can be caused by a number of factors. If solids come into contact with the membrane surface they can damage the membrane surface or skin layer, allowing the feed solution to pass directly to the porous film. This can be avoided by adequate pretreatment of the feed. However, operating with a concentrated solution might result in the formation of crystals in the concentrated boundary layer where they can tumble over the membrane surface and create pin-holes or tears. Also, any inserts in the tubes must be positioned carefully to avoid potential contact damage to the membrane.

Physical (commonly referred to as chemical) damage could result from inadequate membrane storage or use that does not correspond to the manufacturer's specifications. Hydrolysis of the cellulose acetate can occur if the pH of the feed is not within the allowable range. The membrane can become brittle if the feed temperature is too low (and in extreme cases ice particles can scratch the membrane surface).

As for the instance of fouling, care was taken to avoid the potential for membrane damage by operating the system within the membrane manufacturer's specifications for feed temperature and pH, by placing inserts carefully and by taking all precautions to prevent the ingress of particles to the system.

2.4 RO MODULE DESIGN

RO units are commonly classified according to the nature of the module chosen. The module design will typically aim to produce the highest permeate flow: membrane area ratio possible for the system. Modules are normally classified according to membrane diameters (in the case of tubes) or spacing (in the case of adjacent sheets) and feed flow arrangement. Common modules are the hollow fine fibre, spaghetti (although essentially redundant now), spiral-wrap, tubular and plate-and-frame modules. A brief description of each of these follows.

The hollow fine fibre module uses a bundle of fine diameter membrane tubes (typically 100μm diameter) set in a cylindrical housing. The advantage of this arrangement is that a large membrane area can be held in a relatively small volume. The feed is passed over the outside of the membrane fibres and the permeate leaves the module through the tubes. The feed may enter through the fibres themselves, the permeate leaving through the module casing drainage points. The latter flow arrangement has two disadvantages. The feed flow is necessarily laminar leading to low mass transfer in the tubes. The narrow diameter tubes are also prone to blockages.

The spiral-wrap module consists of sheets of membrane wrapped around a central feed core and glued around the edges. Alternate spaces between the membrane sheets act as feed and permeate channels. The layers of membrane between which the feed enters are separated by a mesh which acts as both a spacer and a turbulence promoter. The advantage of this system is that a large membrane area is available in a relatively small volume (though in a lower ratio than that of the hollow fine fibre module) with forced convection promotion.

The plate-and-frame modules are similar to filter presses except that they utilise membranes in place of filter cloths. The membrane sheets are placed on frames (usually circular) and the feed is passed over them. They generally require large packing volumes for relatively small membrane areas.

The tubular RO system, which forms the basis of the investigation for RO performance used in this thesis, is described in Chapter 3.

Chapter 3

STEADY FLOW IN TUBULAR REVERSE OSMOSIS

This chapter discusses the behaviour of tubular reverse osmosis (TRO) membranes under conditions of low linear feed flow velocity. It is not the intention to investigate the particular membrane performance with respect to the theory but to form a basis for performance comparison with the other techniques investigated (i.e., pulsed flow, baffled flow and baffled-pulsed flow). Some of the differences between laminar/transition flow behaviour and the theoretical performance are discussed.

3.1 TUBULAR REVERSE OSMOSIS

TRO is attractive for applications where the relatively more volume-efficient smaller membrane-diameter modules may be subject to blockages or where the system may need to be sterilised or cleaned with sponge balls.

Solids should be avoided in any RO feed but in some instances, the dangers of supersaturation of the feed solution and subsequent crystallisation make TRO advisable, particularly if the system can be operated under laminar feed flow where particles tend to flow nearer the tube centre than in turbulent flow (Kennedy et al., 1974). The possibility of tube blockages is reduced in TRO. Under conditions of extreme fouling, sponge balls are passed down the tube to clean the membrane surface. This process might be automated by reversing the flow at (for example) 15 minute intervals.

3.2 EQUIPMENT

3.2.1 Description of Equipment

The apparatus used is described in Appendix B.

The baffle supports, covered by sheaths the equivalent diameter of the baffle spacers (3 mm diameter), were inserted in the tubes. This was done to negate any effects caused by the supports themselves. Although they could be a source of some mass transfer enhancement (Thomas and Watson, 1968), it was deemed a necessary precaution.

The system is depicted in Fig. 3.1.

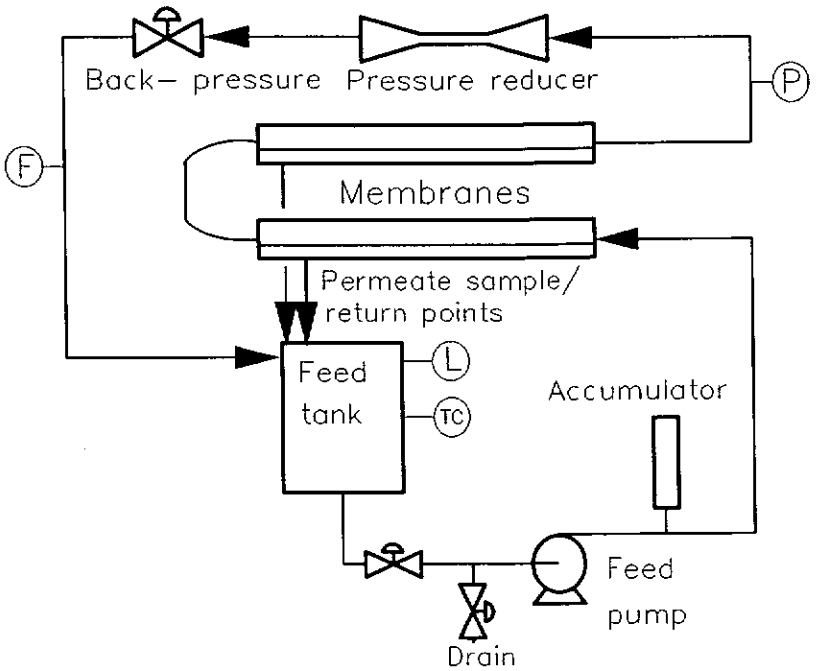

FIGURE 3.1 : *Diagram of equipment for the open tube tests*

3.3 RESULTS AND DISCUSSION

3.3.1 Permeate Flow Trends and Their Significance

Figures 3.2 and 3.3 show the trends of permeate flow with pressure. The detailed results are given in Table D.1. The symbols shown represent the experimental values while the curves show the values predicted for the tubes by the Sourirajan theory. The theory predicts a rise in permeate flow proportional to the pressure on the fluid.

The curves should intersect the pressure axis at the osmotic pressure of the feed solution. For these experiments this value should be around 0,55 MPa. The value is not exact because the concentration varied slightly. This variation was incorporated in the final model. While the experimental results tend to this pressure, the predicted values tend slightly lower to about 0,30 MPa.

It was suspected that the concentration of the feed solution might have been incorrectly measured. However, both gravimetric tests and direct measurements of the osmotic pressure on the feed solution showed the conductivity-based concentration measurements to be accurate. It was decided to accept this aberration in the model because it was consistent throughout the experiments. Furthermore, the aim of this work was to compare mass transfer under different hydrodynamic conditions and not to establish absolute values for coefficients (although a combination of the two would be preferable).

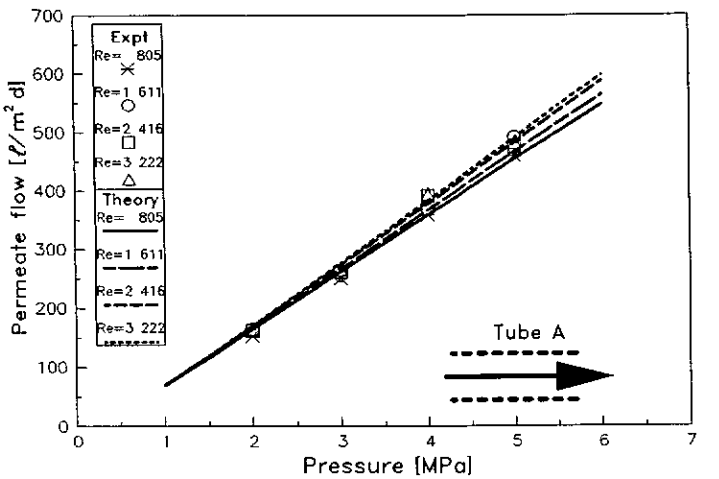

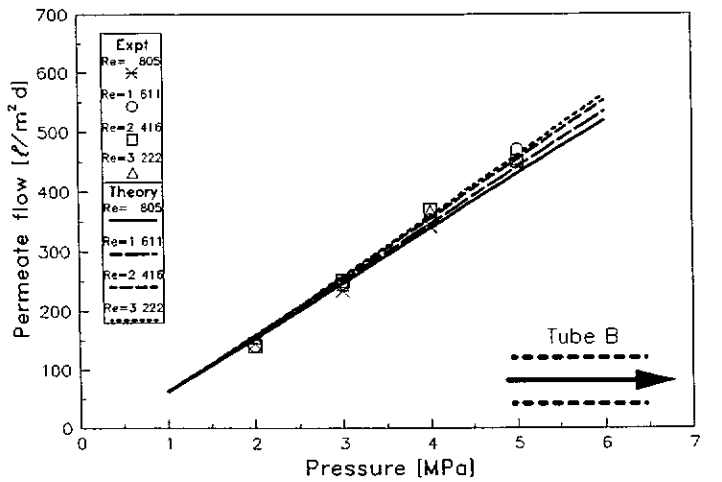

FIGURE 3.2 and 3.3 : *Variations in permeate flow with pressure showing experimental results (as symbols) and the theoretically predicted trends (as lines). Standard RO configuration with baffle holders mounted in the tube. At a temperature of 25 °C. Open tubes A and B respectively.*

The effect of pressure is noticeably more important than that of flow rate : there are only marginal differences for permeate flow across the range of feed flow rates. It is difficult to discern from the experimental results that the highest feed flow delivers the highest permeate flows. The model predicts this trend.

Tube B delivers lower permeate flows than tube A. This was shown to be the case throughout all the experiments. This is borne out by the higher value for pure water permeability constant, A.

Tube A	Tube B
6,64 x 10^{-14} kg-mol H_20/m^2.s.Pa	6,28 x 10^{-14} kg-mol H_20/m^2.s.Pa

3.3.2 Salt Passage Trends and their Significance

Figures 3.4 and 3.5 show a rapid decrease in salt passage with pressure. The detailed results are given in Table D.1. The rate of decline was considerably reduced as the pressure increased above about 3 MPa. This is anticipated by the theory since at a low system pressure the driving force effect is limiting (Eqn 2.1). However, as the salt passage decreases so the removal of retained solute from the membrane wall must improve to achieve the same performance. This can only be achieved physically by higher rates of mass transfer and thus the latter effect becomes limiting (Eqn 2.4).

The limiting mass transfer from the membrane is physically realised by the differentiation between the salt passages at the different flow rates. The increased flow in the tube should lead to higher mass transfer. Further the lowest flow rates deliver the highest salt passages.

The predicted curves follow the experimental data trends. Tube B rejects salt slightly better than tube A. This is borne out by its lower solute permeability coefficient, $\left(\frac{D_{AM}}{K\delta}\right)$.

Tube A	Tube B
4,09 x 10^{-7} m/s	3,58 x 10^{-7} m/s

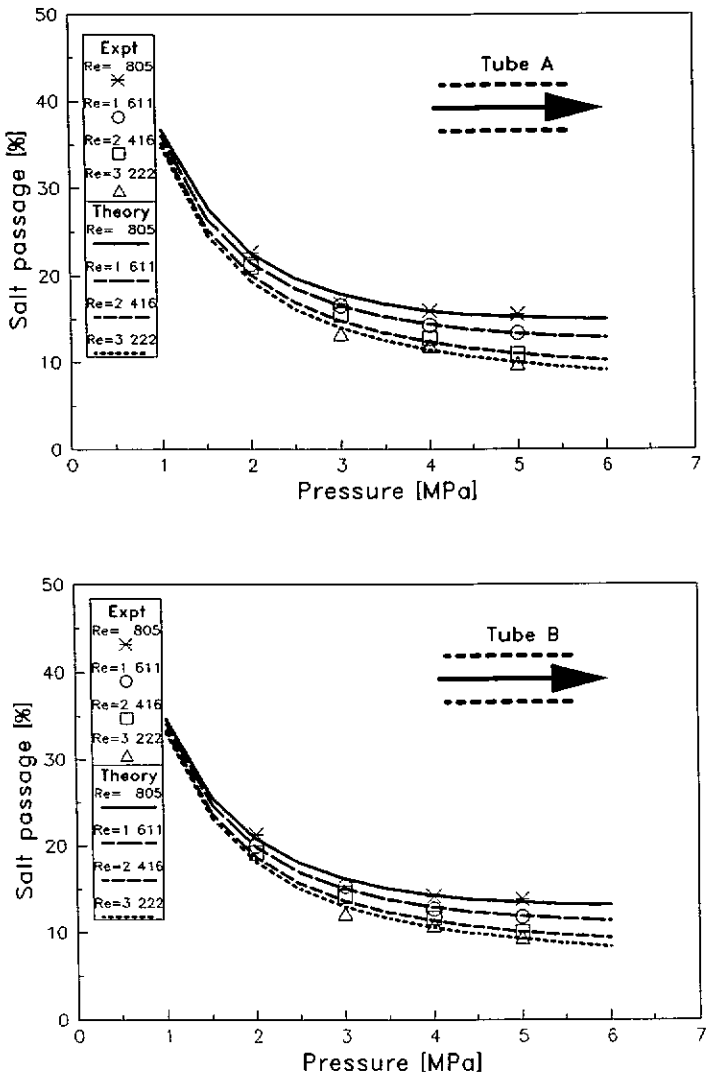

FIGURE 3.4 and 3.5. : *Variation in salt passage with pressure showing experimental results (as symbols) and the theoretically predicted trends (as lines). Standard RO configuration with baffle holders mounted in the tube. At a temperature of 25 °C. Open tubes A and B respectively.*

3.3.3 Mass Transfer Considerations

The calculated mass transfer coefficients (Appendix D.1) are shown as a function of feed flow in Fig. 3.6. They approximate the exponential relationship of $k \propto Re^n$ across the laminar and transition flow regimes. Similar hydrodynamic conditions are experienced in both tubes, indicated by the coincidence of the k values, despite the

differences in A and $\left(\frac{D_{AM}}{K\delta}\right)$. Mass transfer coefficients can be seen to be a convenient appraisal of membrane performance because they combine both salt passage and permeate flow values, which differ according to the particular membrane.

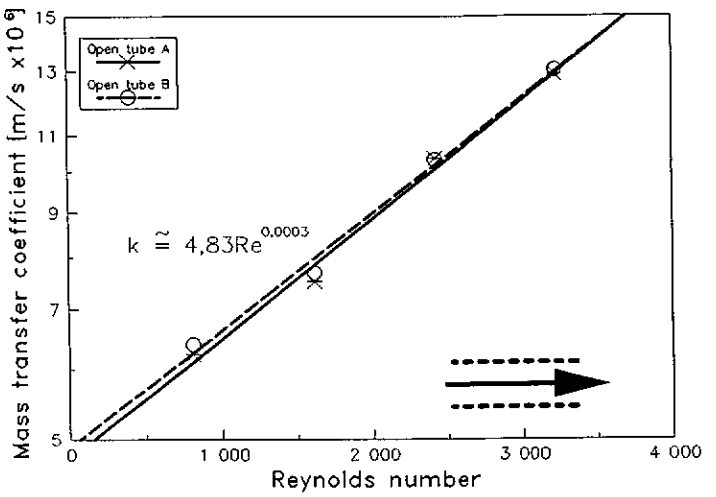

FIGURE 3.6. : *Mass transfer coefficient with Reynolds number. The mass transfer coefficients are plotted on a log scale to indicate the approximation to* $k \propto Re^n$ *for tubes A and B.*

It is encouraging that the model predicts virtually the same mass transfer coefficients for both tubes since it indicates that, despite the suspected differences in the downstream piping of each tube, conditions are comparable.

3.3.4 Error Considerations

An error analysis is described in Appendix C.1.3.

The maximum deviation (determined from tube B) from the calculated value of k is 1,75 x 10^{-6} m/s for Re = 3222 in Fig. 3.6. At Re = 805 it decreases to a maximum deviation of 0,8 x 10^{-6} m/s. The scatter of the data lies within these limits.

3.4 CONCLUSIONS

The combination of experimental data and theoretical modelling of the steady open tube experiments was considered successful. Despite some discrepancies between the

predicted and experimental results, the trends are similar. The modelled parameters predict the experimental data adequately : facilitating smoothing for better comparison. Mass transfer coefficients were considered a good basis for RO performance description because they effectively combined the variables of permeate flow and salt passage.

The error estimates employed indicate that any scatter in the mass transfer coefficients is within the limits of experimental error.

These results form a set against which alternative operating strategies can be compared.

Chapter 4

PULSED FLOW IN TUBULAR REVERSE OSMOSIS

4.1 PULSATING FLOW

Concentration polarisation may be reduced by pulsing the feed flow. Kennedy et al. (1974) reviewed pulsating flow in pipes. They showed that at high pulsing frequencies the laminar flow velocity maximum occurs near the wall and not at the centreline. Howes et al. (1990) mathematically modelled two-dimensional pulsed flow in open tubes and over a series of baffles. They reported their results with the aid of colour graphics to *illustrate particle tracking* simulations. Their prints are reproduced in Figure 4.1. It is possible to observe the behaviour of the different horizontal flow regimes from these prints. The tracking of particles is achieved using numerical integrations of the flow equations for each time interval. The spatial evolution of the initial horizontal fluid sectors is shown as spreading elements of colour.

Figure 4.1a shows the dispersion of the flow under steady, unbaffled laminar flow. No radial mixing of the flow is observed. The flow in the interfacial region is essentially stationary. Pulsing the unbaffled flow (Figures 4.1b and 4.1c) show that pulsing the flow does not necessarily improve the radial mixing. It is interesting to note the apparent flow maximums close to the wall in Figure 4.1b at t =0.5 (predicted by Kennedy et al.). This effect was not discussed by Howes et al.

Solid particles tend to migrate away from the wall in ordinary laminar flow and this effect is heightened when the flow is pulsed. By extrapolating these findings to TRO membranes, Kennedy et al. concluded that these phenomena could reduce fouling and counteract concentration polarisation.

Their experiments showed that the permeation rate increased with pulse frequency. They concluded :

> *To duplicate the observed permeation increases by recycling the concentrate, for example, would require up to 80 % recycle in addition to at least a six-fold increase in velocity.*

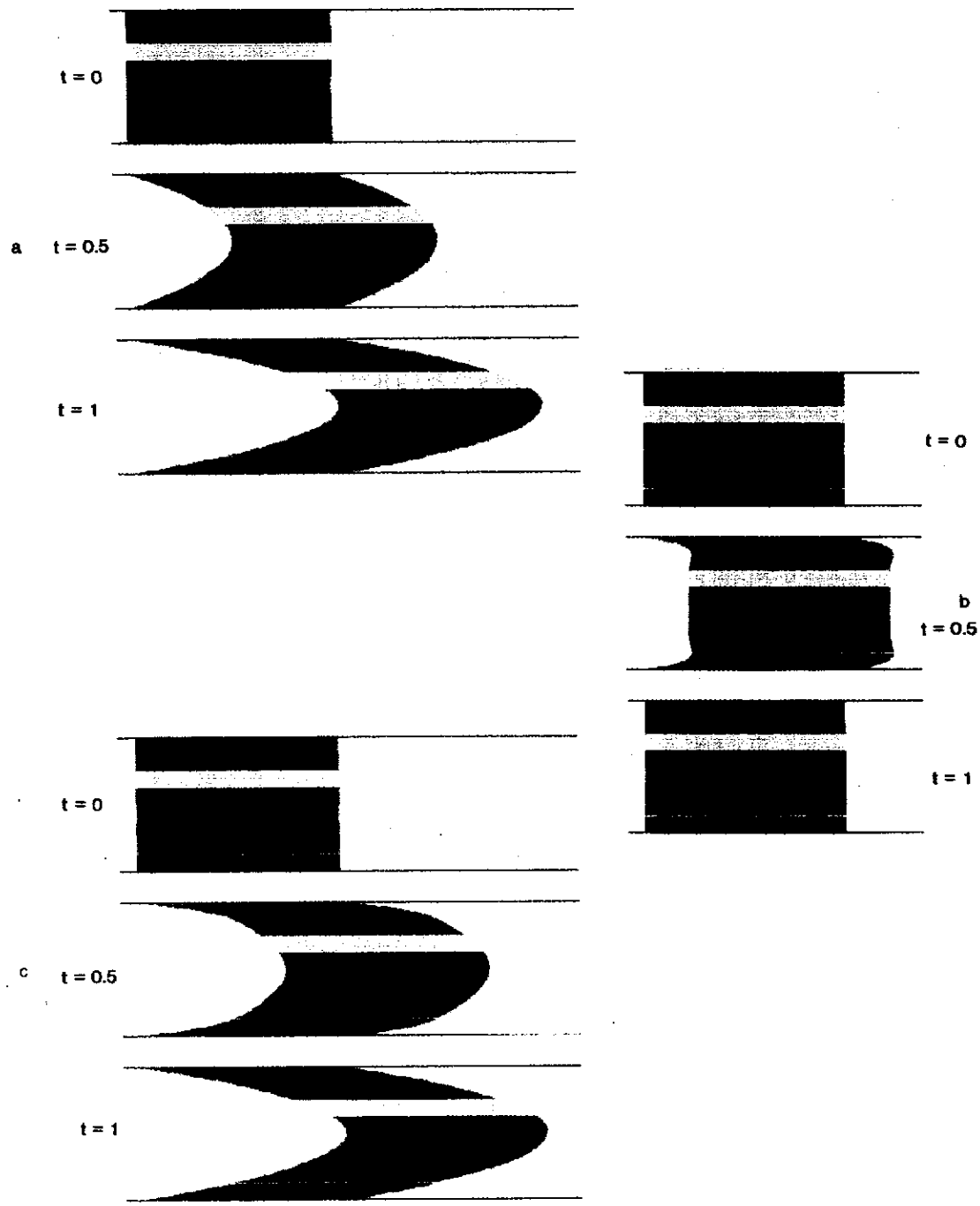

FIGURE 4.1 : *Results for an unbaffled channel : (a) net flow at Re_n = 100, (b) oscillatory flow at Re_o = 100, St = 1,0, (c) coupled net flow and oscillatory flow at Re_n = 100, Re_o = 100, St = 1,0 (from Howes et al., 1991).*

Bauser et al. (1986) attempted to reduce concentration polarisation by applying a constant and an oscillating transmembrane pressure to a number of ultrafiltration membranes, using a protein solution for the feed. The results were reported as ratios of the permeate fluxes under oscillatory versus constant transmembrane pressures. The results showed two peaks at high amplitudes and high frequencies, with a maximum flow gain of 50 %. The effect showed greater improvements for frequency increase as opposed to an increase in amplitude. The only attempt to explain this was :

> [The peaks] *are apparently due to resonance phenomena; they depend on membrane-support geometry but await further clarification.*

Ilias and Govind (1990) reported potential applications for pulsed flow in ultrafiltration.

There are no reported decreases in salt passage for TRO. Kennedy et al. (1974) used a sucrose solution and TRO membranes that had a 2 % sucrose passage. They assumed the solute passage constant (possibly to suit their calculations).

A variation of pulsed flow is agitation by stirring. Lora and Arnal (1990) agitated the feed solution over flat sheet RO membranes. They reported water flux rate increases of 90 % for brack water (1 000 mg/ℓ NaCl) and 140 % for sea-water (35 000 mg/ℓ NaCl) solutions. This finding is significant because the feed solution is not highly viscous as appeared to be the case with most other investigations. Improvements in the performance of RO systems by the destabilisation of the concentrated polarised layer are thus not limited to viscous solutions. They also reported some decreased salt passage. Inspection of the membrane surfaces revealed reduced fouling on the membranes over which the feed had been agitated. After 500 hours of operation, the flows through the agitated membranes were roughly double that of the steady case.

4.1.1 Pulsating and Oscillating Flow

Pulsating flow does not necessarily imply oscillating flow tangential to the feed flow direction. The flow will only oscillate once the reverse pulse changes the direction of the flow in the tubes.

This effect leads to an initial decrease in or constant permeate flux for increasing frequency. A local minimum in flow occurs just before the frequency (or amplitude) at which flow reversal takes place (Kennedy et al., 1974). At this frequency, there would be no flow during the negative pulse and a concentrated polarisation layer would be established during this phase of the cycle, leading to a decrease in permeate flux and quality.

This behaviour is depicted in Figure 4.2 which isolates the trends in the permeate flux results of Kennedy et al. (1974).

To examine this mathematically, consider the behaviour of a particle under the simultaneous influence of a sinusoidal pulse and bulk flow. Its distance down the tube at any time may be described by :

$$s = \bar{u}t + a\sin(wt) \tag{4.1}$$

where s = the distance of the particle from the tube inlet [m]

$\bar{u}$ = the mean feed flow [m/s]

t = the time elapsed since the particle entered the tube [s]

a = the mean-to-peak amplitude of the oscillation in the tube [m]

w = the frequency of the oscillation [rad/s]

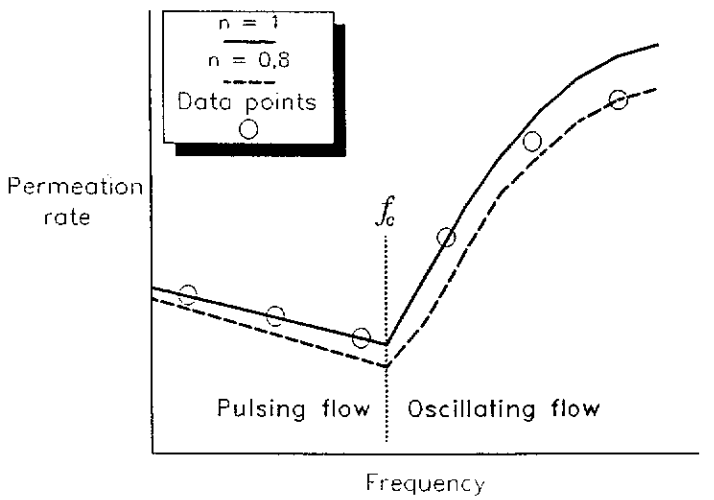

FIGURE 4.2 : *Predicted graph (based on the work of Kennedy et al., 1974) of permeation rate as a function of pulsing frequency for constant amplitude and feed flow. The lines represent the theoretically predicted curves of the square wave theory (discussed in Section 4.1.2.1.) and the data points represent the experimental data.*

The instantaneous velocity (u) of the particle at any time can be determined by differentiating the distance (s) with respect to time :

$$u = \frac{ds}{dt} = \bar{u} + aw\cos(wt) \tag{4.2}$$

At the critical frequency or the frequency of incipient oscillation, the velocity will be zero during the maximum reverse flow (when $\cos(wt) = -1$). Hence, the critical frequency (w_c) can be determined for a given amplitude or *vice versa* :

$$w_c = \frac{\bar{u}}{a} \tag{4.3}$$

Kennedy et al. derived a similar expression for their equipment for critical frequency (f_c) in terms of Hertz :

$$f_c = \frac{\bar{u}}{2\pi \ a} \tag{4.4}$$

4.1.1.1 Graphical interpretation of the critical frequency

Figures 4.3 to 4.8 indicate the effect of increasing frequency at a fixed amplitude on a given feed flow. Below the critical frequency (Figures 4.3 and 4.4), the velocity of the particle remains greater than zero and the particle moves forward continuously. The reverse pulse only retards its progress.

At the critical frequency (Figures 4.5 and 4.6), the particle is stationary for $\cos(wt) = -1$. The distance vs time line appears horizontal at that time. For frequencies above the critical (Figures 4.7 and 4.8), the velocity cycles below zero and the particle moves backward intermittently.

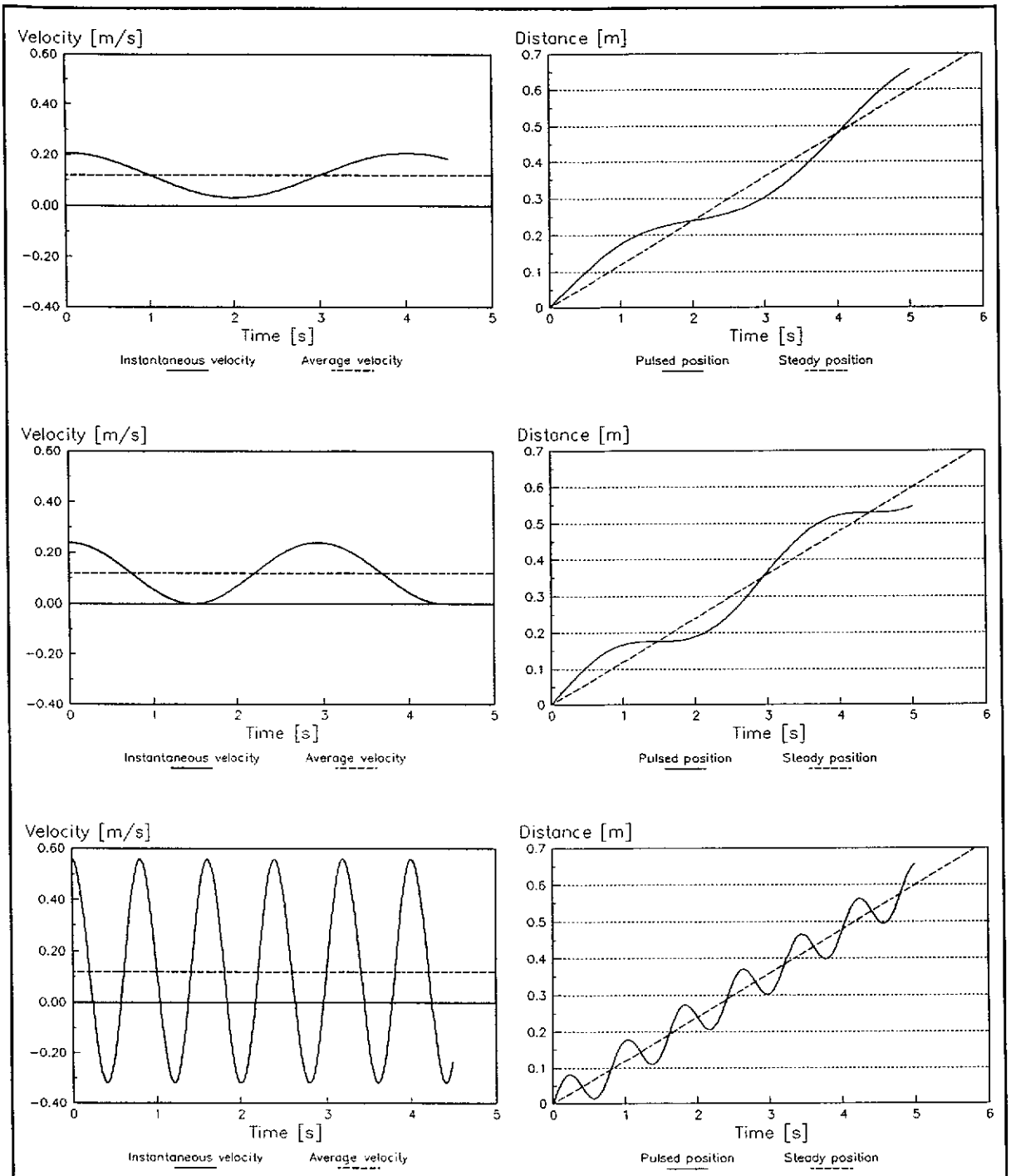

FIGURES 4.3 to 4.8 : *The effect of increasing pulsing frequency on a particle's velocity and position in the tube relative to the feed flow. Feed flow = 0,18 m/s and amplitude = 0.24 m.*

Pulsed flow will refer to any flow that is regularly pulsed whereas oscillatory flow will be pulsed flow where the amplitude and frequency produce a condition where flow reversal occurs. It is useful to employ a simple ratio to categorise this definition.

4.1.1.2 The Pulsing Number

The frequency and amplitude of the pulse and the mean flow velocity are used to determine whether the flow in the tube is merely pulsing or oscillating. This was further refined to produce the Pulsing number (Pu) for the purpose of this work :

$$Pu = 2\pi \frac{fa}{\bar{u}} \tag{4.5}$$

For $Pu < 1$, the flow will be pulsed
for $Pu = 1$, the flow will be critical
for $Pu > 1$, the flow will oscillate.

4.1.2 Theoretical Mass Transfer Considerations

4.1.2.1 The square wave theory

The extent to which increased absolute velocity affects mass transfer away from the concentrated layer adjacent to the wall can be approximated as follows. The quasi-steady state theory of Keil and Baird (1971) is used. There may be some argument as to whether a *steady-state* theory may be applied to the pulsing situation because the development-time of velocity profiles may be longer than the period of pulsation. However, the main concern here is the concentration polarised layer which occurs in a thin film near the tube wall where the velocity profiles are formed rapidly. Furthermore, Kennedy et al. (1974) achieved satisfactory correlation between the theoretical and experimental results using this method.

In steady flow,

$$k = K \; Re^n$$

(*cf* 4.3.3.3) or

$$k = K \; u^n$$

assuming that for pulsating flow the average mass transfer coefficient is :

$$k_p \propto \frac{1}{T} \int_0^T | u_p (t) |^n dt$$

The ratio of the pulsed mass transfer coefficient to the unpulsed mass transfer coefficient is :

$$\frac{k_p}{k} = \frac{1}{T} \int_0^T \left| \frac{u}{\bar{u}} \right|^n dt \tag{4.6}$$

$$= \frac{1}{T} \int_0^T \left| 1 + \frac{u_p}{\bar{u}} \right|^n dt \tag{4.7}$$

where T = the period of the pulse [s]
$u(t)$ = instantaneous velocity [m/s]
$u_p(t)$ = the velocity of the pulse [m/s]
$\bar{u}$ = average unpulsed velocity [m/s]
$n > 1$ for laminar flow, and
$n = 0.8$ for fully turbulent flow.

For a sinusoidal pulse, this translates to :

$$\frac{k_p}{k} = \frac{1}{T} \int_0^T \left| 1 + 2\pi \frac{af}{\bar{u}} \sin(2\pi f t) \right|^n dt \tag{4.8}$$

However, Baird et al. (1966) suggest that the sine wave oscillation be modelled as a square wave. The average half cycle oscillating velocity (u_p) is used. This approximation leads to the simpler relationship for the ratio :

$$\frac{k_p}{k} = \frac{1}{2} \left| 1 + \frac{u_p}{\bar{u}} \right|^n + \frac{1}{2} \left| 1 - \frac{u_p}{\bar{u}} \right|^n \tag{4.9}$$

For the sine wave, $\bar{u}_p = 4af$. Thus, as f decreases from f_c to zero, $\frac{k_p}{k}$ approaches unity. Using Eqns 4.6 to 4.9 it could be possible to calculate the pulsed flow mass transfer coefficients from the open tube, steady flow coefficients.

The square wave theory assumes that the increase in mass transfer is due purely to the increased linear flow velocity induced by the pulsing. It does not account for natural convection as does the theory of Ilias and Govind (1990). Pulsing produces eddies and swirls which enhance mass transfer.

Another difficulty with the square wave theory is that the choice of the exponent, n, must, to some extent, be decided by trial and error. Kennedy et al. (1974) state :

> *For a transition regime open tube Reynolds number between 5 000 and 10 000* (sic), *the value of n is approximately unity; for slightly lower Reynolds numbers, n may be greater than unity.*

All the experiments in this work involve Reynolds number between 0 and 4 000.

4.1.2.2 The Ilias-Govind numerical simulation

Ilias and Govind (1990) reappraised the data of Kennedy et al. (1974) to check their own computational method for mathematically predicting the permeate flux behaviour of a TRO system under the influence of pulsed flow.

They solved their equations using the finite difference method. Their analysis showed a better agreement with the data than that of Kennedy et al. (1974). They attributed this to the failure of the square wave theory to account for natural convection.

An interesting aspect of their findings, although unstated, is the absence of any decrease in permeate flux for $Pu < 1$. This would appear to indicate that unidirectional pulsing does improve membrane performance, albeit marginally. No minimum occurs in flow with increasing frequency.

Their method requires considerable computation. It was not investigated for this reason and because it was not the purpose of this investigation to model the flow in the tube but to compare the effects of different operating modes on TRO performance. Their theory remains the best reviewed for modelling the effects of pulsed flow.

This theory also does not take into account the effects of eddies induced by the pulsing. As such it should under-predict results even though this does not appear to be the case. The smoothly accelerating sinusoidal pulse might be less prone to eddy formation than, say, a square wave pulse.

4.1.3 High Frequency Pulsation

The results of ultrasonic vibrations on RO fall into four categories, (Herrmann, 1982) :

a) displacement of the water-solute equilibria at ultrasonic frequencies,

b) displacement of the water molecule-cluster equilibrium at still higher frequencies,

c) thermally equivalent agitations, and

d) cavitation, more readily produced at relatively low frequencies (commonly 20 kHz) and at low hydrostatic pressures (e.g. 100 kPa).

Herrmann (1982) investigated the water-solute equilibria displacement and concluded that :

> *There is no ultrasonic or electromagnetic excitation frequency which has a specific effect on the permeation process, aside from the normal mechanical-agitation or normal temperature change effects.*

However, he did find that ultrasonic vibration of a fouled membrane during the depressurised cleaning cycle caused a subsequent marginal 3 % improvement in permeate fluxes compared to conventional low-pressure flushing.

Herrmann (1982), quoting Oesterle, stated that electric fields applied to the membrane can increase the rate of permeation through the RO membrane 2,5 times. Fields of 30 Hz to 10 kHz were applied. It was explained that the electric fields caused the dissolved particles to vibrate at their characteristic relaxation frequencies, which should have also caused the mechanical vibration of the membrane and thus yielded similar effects to ultrasonic vibration. Herrmann concluded that this was not so.

In a private communication, Dr Alani (1992) has shown that the application of an electric field to a pulsed flow can markedly increase the flux of a BSA solution through an ultrafiltration membrane. No indication of the field strength of nature (i.e. oscillating or steady) was given. Fluxes were highest for pulsed flow in an electric field, followed by pulsed flow in the absence of an electric field and were marginally lower for steady flow in an electric field. Pulsed flow in an electric field produced 20 to 25% higher fluxes than pulsed flow with no field over a range of concentrations.

4.1.4 Possible Effects of Pulsing Wave Form

Gupta et al. (1992) investigated the effects of different pulse profiles and displacements on apple juice feeds to ceramic (Ceraflow) and carbon tubular (Carbone

Lorraine) membranes. Their paper also reviewed their previous work on pulsed flow in carbon (Carbosep) membranes. They found significant increases (up to 45%) in the long term permeate flux when a regular pulse was applied to the feed flow.

Their findings are significant in that they propose a different mechanism for the increase in permeate flux to that previously put forward. Their experimental apparatus employed on pulsing, piston pump, placed between the feed pump and the inlet to the membrane system. The pump effected measurable pressure fluctuations within the membrane system. Four pulse cycles were examined. All cycles lasted 1 s.

The pulse shapes are summarised in Figure 4.9. Wave shapes *a* and *b* and wave shapes *c* and *d* are reversals of one another. Theory based on the flow destabilisation of the laminar boundary layer alone should predict no difference in the effects of reverse shape pulses. In their experiments, Gupta et al. found that the *stable* permeate flux improved in the following order (with increases in permeate flux after 60 min shown in brackets); steady flow, wave shapes *b* (35 %), *a* (40 %), *c* (47 %) and *d* (55 %). The increases are highest for the waves with the highest time-mean value of fluid acceleration.

The system pressure fluctuation caused by the pulsing pump arrangement was examined. *Wave a generated the highest pressure but not the highest flux. Wave d begins with a drop in pressure (which may destabilise the boundary layer) followed by a fast pressure rise* (which should increase the driving force across the lower resistance layer). Another factor is that pressure reduction immediately after the instantaneous increase in driving force may counteract the action's effect whereas the synergy of the negative-positive pressure variation in wave *d is beneficial to the permeate flux*. However, this does not explain the absence of this effect for waves *a* and *b*. The authors make no attempt to explain this.

Direct comparisons cannot necessarily be drawn between the effects of pulsed flow in microfiltration systems and reverse osmosis systems because of the nature of the separation mechanisms but the significance of the findings of Gupta et al. to this work is that the manner in which the pulse is applied to the feed flow (and not the pulse alone) must be considered. Where the pulse is likely to introduce pressure modulation (typically the case for an unbalanced piston action) as well as an instantaneous flow rate variation, both steps must be considered in assessing the effectiveness of the pulse.

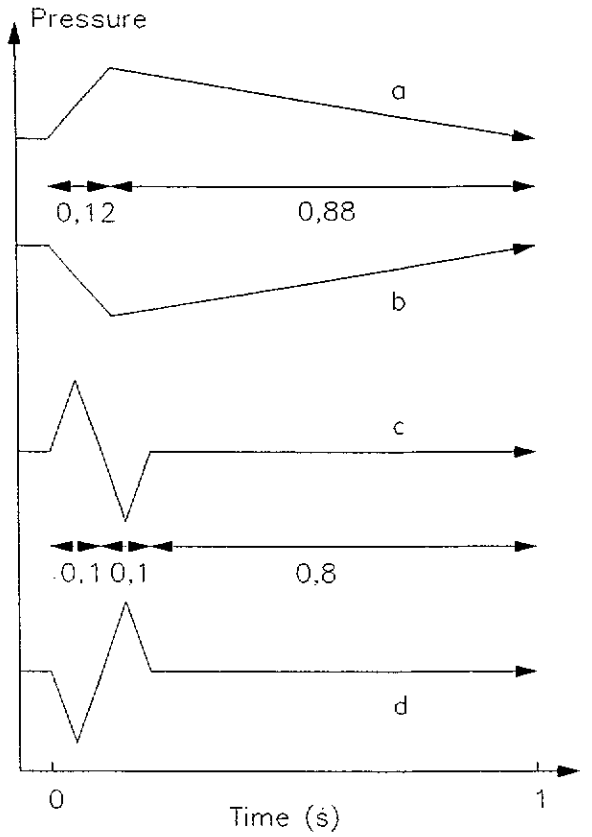

FIGURE 4.9 : Pressure variations in the pulse profiles used by Gupta et al. (1992) showing the order of respective variations occurring in each cycle.

4.1.5 Pulsing Energy

Ilias and Govind (1990) calculated the theoretical additional energy required by a pulsing pump. They show that this power is of the order of one thousandth that of the system energy. It should be noted that their theory makes no allowance for the type of pulsing pump used. It only reflects the power required to maintain the pulsations. However, Finnegan and Howell (1989) report a 6 to 53 % increase in power requirement for the pulsing, stressing however that despite the energy penalties, permeation flow increases warranted the increased energy requirements.

Theoretical calculations by Gupta et al. of total hydraulic power dissipated per unit volume of permeate reveal that the values are lowest for wave forms *c* and *d*, with wave form *c* with a small stroke volume being the most economically attractive with a 32 % power reduction over the steady flow base case. The unbalanced pulsing pump would be required to counteract the effects of the feed pump, requiring a

significant additional energy factor and this was bourne out by comparison between theoretical and physical energy considerations; the experimental values were up to 60 % higher than the theoretical values for this system. Such discrepancies were attributed to the flow resistance effects of pulsations.

4.2 EQUIPMENT

4.2.1 Diagram of the Equipment

The diagram of the equipment used in this section of the work is shown in Figure 4.10.

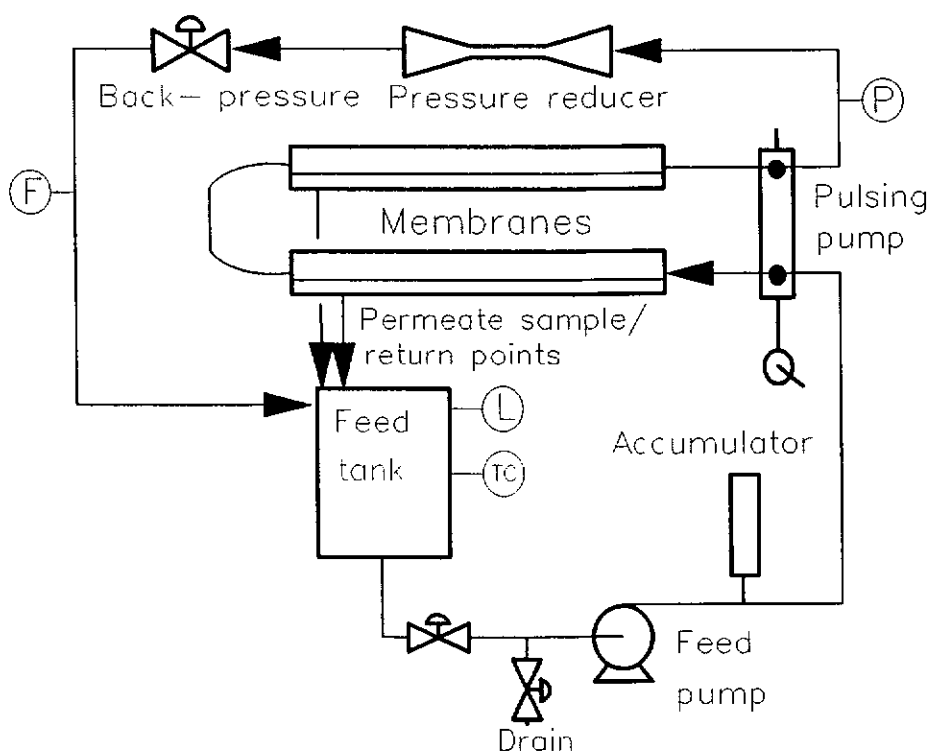

FIGURE 4.10 : *Schematic diagram of the equipment used for the open tube, pulsed flow experiments.*

4.2.2 Pulsing Pump Development

The object of the pump design was to devise a low energy, pulsing pump that could be modified to generate a range of amplitudes and frequencies.

All the papers that presented pump designs appeared to use two synchronised piston pumps positioned at the inlets and outlets of the membrane systems (Kennedy et al., 1974; Mackley et al., 1990 and Finnegan and Howell, 1989/90). There are a number of problems with this design.

The essence of the design used in this work is that the double-acting pulsing-pump bridges the inlet and the outlet of the membrane loop. A piston, placed in what is effectively a by-pass to the unit, can oscillate the flow through the membrane-module. The only pressure that it needs to operate against is the pressure drop through the membranes: which is dependent on the flow rate and the number of membranes being used in series: in this case 1 % of the system pressure (but typically between 2 and 10 %).

4.2.3 Pump Design Specifications

The final pump design is diagrammatically depicted in Figure 4.11.

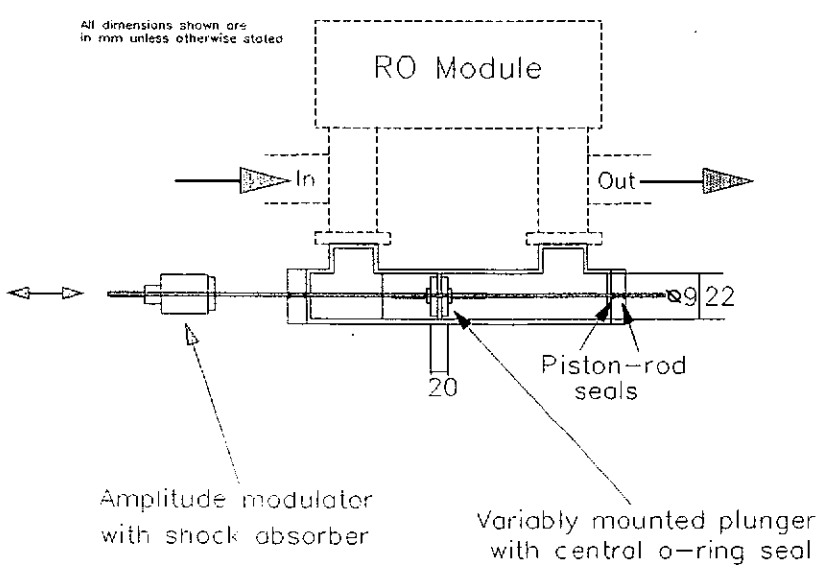

FIGURE 4.11 : *Cross-section of the double acting pulsing pump. All metal parts are stainless steel.*

The piston rod was designed to run the entire length of the pump to maintain a linear travel path for the plunger (to counter any lateral motion that might be exerted by the drive). The connection between the drive and the piston rod was also pivoted to absorb any such motion.

The end of the rod (not connected to the drive) had a small hole drilled through it. A cord was connected to this and a precision potentiometer was used to measure the displacement of the plunger electronically. Hence the pump action was characterised.

The rod design did have a shortcoming in that it required an extra set of piston shaft seals. These were the parts of the pump most prone to failure. Whilst they were successful as water seals, each outside pair had to withstand high, friction-induced temperatures as there was no water for cooling or lubrication.

The amplitude was set by the location of a locknut. This acted as a base-line an reference point. The other amplitudes could be fixed by clipping teflon spacers onto the piston rod. The displaced volumes caused by the pulses in the RO tubes was calculated by determining the volume displaced by the pump during one oscillation at a given amplitude (using the dimenisions within the pump chamber, excluding the rod and plunger volumes) corrected for the pump-tube diameter differences (excluding the volume of the baffle holders).

Compressed air was used to actuate the piston. A variable-period recycling timer was used to regulate the frequency of oscillation. The period could be adjusted between 0,2 and 19,8 Hz.

4.2.4 Pulse Action

It is possible that the sinusoidal pulse has no effect at frequencies lower than the critical, $Pu < 1$. This waveform choice was probably a product of the previous investigators' needs to synchronise two pistons (normally with a central cam or oscillator) and to provide a conveniently modelled wave form. With the device described above there is more flexibility with regards to the pump action.

An approximately square-wave pulse is attractive because, provided the speed of oscillation (adjusted for the difference in the pump and tube diameters) is greater than the velocity of the fluid, **one will always have flow reversal**. The liquid will also be subject to shear caused by the sudden acceleration at the beginning and end of each stroke. Effectively, the flow condition within the tube will become a four-stage cycle : (1) normal forward, (2) fast forward, (3) normal backward and (4) fast backward.

4.2.5 Modelling of the Wave Form

Modelling such a stroke is more difficult than with sinusoidal oscillation. A computer program was written to read the current continuously through the potentiometer. These readings were averaged (approximately 50 ms) and stored in an array. After about 500 readings had been taken (between 6 and 60 cycles), these values were stored for analysis.

These data were reduced to a single composite wave form. Regressing for the slopes of the pulse phases gave the pulse velocities and duration.

The computed waveform was used to generate an accurate velocity profile for the pulse. This, together with the mean flow, can be numerically integrated to compare the mass transfer coefficients. More details of the modelling are given in Appendix E.1.

4.3 RESULTS

4.3.1 Pump Waveform

The nature of the waveform (an example of which is shown in Figures E.2 and E.3) warrants some discussion. The results are presented in Appendix E. The wave forms were not perfectly symmetrical. The reverse pulse was slightly faster than the forward pulse but occurred over a shorter duration. This was probably caused by the pulsing pump ram and not any hydrodynamic condition, since this effect was also noticeable when only the pulsing ram was operative (no feed flow).

This action caused little difficulty for modeling the waveform. The speed at which the ram moved was dependent on the amplitude of the stroke. Increased amplitude thus implied increased linear velocity. Both of these effects were accounted for in the subsequent modelling.

4.3.1.1 Square-wave theory

Since the velocity for each cycle-phase could be adequately determined, the square wave theory (Eqn 4.9) could be modified without any approximation to :

$$\frac{k_p}{k} = \frac{1}{T}\left\{T_{\uparrow}\left|1 + \frac{u_{p\uparrow}}{\bar{u}}\right|^{n} + T_{\downarrow}\left|1 - \frac{u_{p\downarrow}}{\bar{u}}\right|^{n}\right\} \qquad (4.10)$$

where T is the period of the relevant pulse cycle [s]
↑ refers to the forward pulse
↓ refers to the reverse pulse.

Using the value of $n = 1$, the mass transfer gains predicted by the square-wave theory are calculated. While this is not strictly correct in terms of the analysis presented by Kennedy et al. (where $n > 1$), it represents the only sensible mechanism of comparison between the ratio of mass transfer coefficients derived from the square wave model and those derived via the separate Sourirajan analyses of the base-case and the pulsed-flow experimental results. The results of the comparison are shown in Tables 4.1 and 4.2. At the lowest flow rate (that of 0,061 m/s) the square wave theory sometimes predicted higher gain than those determined experimentally. This is unusual as the value of the exponent could theoretically be higher : allowing for even higher values of the mass transfer gain. However, as the flow tends to the turbulent regime (where the exponent should decrease to 0,8), the theory progressively underpredicts the experimentally determined gains. Values for the exponent, n, were derived iteratively (from the experimental gains and the pulse characteristics determined in Appendix E) and those required to produce the magnitude of the experimental gains were generally found to be higher than the theoretical value of one. Such findings indicate that the square-wave theory does not adequately describe the natural convection and the mixing capability of the pulsing-induced eddies.

However, when assessing the results, one must bear in mind the implications of the error analysis conducted in Appendix C. Large variations in the value of the mass transfer coefficient, particularly in the range produced by pulsing, are not necessarily indicative of great changes in RO performance. The theory serves as a rough guide to the trends one could expect from a pulsing system.

TABLE 4.1 : *Comparison of gains in mass transfer coefficients predicted by square wave theory and those calculated from the experimental analysis*

Amplitude	Frequency	Feed flow	Square wave theoretical gain	Experimentally determined gain	
cm	Hz	m/s		Tube A	Tube B
16,7	1,25	0,061	7,20	6,93	5,92
		0,123	3,79		
		0,184	2,67	6,94	2,47
		0,246	2,10		
13,3	1,25	0,061	5,34	6,47	5,06
		0,123	2,69		
		0,184	1,82	7,44	3,88
		0,246	1,37		
9,3	1,25	0,061	3,83	7,17	3,69
		0,123	1,94		
		0,184	1,31	5,04	1,91
		0,246	0,99		
5,6	1,25	0,061	2,30	7,17	3,69
		0,123	1,15		
		0,184	0,78	5,04	1,91
		0,246	0,59		

TABLE 4.2 : *Comparison of gains in mass transfer coefficients predicted by square wave theory and those calculated from the experimental analysis. Frequency variation (excluding 1.25 Hz: shown in previous table).*

Amplitude cm	Frequency Hz	Feed flow m/s	Square wave theoretical gain	Experimentally determined gain	
				Tube A	Tube B
9,3	0,25	0,061	0,82	3,71	2,71
		0,123	0,44	2,52	2,07
		0,184	0,32	1,96	1,56
		0,246	0,25	1,74	1,37
9,3	0,50	0,061	1,54	5,22	3,69
		0,123	0,78	3,45	2,57
		0,184	0,53	2,44	1,87
		0,246	0,40	2,08	1,57
9,3	2,50	0,061	7,42	8,27	5,15
		0,123	3,75	5,33	3,49
		0,184	2,53	4,53	2,93
		0,246	1,92	3,46	2,28

4.3.2 Mass Transfer Coefficients in Pulsed TRO

A series of experiments were conducted at four frequencies and two amplitudes. Since these were carried out in open tubes the same values for A and $\left(\frac{D_{AM}}{Kb}\right)$ were used as in the open tube, steady flow analysis. The full set of results is presented in Appendices D.2 and D.3.

Each mass transfer coefficient corresponds to one run at 4 MPa, a given feed flow rate, a temperature of 25 °C and a given feed concentration. A permeate flux and a salt passage were determined for each run. The details of the regression procedure used to determine the mass transfer coefficient are described in Appendix C.

Zero frequency represents the open tube, steady flow. The reported gains in mass transfer coefficient are the ratio of the pulsed flow coefficient to the steady flow coefficient at the corresponding average Reynolds numbers.

4.3.2.1 Frequency variation

Figures 4.12 and 4.13 show the trends in mass transfer coefficient for increasing pulsation frequency with constant amplitude. Both tubes exhibit increasing k for increasing frequency. The increase tails off after an initial rapid rise (Table 4.1).

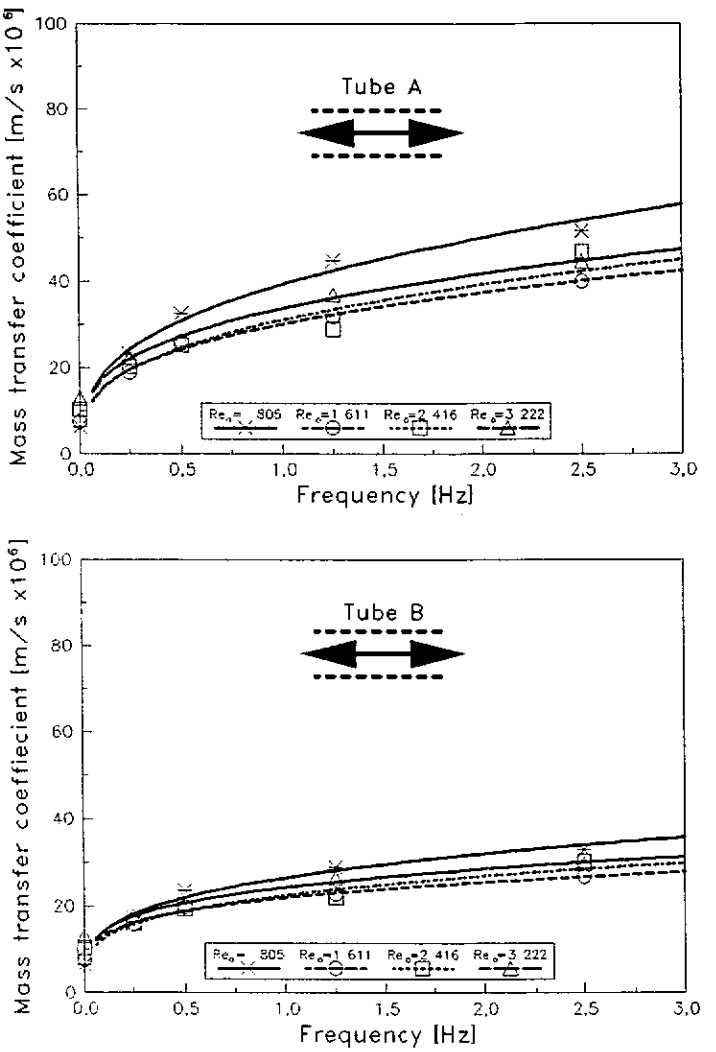

FIGURES 4.12 and 4.13 : *Variation in mass transfer coefficient with frequency of oscillation for open tubes A and B. The four data ranges represent the four average Reynolds numbers, Re. The curves are merely intended to highlight the trends in the data. Amplitude of oscillation = 93 mm.*

Such behaviour is predicted by the square wave theory. The increasing frequency leads to more frequent flow reversal (ie. $\frac{1}{T}$ increases). In this case it also leads to higher pump speeds (ie. u_p increases).

The error analysis (Appendix C) reveals that the highest values of k obtained for tube A could lie below the lowest values obtained for tube B. As such, the trend of increasing mass transfer coefficient with frequency remains meaningful but the comparative increases with average Reynolds number (Re_o) are probably an artefact. It could be said, with 90 % certainty, that the apparent differences in mass transfer coefficient for similar hydrodynamic conditions (i.e. tubes A and B) are within the range of experimental error. Furthermore, experimental error could account for the absence of any trends with increasing flow rate. The highest average Reynolds numbers should return the highest coefficients but this is not the case.

The greatest gain in mass transfer coefficient occurs at lowest average Reynolds numbers for both tubes (see Figures 4.14 and 4.15). This would be expected since the lowest Reynolds numbers would be associated with the highest concentration polarisation and stand to gain the most from better fluid mixing. The rate of increase in gain diminishes for increasing frequency.

4.3.3 Amplitude Variation

The results of amplitude increase (Figures 4.16 and 4.17) are similar to those for increasing frequency. This would be expected because the speed of the fluid is proportional to the magnitude of the amplitude in the tube for a given frequency. (For this reason, only two flow rates were investigated). According to the square pulse theory, the mass transfer coefficient should increase with increasing u_p.

The afore-mentioned comments on experimental error (*cf* 4.3.2.1) stand for these data sets as well. However, in this instance, the trend of enhanced mass transfer with increased linear velocity in the tube is clear (i.e. the lowest flow rates exhibit the greatest gain in mass transfer under pulsed conditions).

The results of gain in mass transfer coefficient with increasing amplitude (Figures 4.18 and 4.19) are similar to those for increasing frequency. Tube A continued to show a larger increase (Figure 4.17) although the results at the higher amplitudes are more erratic, indicative probably of the *narrow range*[1] mass transfer effect. Re-appraisal of the raw data shows very small differentials between the experimentally determined values of permeate flux and salt passage over the range of these

1 The *narrow range* effect is fully discussed in Appendix C.4.2. At the lowest values for salt passage and the highest values of permeate flux, relatively small gains in salt passage or permeate flux result in comparatively large gains in mass transfer coefficient. Thus a small experimental error could be unduly magnified in terms of the value of the mass transfer coefficient.

experiments. Any small experimental deviation is then magnified when the mass transfer coefficient is calculated. Furthermore, no logical explanation can be reached as to why the mass transfer coefficient should decrease with increasing open tube amplitude oscillation.

A hypothesis extended to account for this apparent trend is that the longer flow path associated with the higher amplitude, causes more severe concentration polarisation effects but this fails on examination of the pulse characteristics: while the periods of the longer amplitude pulse strokes are comparatively higher, the velocities are also higher than during the shorter pulses. The contradictory nature of these characteristics makes it difficult to draw categorical conclusions from the results.

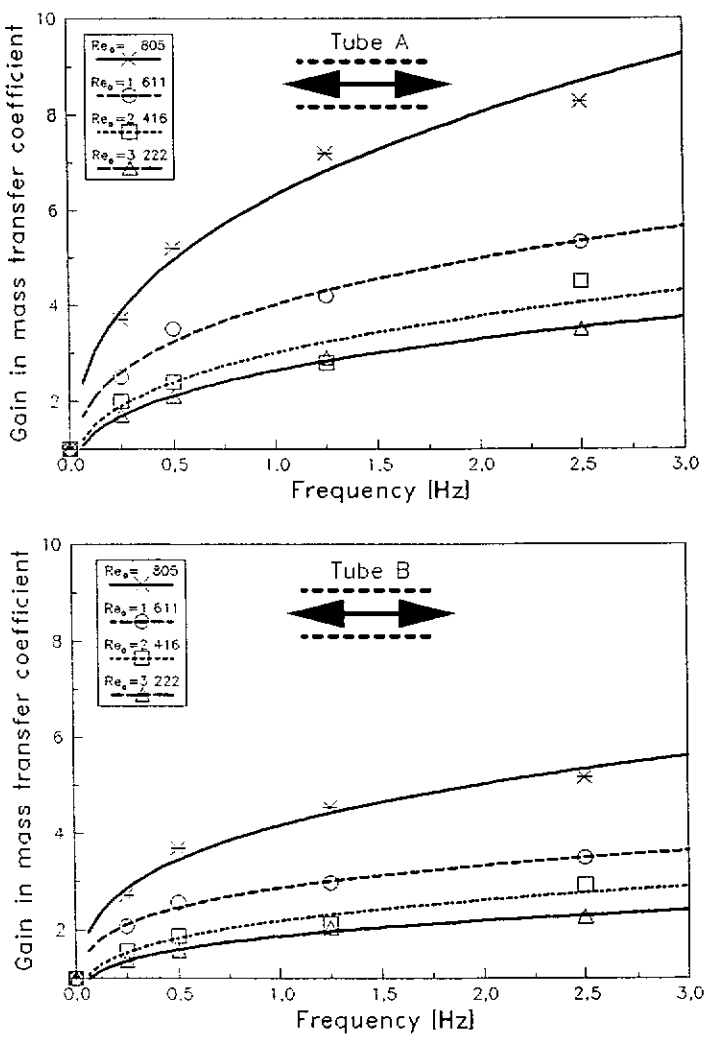

FIGURES 4.14 and 4.15 : *Gains in mass transfer coefficients for pulsed flow, open tubes, as a function of increasing frequency. The four data ranges represent the four average Reynolds numbers. The curves are merely intended to highlight the trends in the data. Amplitude of oscillation = 93 mm.*

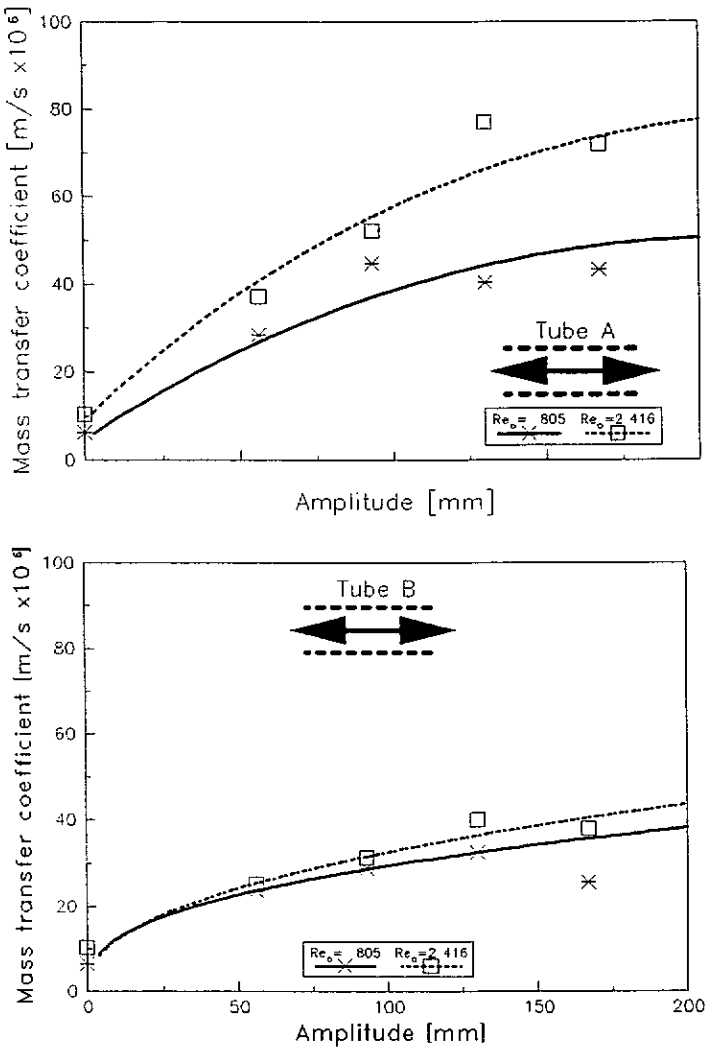

FIGURES 4.16 and 4.17 : *Graphs of mass transfer coefficient as a function of amplitude of oscillation for open tubes A and B at a frequency of oscillation = 1,25Hz. The two data ranges represent the two average Reynolds numbers. The curves are merely intended to highlight the trends in the data.*

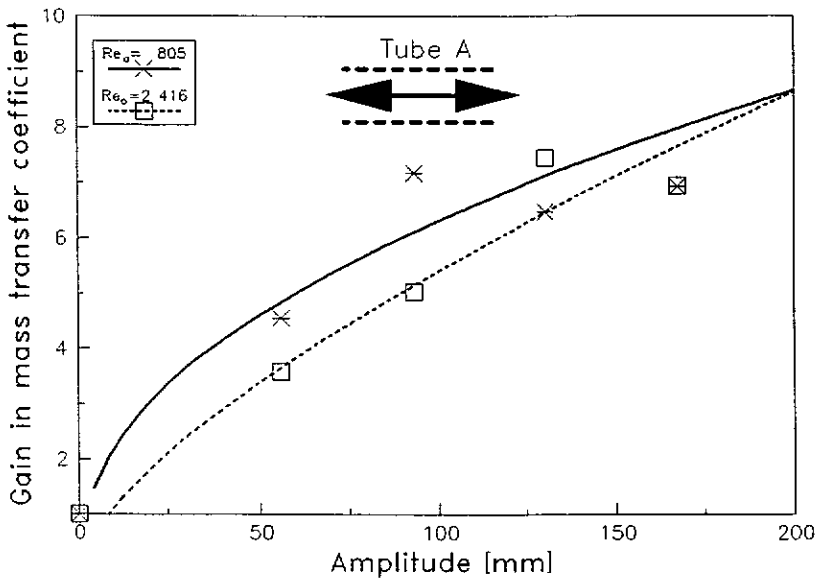

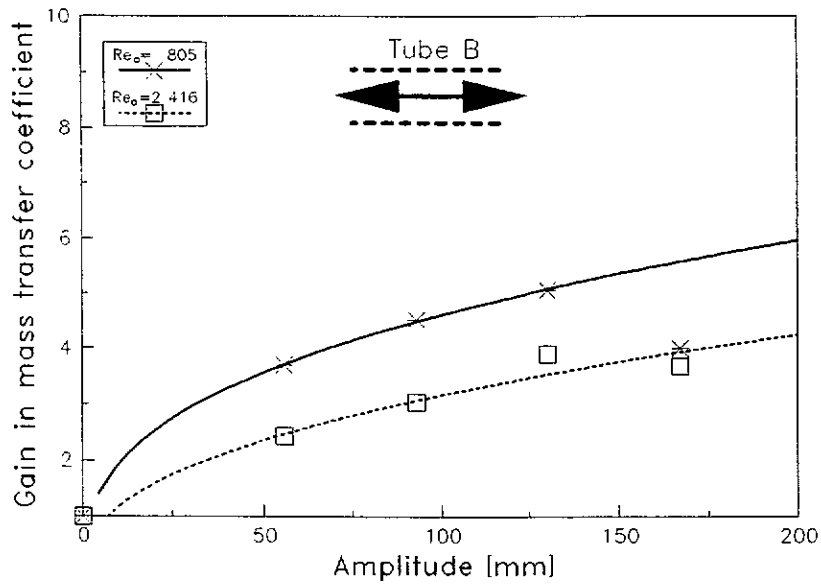

FIGURES 4.18 and 4.19 : *Gains in mass transfer coefficients for pulsed flow, open tubes, as a function of increasing amplitude. Frequency of oscillation = 1,25 Hz. The two data ranges represent the two average Reynolds numbers. The curves are merely intended to highlight the trends in the data.*

4.4 CONCLUSIONS

Pulsing the feed flow to a TRO system increases the solute mass transfer in the system. Increasing the frequency and the amplitude of the pulse have beneficial effects.

A novel pulsing pump design was shown to operate satisfactorily. Despite inconsistencies in its speed of operation for different frequency settings, a problem which could be remedied by a different drive mechanism, the pump is simpler and requires less energy than the pumps reported in the literature.

The square-wave theory predicts pulsed mass transfer coefficients below those calculated on the basis of the Sourirajan analysis. The square wave theory neglects natural convection and the mixing effects of eddies generated by the rapid acceleration at the beginning and end of each of the pulse cycles.

Analysis of the results is made difficult by the large increases in mass transfer coefficient for relatively small increases in performance (described in Appendix C.4.2). Most problematic of the consequences of this *narrow range* effect is the divergence of the results for the two open tubes. Hydrodynamic effects in the tubes should be similar, but this does not appear to be mirrored in the results. An error analysis reveals that the regions of uncertainty for both sets of results do overlap, making it conceivable that the deviation is a result of experimental error. Given the analysis tools developed during the course of this work, similar difficulties could be avoided by immediate appraisal of the experimental results within an RO model. The ultimate effect of the analysis, while demonstrating that pulsing the feed flow does improve the mass transfer within the tube, has also shown the difficulties likely when dealing with a system that is operating close to its optimum limiting performance.

The apparent hydrodynamic discrepancies do fall within the range of experimental error as do the deviation of the results for the different flow sets from the expected trend of increasing mass transfer coefficient for increasing average Reynolds number : increased linear fluid velocity should imply increased mass transfer. The capabilities of the model are thus not necessarily at fault.

Chapter 5

STEADY FLOW IN BAFFLED TUBULAR REVERSE OSMOSIS

5.1 INTRODUCTION

This Chapter examines the performance of steady flow in a baffled tubular reverse osmosis system in terms of the mass transfer coefficient.

Baffles of elliptical and doughnut shape were tested. The term, superficial Reynolds number, is used to indicate that flow regimes (e.g. laminar or transition) normally associated with certain Reynolds number values for open tube flows do not necessarily apply for baffles.

Baffles have been used in many applications to improve the heat or mass transfer from the tube wall to a fluid. They create eddies that enhance convection by increasing turbulence and improving fluid mixing. Typically most baffled systems used in previous studies consisted of a series of regular obstructions placed in the flow path : disks, spheres, spirals etc. (Thomas and Watson, 1968, Pitera and Middleman, 1973 etc.) on the one hand and constrictions of the tube walls *per se* on the other (Bellhouse et al., 1973). The local linear velocity is increased through the constriction as is the shear rate at the membrane surface. Simple film theory models indicate that mass transfer is enhanced by increasing the shear rate. Additionally, at sufficiently high Reynolds numbers, secondary flows may be generated by the obstructions which in turn result in turbulent eddies (Sobey, 1980). Both of these effects enhance mixing adjacent to the membrane wall and should reduce concentration polarisation at the cost of increased pressure drop.

Baffles are not ideally suited for use in reverse osmosis though, because they can damage the delicate membrane surface either during insertion or through vibration against the tube wall during operation. They also increase the capital and running cost of the membrane system. These drawbacks must be weighed up against the possible improvement in membrane system performance.

5.1.1 Convection and Turbulence Promotion

A distinction must be made between convection and turbulence promotion. It is possible to use baffles in a tube and still maintain laminar flow conditions. Under

such circumstances, the baffles would induce secondary flow of a steady nature. To include such situations, the term *convection promotion* will be used instead of the more commonly used, *turbulence promotion*. Examples of convection promotion include the coiled tube heat exchangers, the coiled tubular membrane oxygenator for blood (Weissman et al. (1968)) and furrowed oxygenator (Bellhouse et al. (1973)). This mechanism must not be confused with the convective transport of solvent to the membrane surface caused by the hydrostatic pressure differential (or driving force) within the membrane.

5.1.2 Detached Baffles and Convection Promotion

A means of avoiding membrane damage by baffles is to mount them on a central support and to keep their projected sectional diameter less than the internal tube diameter. All the inserts reviewed in this chapter have operated on this principle. A Kenics mixer was mounted on a central rod (Pitera and Middlemans (1973)). A spiral and twisted tape were mounted on wire runners placed on the membrane (Thomas and Watson (1968)). The latter has the disadvantage of blocking some of the membrane area.

5.1.3 Baffle Geometry Optimisation

The optimisation of baffle geometry was reviewed by Shen and Probstein (1979). Their main concern was to find the optimum inter-baffle distance to tube diameter ratio, $\frac{\Delta l}{d}$. Decreasing the ratio should bring about better fluid mixing and a reduction in concentration polarisation. Shen and Probstein (and four other groups of researchers they reviewed) concluded that there were insignificant performance improvements for $\frac{\Delta l}{d} < 4$. The $\frac{\Delta l}{d}$ for this work was set at four.

Other conclusions regarding promoters' geometry can be summarised as follows (Thomas and Watson (1968)) :

* *The optimum spacing between promoters in the direction of the flow is between 8 and 12 times the dimension of the promoter normal to the flow.*

* *The optimum dimension of the promoter in the direction normal to the flow and the optimum distance from the transfer surface depends on the particular flow configuration e.g. flow within a tube or channel.*

With regards to baffle design there is less clarity. Increases in the rates of heat and mass transfer by detached baffles had been studied using a variety of different geometries (reviewed by Thomas and Watson, 1968). Data exist for rings, disks, streamlined inserts, wire and sheet metal spirals and Kenics static mixers inside cylindrical tubes; rings in the annular region between concentric tubes; cylindrical rods located at the

edge of the laminar boundary layers; and cylindrical rods in confined rectangular channels. However, a measure of the relative merits of the different baffle types was not found in the literature.

5.1.4 Summary of Results Achieved with Convection Promoters

Convection promoters have been shown to improve the performance of membrane systems. Thomas and Watson (1968) found that inserting a detached spiral convection promoter caused a marked decrease in the salt passage of a dynamically formed Zr(IV) oxide TRO membrane. At their lowest Reynolds number of 2 100, the spiral caused the salt passage to decrease from 75 to 25 % while at a Reynolds number of 15 200, the salt passage only decreased from 10 to 7 %. A twisted tape insert decreased the salt passage from 46 to 31 % and 19 to 18 % at the same superficial Reynolds number respectively. Both promoters had pitches of 1,35 cm in 0,54 cm (sic) diameter tubes which was stated to be near the optimum.

What they reported as an *unexpected result*, was that throughout the experiments, they found a 10 to 50 % increase in permeate flow (the absolute rates were not stated). This increase was independent of superficial Reynolds number. Their explanation was that the increase in shear stress in the convection promoter region thinned the dynamically formed membrane layer on the surface of the tube, thus reducing the resistance to permeation. However, they did not explain how, with the membrane-thinning, they still returned such low salt passages.

Pitera and Middleman (1973) worked in the lower Reynolds number region (10 to 1 500), in which they stated that *previously studied inserts showed poor improvement.* They used a Kenics static mixer and a series of fixed, helical elements of alternating left- and right-hand pitch. They used two tubes in series. One tube was open and the other contained the promoters. The fact that the tubes were shown to have different pure water permeabilities made for difficult comparison of the performance improvement. They did not measure the improvement in mass transfer coefficient. At the lowest Reynolds number, more than half of the fluid entering the tubes permeated the membranes, which invalidated the assumptions of their analysis. The concentration of solute at the wall was reduced by approximately 40 % for all the reported results. They felt that their results, adjusted for the tube differences would have shown a 30 to 40 % increase in permeate flux and an improvement of 15 to 30 % in permeate quality for the promoted tube.

5.1.5 Flow Through a Furrowed Channel

Another means of forcing convection in any RO system is to modify the membrane surface. Sobey (1980) modelled the steady and pulsed flow through the Oxford

membrane oxygenator (Bellhouse et al. (1973)). This consisted of a membrane which was deformed onto triangular channels to form regular depressions as shown in Figure 5.1.

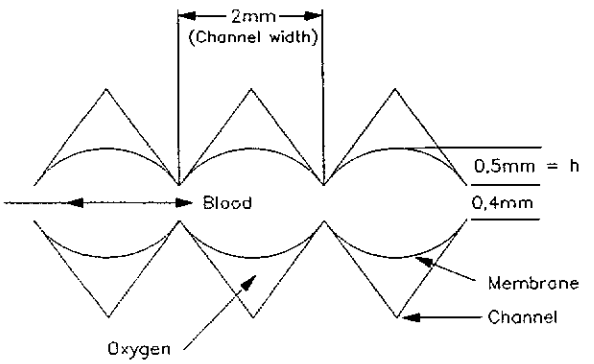

FIGURE 5.1 : *Configuration of the Oxford membrane oxygenator developed by Bellhouse et al. (1973).*

The device transfers oxygen into and removes carbon dioxide from blood. It is able to reduce concentration polarisation of the viscous liquid significantly without using turbulent flow. Unsteady laminar flow does not damage the blood. It is significant to this work in that it represents a practical applications of baffled (and pulsed-baffled) mass transfer enhancement. Sobey's mathematical modelling of the system describes the flow (in particular, *unsteady-laminar* flow) through a series of apertures, similar to the baffled system used in this work.

Beginning with the Navier-Stokes equation of motion for a Newtonian fluid[1], Sobey used a finite difference method to solve for a two-dimensional system. He then mathematically varied the Reynolds number and the geometric parameters to predict effects of their changes. His results compared well to the solutions for the boundary-layer theory of Smith (1976). (This is an approximate solution valid in the limits of large Reynolds number and small change in channel width).

As the Reynolds number is increased from a zero, a vortex forms in the centre of the membrane depression, filling the major part of the depression at a Reynolds number of 15. As the Reynolds number is increased, the vortex expands into the mainstream and shifts slightly towards the exit of the depression. At a Reynolds number of about

1 While blood exhibits non-Newtonian characteristics, the assumption of Newtonian behaviour and laminar flow in the large arteries is generally accepted (Hadingham and Buhr (1970)).

600, a small, counter-rotating vortex, forms on the downstream wall. This vortex formation would imply that as long as the Reynolds number was above about 500, the wall flow would be constantly replaced by the main stream flow, reducing concentration polarisation.

By varying the channel width while keeping the depth (h) constant showed a maximum effect at a ratio of about five. Varying the hollow depth, keeping the length constant shows a maximum vorticity at the apex of the depression (necessary to ensure good mixing throughout the region but somewhat dependent on the arc furrow geometry) at the ratio of 3:4. The theory of Smith (1976) is shown to be a good approximation of these solutions although they are rather limited in their application.

5.1.6 Disadvantages of Convection Promoters

Inserts occupy a sizable volume in the tube : reported volume fractions range from 20 to 50 % (Pitera and Middleman, 1973). (In this study the volume fractions fell in the low twenties). Thus the volumetric flow is reduced because of the decrease in area available to flow. By introducing baffles one may be converting, in an expensive manner, a tubular membrane system designed to handle large flows (albeit somewhat inefficiently) into a thin channel membrane, operating more efficiently, but with a low throughput.

Baffles might also create stagnant regions where foulants collect. Baffles should create the opposite effect by increasing the shear at the membrane wall, thereby scouring the membrane surface of foulants. If incorrectly placed, though, they might cause stagnant regions. This might be avoided by using streamlined shapes or inserts that present minimal surface area to the flow. These have the corresponding drawback of being less effective. Alternatively, twisted shapes can be utilised.

One of the main reasons for choosing a tubular membrane over a spiral wound or hollow fibre system, is that the former may be cleaned by sponge balls. Baffles negate this advantage.

5.1.7 Mathematical Modelling of Baffled Flow

Mathematical modelling of flow through a baffled tube was graphically represented by Howes et al. (1990). The results of their work is shown in Figure 5.2. The bands of colour correspond to particles in a particular horizontal fluid regime at the initial condition. The application of a laminar net flow is seen to disturb the vertical alignment of the particle regimes and mix the flow. Figures 5.2a and 5.2b examine the effect at Re=100 and Figures 5.2c and 5.2d at R=300.

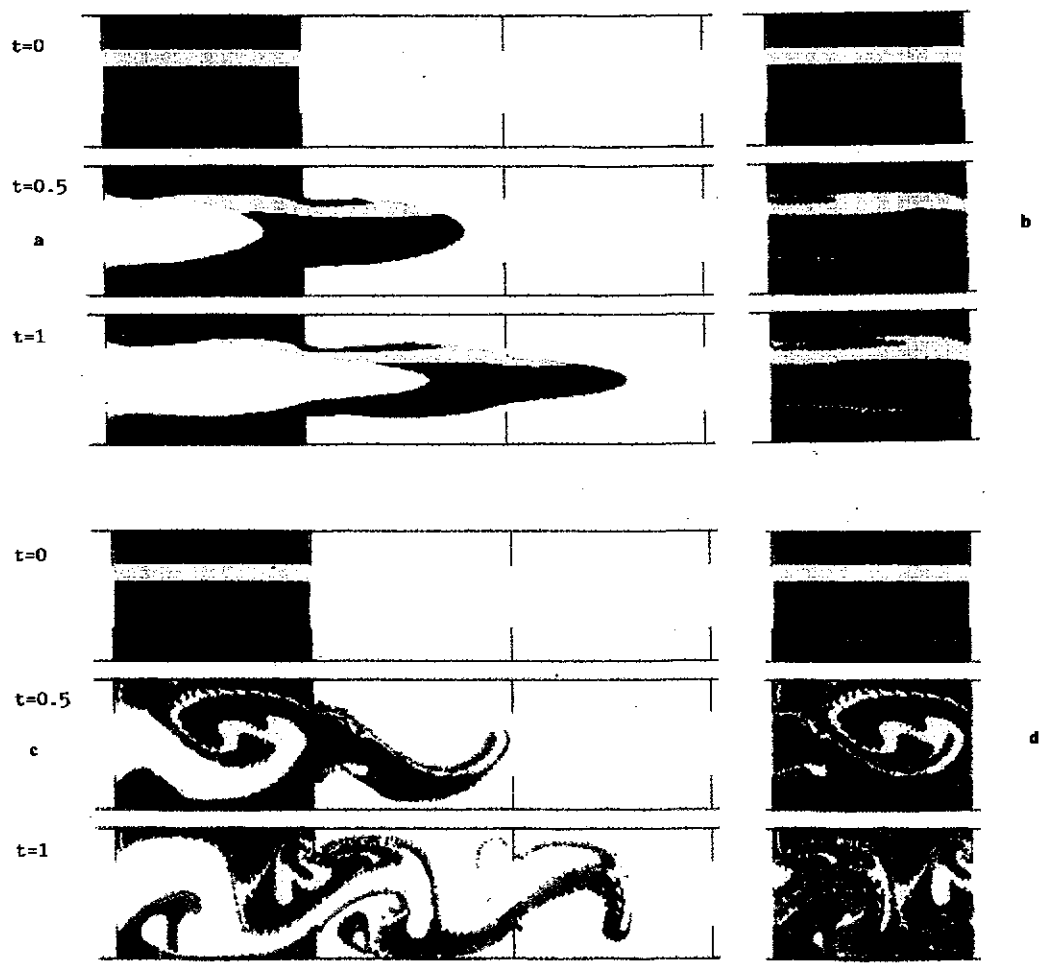

FIGURE 5.2 : *Results for baffled channel with no oscillatory flow : (a) and (b) net flow at Re_n = 100, and (c) and (d) net flow at Re_n = 300 (from Howes et al., 1991).*

That the baffles would induce mixing (and this an improvement in mass transfer) under conditions of laminar flow is clear from the figures but they also serve to highlight some of the potential drawbacks of baffled flow. While the bulk flow impinges on the central boundary layer regions, dead volumes are visible adjacent to the baffles.

These could give rise to fouling and might even result in sever concentration polarisation in these areas. However, the disturbance of the flow regions is clear as is the vortice shedding off the sharp edges of the baffles.

5.1.8 Energy Considerations

The main disadvantage of convection promoters in the flow path is the increased pressure drop. This will manifest itself in higher operating costs and decreased downstream operating pressures for a given flow, leading to lower driving forces for permeation rates and increased salt passage. However these effects may be offset to some extent by the ability to operate at lower flow rates, achieving similar performance but an increased water recovery.

The increased pressure drop caused by orifices alone in the line may be calculated as follows :

$$\Delta P = 2n_b \frac{u_b^2}{2} \rho$$

$$= n_b \left(C_c \frac{r^2}{r_b^2} u \right)^2 \rho \qquad (5.1)$$

where n_b = the number of baffles
C_c = the contraction coefficient specified for the orifice
u_b = the local linear velocity through the baffle aperture [m/s]
u = the open tube linear velocity [m/s]
r_b = the baffle aperture radius [m]
ρ = the fluid density [kg/m^3]

[Perry and Green (1986)]

Thomas and Watson (1968) quantified the increased energy requirements compared to the performance improvement. In the Reynolds number range 5 000 to 15 000, less pumping power was required to increase the mass-transfer coefficient by using a detached-spiral convection promoter than by increasing the turbulence by increasing the feed flow. They had previously shown that, at constant Reynolds number, a simple comparison of mass transfer coefficients based on pumping energy can be made using the expression :

$$\left[\frac{k_b}{k}\right] = \left[\frac{f_b}{f}\right]^n \tag{5.2}$$

where k = the mass transfer coefficient [m/s]
f = the Fanning friction factor
b = refers to the baffled condition

n was calculated from experimental results. They found that less pumping power was required to achieve the high mass-transfer coefficients using the baffles if n was greater than 0,28.

5.2 EQUIPMENT

The equipment differs from that discussed in Appendix B in that the baffles are included. The dimensions of the baffles are as follows :

Doughnut baffles	
Characteristic	**Dimension**
Aperture	7 mm
Outside diameter	12 mm
Thickness	2 mm
Angle	0 °

Elliptical Baffles	
Characteristic	**Dimension**
Aperture (horizontal)	7 mm
Aperture (vertical)	10 mm
Outside diameter (horizontal)	12 mm
Outside diameter (vertical)	17 mm
Thickness	2 mm
Angle	45 °

Overall geometry	
Characteristic	**Variable**
No. of baffles	9
$\frac{\Delta l}{d}$	4
Baffle spacing (center-to-center)	50 mm
Baffle holder diameter	1,6 mm
Spacer diameter	3 mm

Figures 5.3 and 5.4 are a pictorial representation of the baffles showing some of the main dimensions.

5.2.1 Elliptical Baffle Design

It was believed that the elliptical baffles should function better than the doughnut baffles for three reasons :

a) the baffles would still shed vortices at their edges;

b) the baffles would direct a fraction of the wall flow towards the centre of the tube and *vice versa*;

c) the shape of the baffles should induce scouring eddies as the flow is directed up to and then deflected away from the wall; and

d) the angled baffles should cause a lower pressure drop than the doughnut baffles.

The mass transfer coefficient caused by these baffles was to be compared to that for doughnut baffles to assess their effectiveness.

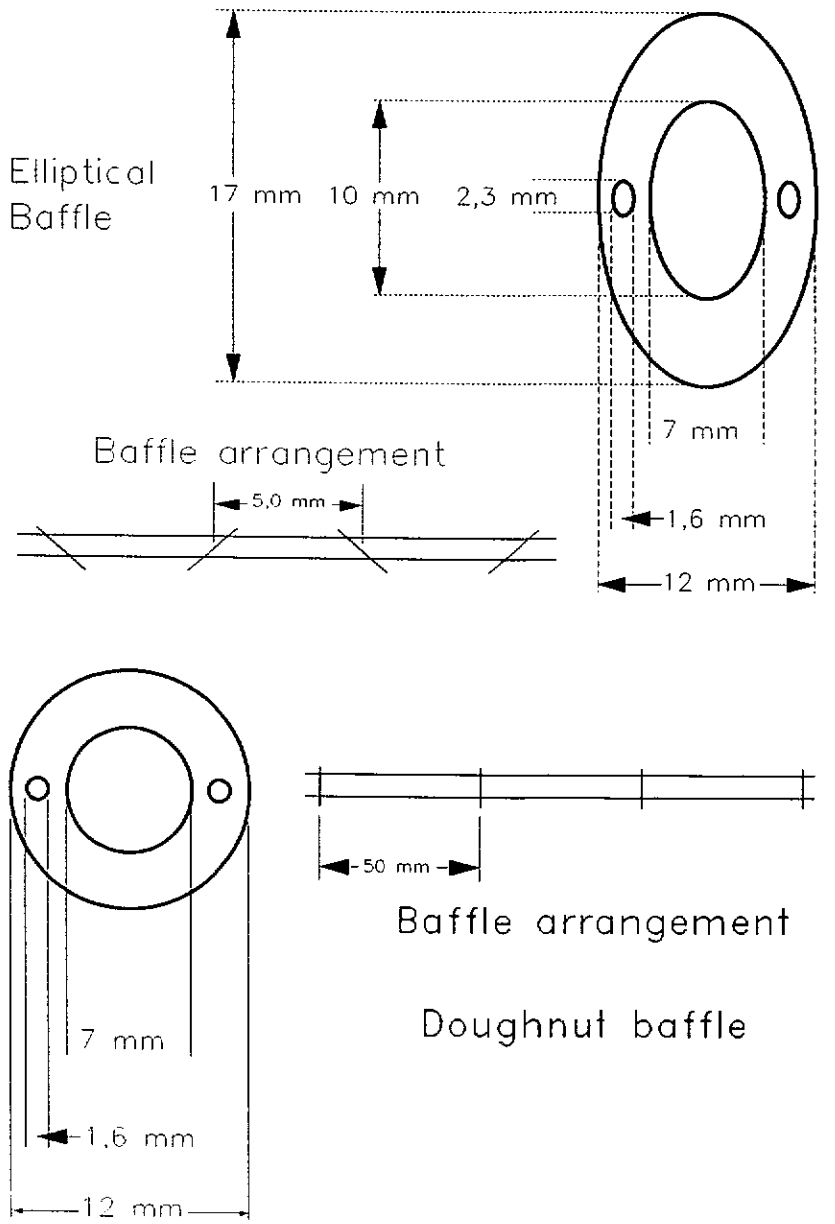

FIGURES 5.3 and 5.4 : *Diagrams of the elliptical and doughnut baffles, their geometries and arrangements.*

5.3 RESULTS AND DISCUSSION

A series of experiments, similar to the open TRO tests, were conducted with the elliptical and doughnut baffles on place. Values for A and $\left(\frac{D_{AM}}{K\delta}\right)$ were determined for all the baffled flow experiments (both steady and pulsed flow). The full set of results is presented in Appendix D.4.

Each mass transfer coefficient corresponds to four runs at four pressures (2, 3, 4 and 5 MPa) at a given feed flow rate, a temperature of 25 °C and a given feed concentration. A permeate flow and a salt passage were determined for each run. The details of the regression procedure used to determine the mass transfer coefficient are described in Appendix C. The reported gains in mass transfer coefficient represents the ratio of the baffled tube, steady flow coefficients to the open tube, steady flow coefficients.

Figure 5.5 shows the trend of increased mass transfer with pressure. The increase is smooth up till Reynolds number 3 222 which appears to be lower than the regressed curve would expect, indicating little theoretical basis for a power law fit. The value of the error in this region is of the order of 8 x 10^{-6} and 7 x 10^{-6} m/s for the elliptically baffled tube A and the doughnut baffled tube B respectively. (The error analysis is described in Appendix C).

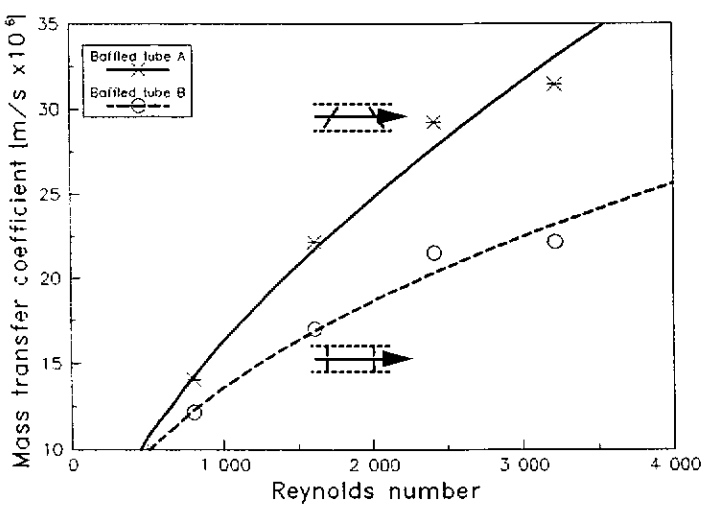

FIGURE 5.5 : *Variation in mass transfer coefficient with Reynolds number for the elliptical and doughnut baffles. The points represent the experimental data while the lines represent a least-squares power law fit. The temperature is 25 °C and the pressure range is 2 to 5 MPa.*

Consequently, the region of uncertainty for both sets of results overlaps. This may explain the discrepancy between the mass transfer coefficients for the two sets of baffles. One cannot therefore categorically conclude that the elliptical baffles perform better than the doughnut baffles.

The curve of gain in mass transfer coefficient as a function of Reynolds number (Figure 5.6) reveals that the gain appears to reach a maximum around Reynolds number of 3 000. This may be due to experimental error in the final result. The gain curve relies on two different experimental groups (*viz.* the open tube and baffled tube results) and a higher value of K for steady flow, open tube and a lower value of K for steady, baffled flow can cause the final gain to be lower than the real value. For this reason, the final value of the gain for elliptical baffles at a Reynolds number of 3 222 has been neglected from the trend regression for the trend line.

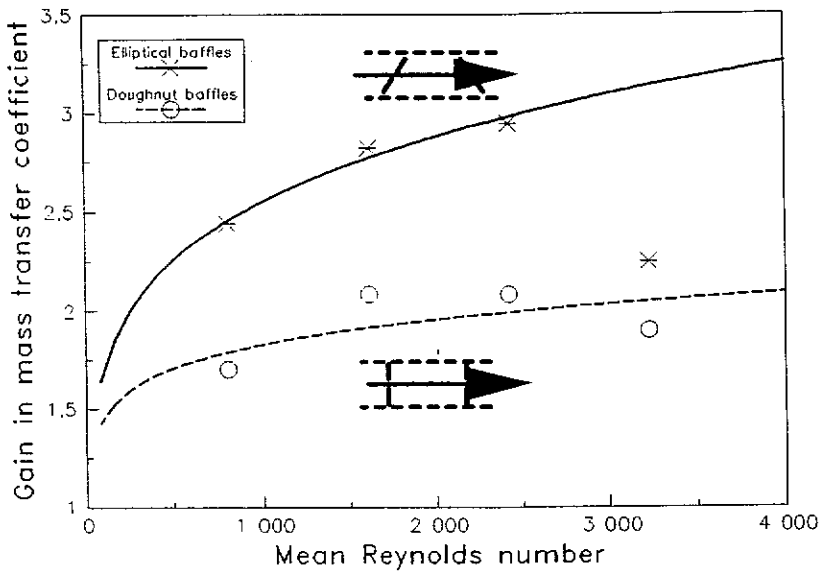

FIGURE 5.6 : *Gain in mass transfer coefficient as a function of Reynolds number at a temperature of 25 °C and a pressure range of 2 to 5 MPa.*

The suspected maximum around the Reynolds number of 3 000 possibly corresponds to the onset of turbulence (transition region :
2 000 < Reynolds number < 4 000. This would imply that the baffles are acting as turbulence promoters and convection promoters. The onset of turbulence

reduces the baffles' effectiveness as the natural convection of the fluid plays an increasingly important role. On the other hand, the gain in this region is still of the order of 200 %.

The high gain in mass transfer coefficient around the Reynolds number of 2 000 contradicts the findings of Pitera and Middleman (1973), who found maximum effectiveness at their lowest Reynolds numbers (10 to 1 500), but corresponds with their review of other baffled systems where the maximum effectiveness occurred for Reynolds numbers between 2 000 and 5 000.

5.4 CONCLUSIONS

Placing baffles in the flow path did increase the mass transfer in the TRO system. For the elliptical and doughnut baffles, gains in the mass transfer coefficient of up to 300 and 200 % respectively were recorded. However, this does not imply that the elliptical baffles necessarily perform better than the doughnut baffles because the error analysis (Appendix C) reveals that the difference in these gains is within the bounds of experimental error.

There appears to be maximum gain in mass transfer around the superficial Reynolds number value of 2 000 at which one would expect the onset of turbulence in the open tube experiments, indicating that the baffles are acting as turbulence promoters as well as convection promoters. The baffles cause gains of about 200 % for the open tube transition flow regime.

Chapter 6

PULSED BAFFLED FLOW IN TUBULAR REVERSE OSMOSIS

6.1 INTRODUCTION

Another technique for convection promotion is to pulse the flow through a baffled tube. In this Chapter, the performance of pulsed flow in a baffled TRO system is examined in terms of the film mass transfer. Both elliptical and doughnut baffles were assessed as convection promoters. The feed flow was pulsed over a range of frequencies and amplitudes.

6.2 PULSED BAFFLED FLOW IN VARIOUS APPLICATIONS

The following sections detail successful heat transfer and mass transfer coefficient enhancement through the use of pulsed baffled feed flow.

6.2.1 Pulsed Flow Through Furrowed RO Channels

Sobey (1980) mathematically modelled pulsed flow through the furrowed channels of the equipment of Bellhouse et al. (1973) which is described in Chapter 5.1.5. Flow patterns are modelled for the quasi-steady state regime using the Navier-Stokes equations of flow.

The results were divided into three main categories : low ratios of mean to high peak flows, comparable mean and peak flow, and mean flows with a low pulsed component.

A low mean flow and a large oscillatory component results in a small separated region forming in the upstream part of the depression. During the deceleration of the pulse, the region expands to fill the entire depression. As the bulk flow reverses, the vortex is ejected from the depression. (No description is given of the possible interaction of such ejected vortices which should also enhance fluid mixing).

For comparable mean and peak flows, large changes occur in the magnitude of the flow rate, but the flow will be unidirectional ($Pu \geq 1$). At the instant of minimum flow, the vortex fills the depression. As the flow accelerates, the vortex is ejected from the depression as the bulk fluid flow begins to displace it. A new vortex

begins to establish itself in the depression as the flow decelerates. However, if the flow just reverses ($Pu < 1$) , the flow structure is more complex. Apart from the main depression vortex, secondary vortices form at the depression entrance and exit when the reverse flow rate begins to decrease. The secondary vortices collapse as the fluid flow changes direction again.

Where small pulsations are superimposed on a large mean flow, the vortex will not be displaced from the depression. In this and the previous case (around $Pu = 1$), Sobey remarks that this is *...a region where the flow patterns make it impossible to decide a priori whether high or low convective mixing would be attained.*

The formation of the vortices, aided by the regular flow obstructions, should enhance fluid mixing considerably. Particularly important are the vortices which fill the depression region, replacing wall flow with centre-flow. This should alleviate concentration polarisation.

6.2.2 The Heat Transfer Analogy

Solutions to heat and mass transfer systems are considered analogous. They are linked under the title of *transport phenomena.* Mackley et al. (1990) examined heat transfer under four conditions : steady flow; steady baffled flow; pulsed flow; and pulsed, baffled flow. These four sets of experiments correspond to those undertaken in this investigation for TRO.

They used oil in a double pass heat exchanger. Except for a ratio of $\frac{\Delta l}{d} = \frac{3}{2}$ and a metal tube in place of a membrane, their equipment was similar to that used in this investigation.

They concluded that, for their experiments, pulsed flow alone offered little improvement over steady flow but that oscillatory flow in a baffled tube, depending on the pulse frequency, could increase the Nusselt number (related to the heat transfer coefficient) by 700 %. A number of photographs of the streamlines created by this flow were taken and are reproduced in Figures 6.1 and 6.2. The position of the baffles and support rod are visible in each photograph. The first set of photographs (Figure 6.1) represent the cases of steady flow and then increasing pulsing frequency for a given amplitude. The feed flow Reynolds number remains essentially constant. Stagnant regions are visible near the wall, particularly in the non-pulsing case.

The second set of photographs (Figure 6.2) represent the case of pulsing, but no net flow at different times in the oscillatory cycle. Here the eddies and their movement within the inter-baffle region are apparent. The eddy structure also appears time dependent.

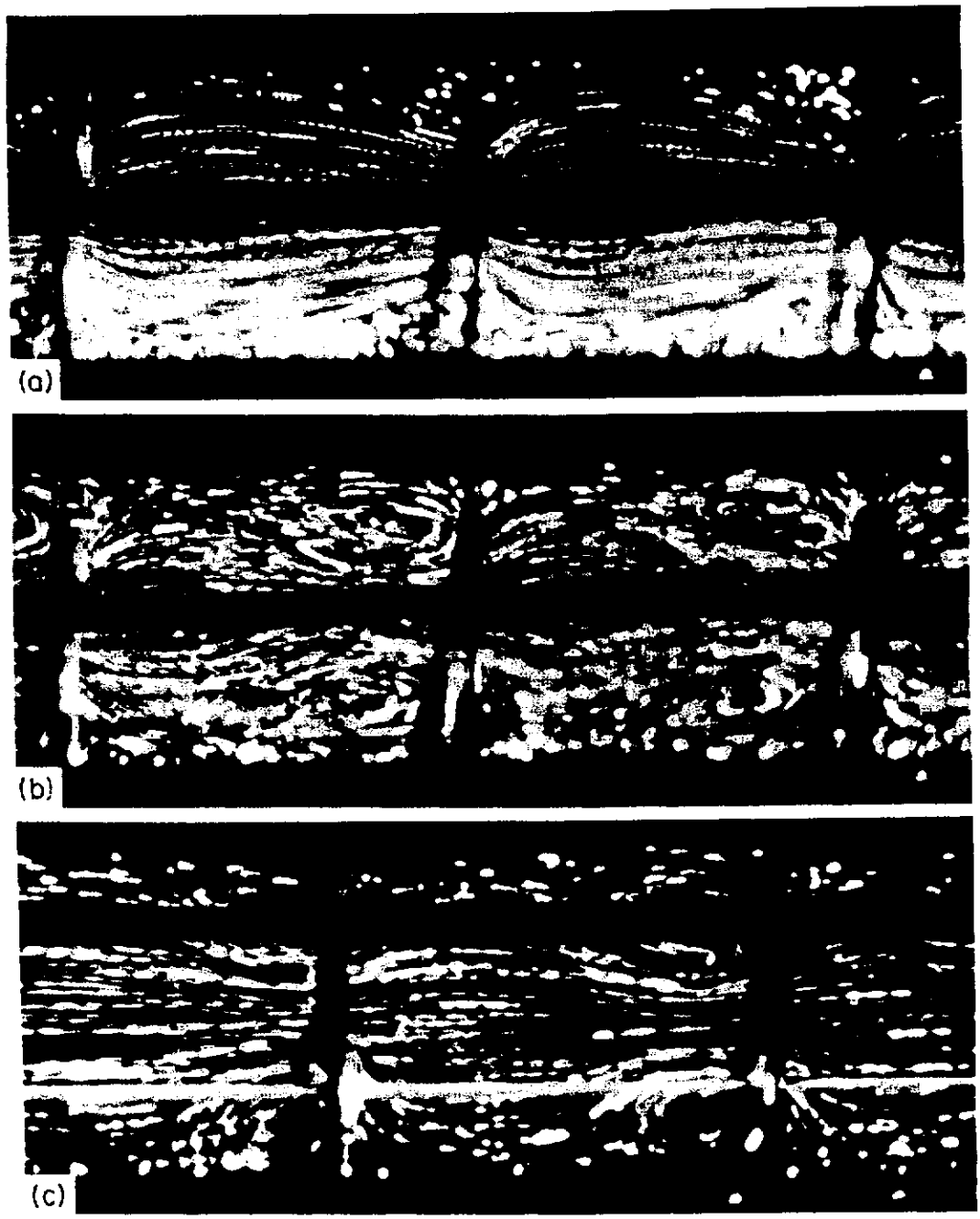

FIGURE 6.1 : *Flow visualisation photographs by Mackley et al. (1990) Reynolds numbers of bulk flow virtually constant.*
(a) No oscillation, (b) and (c) increasing oscillation

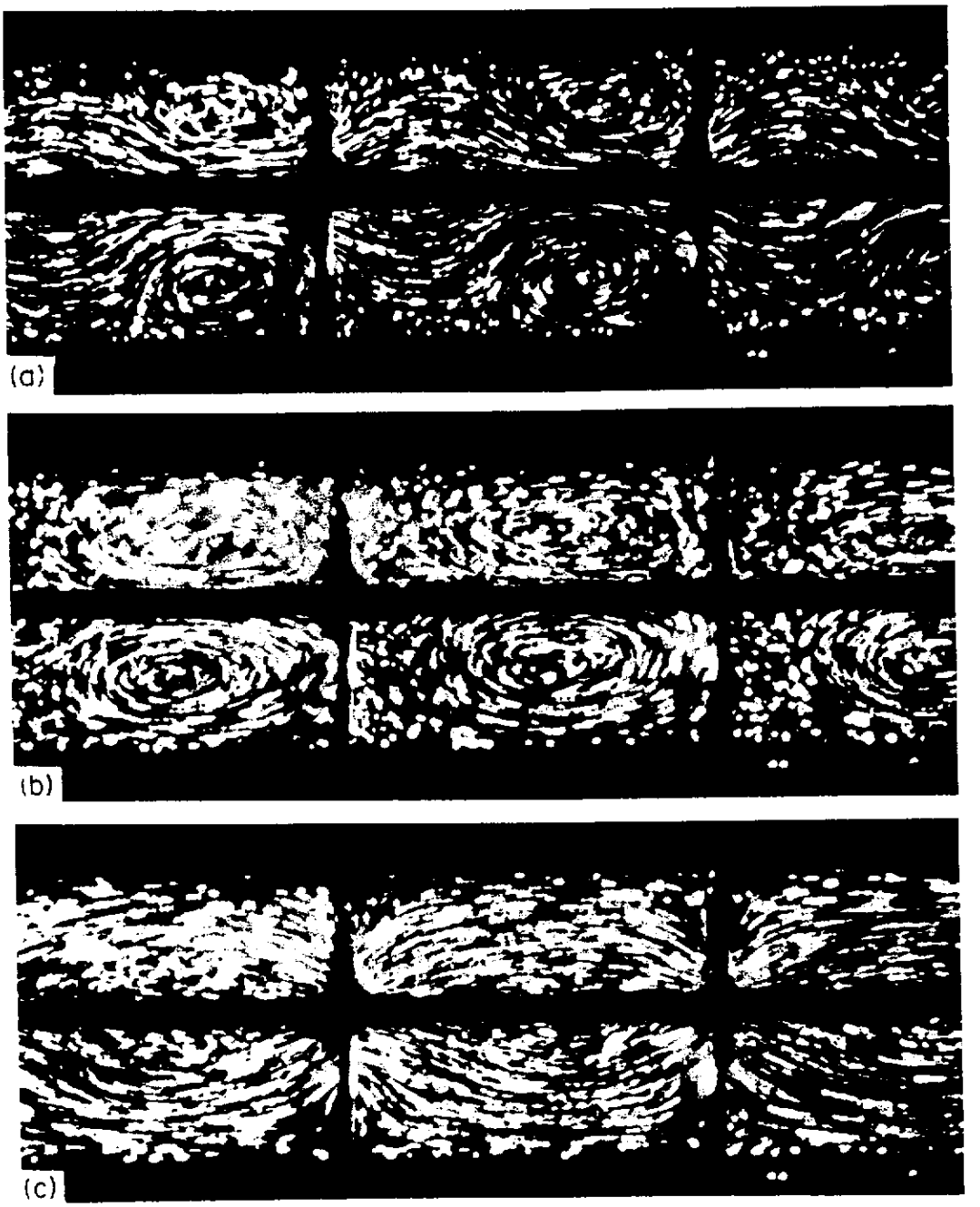

FIGURE 6.2 : *Flow visualisation photographs by Mackley et al (1990). No bulk flow. Photographs taken at different times in the oscillatory cycle*

From these experiments, Mackley et al. (1990) concluded that a reversing-oscillatory or pulsing flow superimposed on a net flow could result in a near plug-flow residence

time distribution with each inter-baffle region behaving as a continuously stirred tank. Under these conditions a significant change could be achieved in heat/mass transfer coefficients since uniform temperature/concentration should exist within each inter-baffle region.

Colman and Mitchell (1990) quantified these observations by injecting a saturated sodium chloride solution into the first baffle space of the channel. They then measured the conductivity of the solution in the baffle spaces down the tube. The residence time down the tube could be calculated and the axial dispersion thus quantified. They showed how the width and the shape of the sodium chloride pulse under conditions of pulsed flow could be observed intact over 30 baffle spacings down the tube, indicating a low axial dispersion. (During steady flow the pulse spread both forward and backward, indicating by-passing and separation). However, Mackley et al. had shown that the effectiveness of the plug-flow characteristic reached a maximum around amplitudes of half the baffle spacing.

6.2.3 Baffled Pulsed Ultrafiltration

Finnigan and Howell (1989, 1990) have applied the above techniques to examine the effects of pulsatile flow on ultrafiltration. They found that the permeate flow increased with pressure and that the incorporation of baffles increased the permeate flow by 71 to 121 % between the superficial Reynolds numbers 570 and 1 710. However, when pulsatile flow was used with the baffled system a further improvement in permeate flow of 18 to 58 % occurred at the higher pressures. This gave an overall improvement over the conventional system of 236 to 268 %.

Their pulse form appears to represent the first reported departure from the sinusoidal wave-form. They used a *sawtooth* pulse but no characterisation was available then. They also used both disk and doughnut-shaped baffles. The disk baffles under-performed relative to the doughnut-shaped baffles. Consequently, improvements reported here are for the doughnut baffles.

The investigation of Finnigan and Howell (1990) into the effects of frequency on water flux proved to be inconclusive at the higher Reynolds numbers (those greater than 1 000). Further, increases in amplitude appeared to be inconsequential. They explained their results in terms of the findings of Sobey who found that in the case of comparable mean and peak pulsed flows, the flow patterns do not indicate that better fluid mixing should necessarily occur.

Finnigan and Howell (1989) assessed increased flux against the increased energy consumption attributed to baffle friction loss and the pulsing pump. Baffled and baffled-pulsing systems gave better performance for the same power consumption than the conventional systems. The kinetic energy associated with the pulsations

varied between 0,9 and 9,8 % of the total power. However, the fact that the system could be run at low flow rates led to the conclusion that *...the power consumption of the baffled systems* is *in fact quite small when operated at these moderate velocities.*

6.2.4 Mass Transfer Considerations

In their investigation of mass transfer enhancement techniques for channelled RO systems Colman and Mitchell (1990) made physical measurements of mass transfer coefficients using an electrolytic solution and electrodes within the channel. Their paper was the only one that reported mass transfer coefficients for RO systems. They showed that mass transfer coefficients in baffled, pulsed RO systems with average superficial Reynolds numbers of 100 can be equivalent to open channel steady flow, Reynolds numbers greater than 10 000.

They found that increases in both the amplitude and the frequency enhanced the mass transfer coefficient.

6.2.5 Mathematical Modelling of Pulsed Baffled Flow

Howes et al. (1990) mathematically modelled a two-dimensional pulsed flow over a series of baffles. They reported their results using colour graphics to show particle tracking simulations which are shown in Figure 6.3.

Figures 6.3a and b, and 6.3c and d illustrate the effect of pulsing with no net flow in a baffled tube. The initial flow regimes, under conditions of low frequency, become symmetrically distributed around the centreline. Vortices are shed off the baffle edges and expand into and out of the interbaffle regions. The mixing effects are even more dramatic when the pulsing frequency is tripled (Figures 6.3c and d) but the application of a nett flow, at the same pulsing frequency, (Figures 6.3e and f) reveals that the net advection of particles appears to approach uniformity along the channel. A comparison of the latter four figures indicates that oscillatory flow fluid mixing has dominated over any net flow radial velocity profile. The dead spaces near the tube wall and baffle junction are minimised as particles from various flow regimes extend into the spaces.

In fact the model appears to have reached a resolution limit as species of colour are intimately mixed throughout the interbaffle region. The consequences of this intense mixing illustrated by these figures should be a dramatic reduction in concentration polarisation as wall flow is merely spatial. A rough indication of the degree of concentration polarisation might be obtained by the degree of persistence of a regime near the wall. However, the model does not account for the removal of this layer through the wall as in the case of reverse osmosis. At best, therefore, this model only serves to illustrate the fluid mixing effects that can be achieved with pulsed, baffled flow.

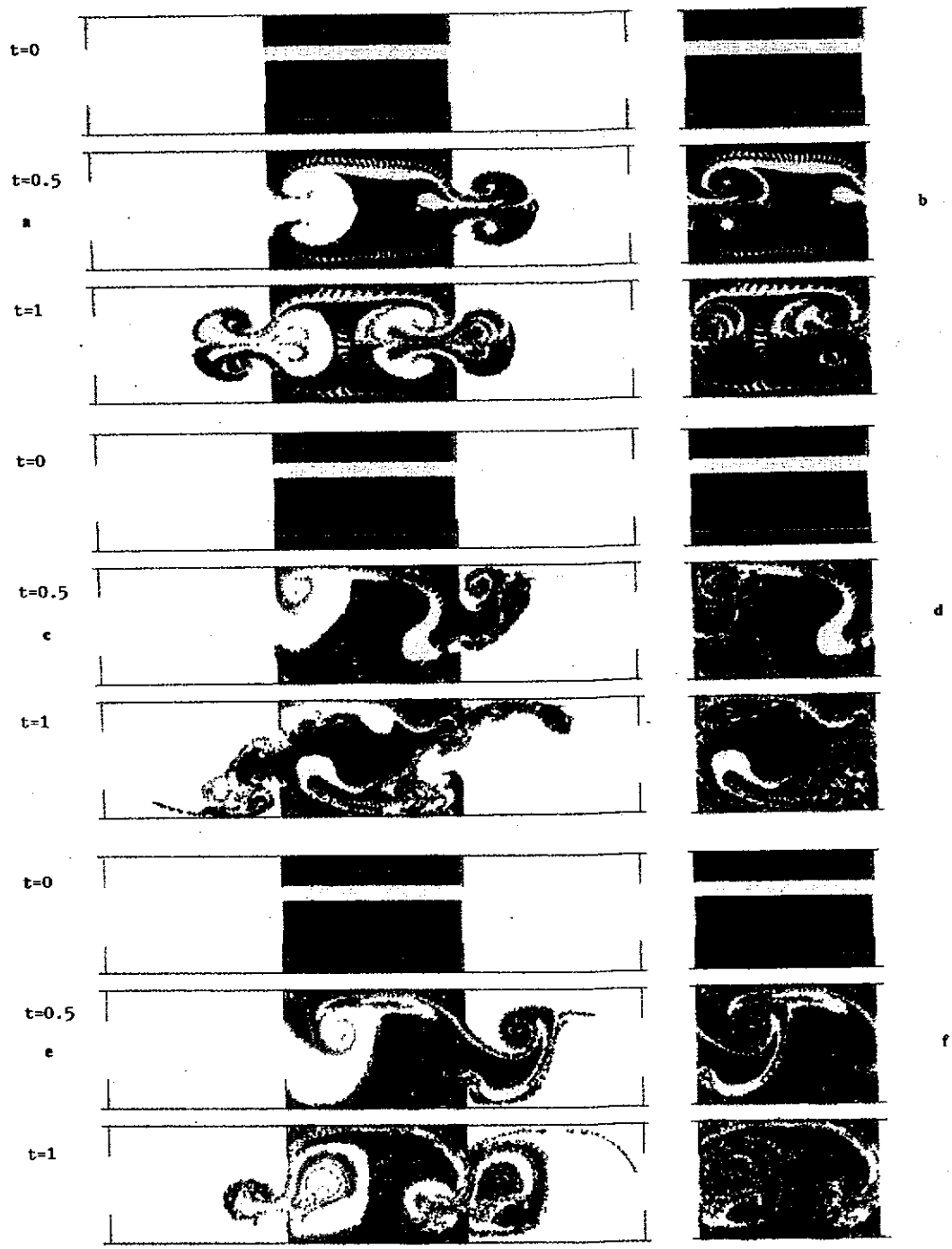

FIGURE 6.3 : *Results for oscillatory flows in a baffled channel: (a) and (b) oscillatory flow at Re_o = 300, St = 1,0 and (e) and (f) coupled net flow and oscillatory flow at Re_n = 300, St = 1,0. The Figures show a series of particle advection plots. The pictures show the position of an array of particles with each particle respresented by a coloured spot. Each figure consists of three pictures taken at successive times during the advection process. The first picture shows the starting position of the particles corresponding to t = 0, the second picture shows the position of the particles at t = 0,5 and the third at t = 1,0 (from Howes et al., 1991).*

6.3 EQUIPMENT

The equipment is no different from that discussed in Appendix B. It represents the collection of all the equipment used in the previous sections.

6.3.1 Elliptical Baffles

In addition to the elliptical baffles' proposed advantages over conventional orifice baffles (Chapter 5), the baffles should enhance the creation of vortices. Doughnut baffles rely solely on their sharp edges to create the vortices. Elliptical baffles should direct the oscillating flow to create counter-current fluid movements during the cycle.

6.4 RESULTS AND DISCUSSION

A series of experiments were conducted at four frequencies and four amplitudes for pulsed baffled TRO. The baffled tube values of A and $\left(\frac{D_{AM}}{Kb}\right)$ were used in these (Chapter 6) calculations. The full set of results is presented in Appendix D.5 and D.6.

Each mass transfer coefficient corresponds to one run at 4 MPa, a given average Reynolds number, a temperature of 25 °C and a given feed sodium nitrate concentration. The permeate flow and a salt passage were determined experimentally for each. The details of the regression used to determine the mass transfer coefficient from all the above values (using the Sourirajan theory, Eqns 2.1 to 2.4) is described in Appendix C.

Zero frequency represents the **open** tube, steady flow. The gains in mass transfer coefficient are the ratios of the pulsed baffled coefficients to the steady flow, open tube coefficients at the corresponding average, superficial Reynolds numbers.

6.4.1 Frequency Variation

Figures 6.4 and 6.5 show the variation in mass transfer coefficient with increasing frequency for pulsed baffled TRO, for elliptical and doughnut baffles respectively.

As with the discussion of the previous results (Chapters 4 and 5) for mass transfer enhancement, these should be prefixed by the caution that the mass transfer coefficients were in a range where they underwent large changes for small performance improvements : the so-called *narrow range effect*. However, the error in this group of experiments was not of the same magnitude as the open tube pulsing experiments (73 and 55 % for the elliptical and doughnut baffles respectively here).

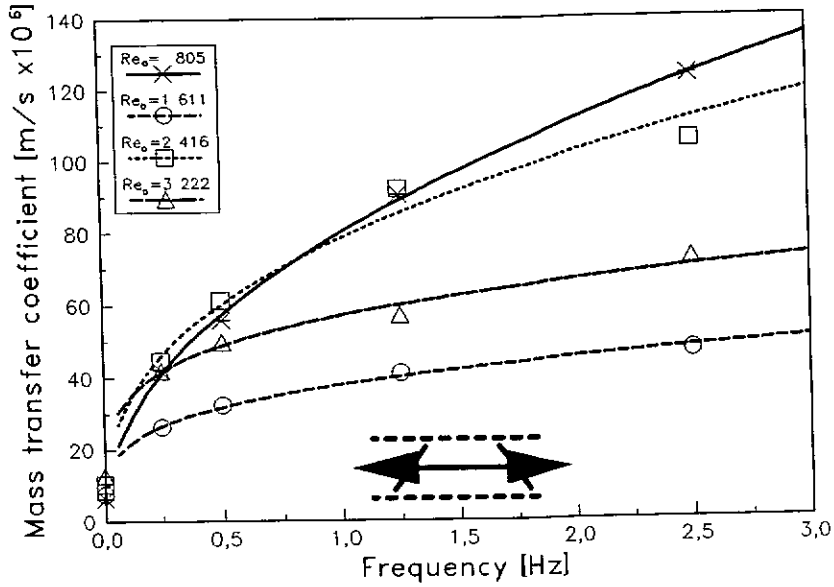

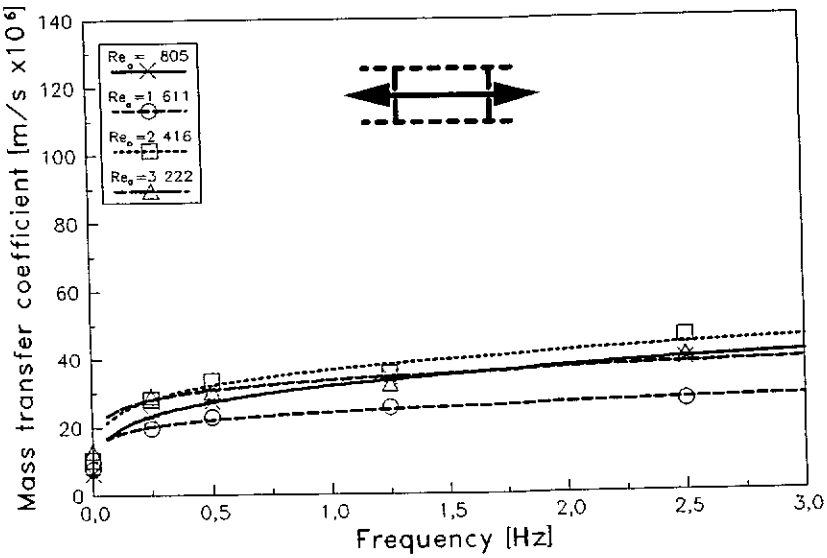

FIGURES 6.4 and 6.5 : *Variation in mass transfer coefficients as a function of frequency for different flow rates at a pressure of 4 MPa and a temperature of 25 °C. Elliptical and doughnut baffles respectively.*

Consistent in both sets of data is the unexpectedly low coefficients for the runs at $Re_o = 1\ 611$. While this might be expected as a result of the effect predicted by Sobey (1980) and observed by Finnigan and Howell (1989, 1990), i.e. unpredictable flow patterns for similar peak and mean velocities, the peak flow in these experiments is well above the mean steady flow. This aberration is probably a result of experimental error. An error analysis (Appendix C) shows that, for each feed flow,

the largest calculated mass transfer coefficient could fall below the lowest value negating the unexpected trend with flow rate. The trend of increasing mass transfer with increasing flow rate was expected.

The error bars on the data for the elliptically baffled tube would overlap those for the doughnut baffles. However, comparing the values for corresponding flows, those of the elliptical baffles are consistently higher.

The discussion of the above paragraphs is confirmed by Figures 6.6 and 6.7. The erratic trend with flow rate is again visible. The large gains due to the elliptical baffles (from about 500 to 2 000 %) far outweigh those of the doughnut baffles which barely attain 500 %. Again it should be mentioned that these gains are, somewhat academic when one considers the marginal real gains in performance (i.e. improvements in permeate flows and quality).

6.4.2 Amplitude Variation

Similar remarks can be made about the trends in mass transfer with amplitude (Figures 6.8 and 6.9) to those made for frequency variation. However, the apparent decrease at high amplitudes (in Figure 6.8) and low increase at low amplitudes (for Figure 6.9) with increasing amplitude corresponds with the findings of Mackley et al. (1990). The results indicate that there is little or nothing to gain from increasing the amplitude past a limiting value. It is not clear what the limiting value is for the doughnut baffles, but would appear to be in the region of 80 mm for the elliptical baffles. Mackley et al. (1990) suggested that the optimum amplitude would correspond to half the baffle spacing (to create a continuously stirred cell). A spacing of 80 mm would correspond to just over the maximum baffle-to-baffle distance for the elliptical baffles. Further investigations in this region would be required to draw any firm conclusion from about the significance of the baffle spacing and amplitude relationship. It is possible, though, that the angle of the elliptical baffle creates additional scope for mixing at higher amplitudes.

The *stirred cell* theory could explain the difference between the frequency and amplitude trends. If the amplitude is too large, it might create axial dispersion, akin to that of once-through flow in adjacent baffle spaces. This would lead to poor fluid mixing and low mass transfer. At the optimum amplitude, the effect of increasing the frequency would be to stir the inter-baffle volumes more vigourously, leading to improved mixing and mass transfer.

The variation in mass transfer with amplitude (Figures 6.10 and 6.11) reinforce the above remarks. The gains for the elliptical baffles are as much as three times those for the doughnut baffles. In this instance, this may be due to the increased scope for amplitude extension allowed by their geometry.

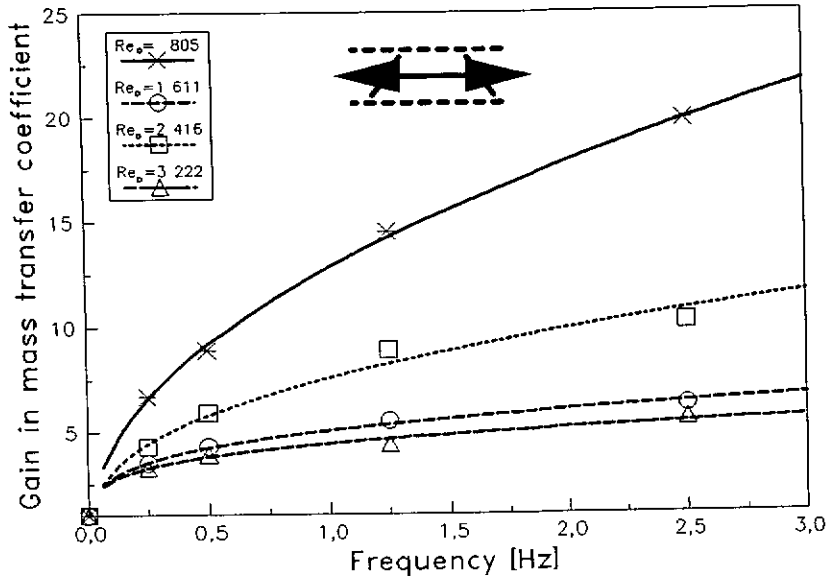

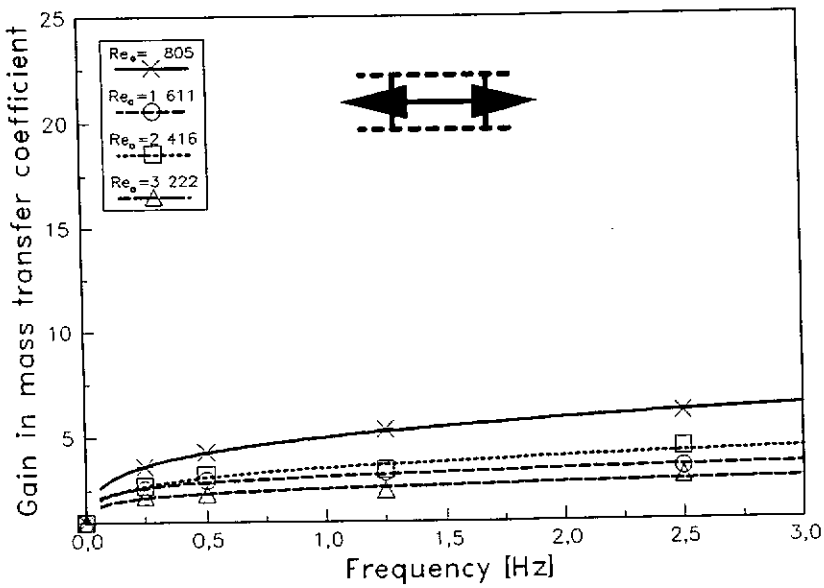

FIGURES 6.6 and 6.7 : *Gain in mass transfer coefficient as a function of frequency for pulsed baffled flow at a pressure of 4 MPa and a temperature of 25 °C. Elliptical and doughnut baffles respectively.*

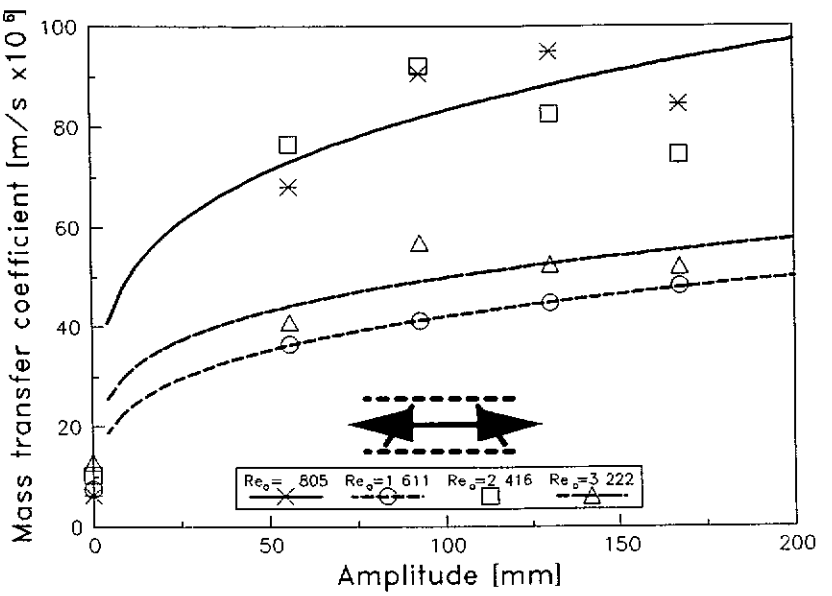

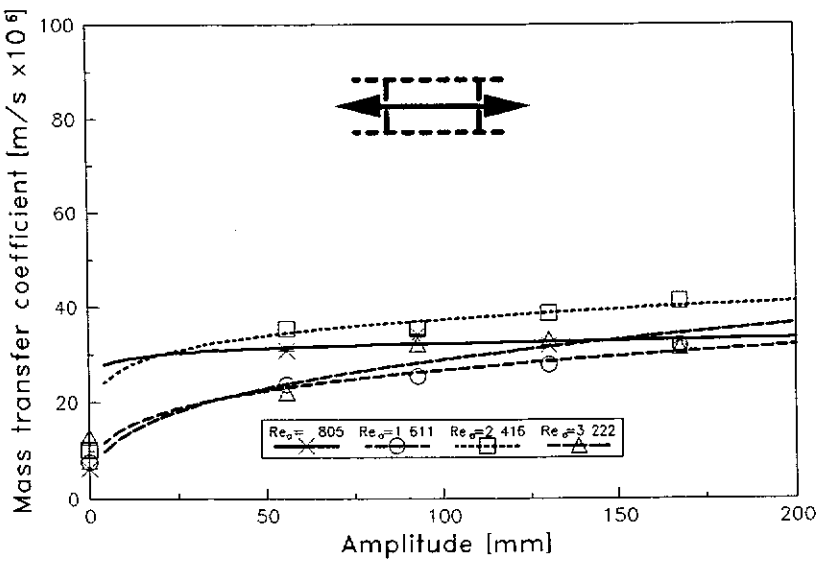

FIGURES 6.8 and 6.9 : *Variation in mass transfer coefficient with amplitude for different flow rates. Data at a pressure of 4 MPa and a temperature of 25 °C. Elliptical and doughnut baffles respectively.*

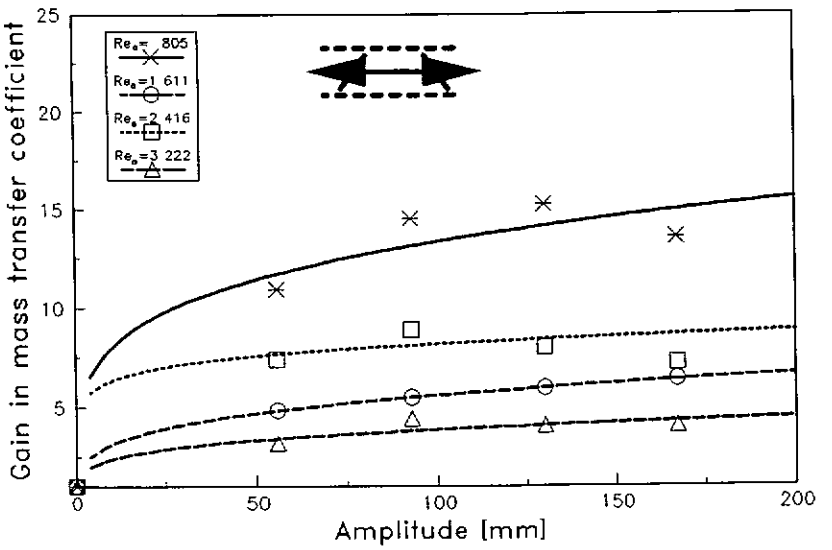

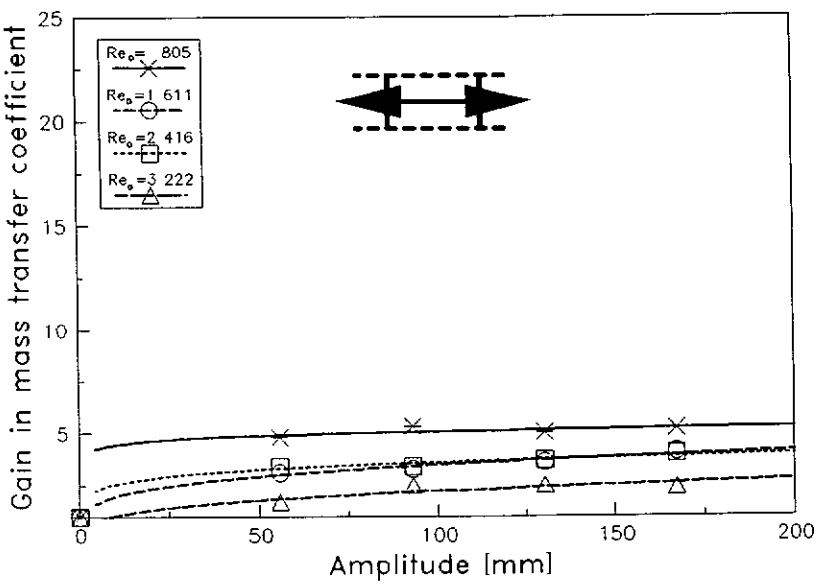

FIGURES 6.10 and 6.11 : *Gains in mass transfer coefficient as a function of amplitude for pulsed baffled flow. Data at a pressure of 4 MPa and a temperature of 25 °C. Elliptical and doughnut baffles respectively.*

6.5 CONCLUSIONS

For corresponding flow conditions the elliptical baffles return higher mass transfer coefficients than the doughnut baffles (Appendix C). This effect may be due to the error associated with measurement of the permeate flow and salt passage. Hence,

the conclusion that the elliptical baffles perform better under similar conditions does not necessarily hold. These differences in mass transfer coefficient lie within the range of the experimental error.

The graph of mass transfer as a function of frequency indicates some unexpected results. The expected mutual increase in mass transfer and flow rate turns out to be erratic. This can be explained in terms of the experimental error for the doughnut baffles but not for the elliptical baffles. It was concluded that this was a function of the indeterminate flow patterns established in this regime.

The mass transfer with amplitude trends are similar for the elliptical and doughnut baffles. There appears to be an amplitude value beyond which no improvement in mass transfer occurs. This corresponds with the findings of Mackley et al. (1990). Further investigation into the exact value of this amplitude will provide more concrete conclusions as to the implications of this phenomenon, for the elliptical baffle design in particular.

Chapter 7

CONCLUSIONS

The conclusions drawn in this Chapter are a summary of those for Chapters 3, 4, 5 and 6 and those of Appendix C. Further deductions are drawn from a comparison of all the methods attempted for film mass transfer enhancement for tubular reverse osmosis systems. All results are discussed in terms of the mass transfer coefficient for each feed flow.

7.1 THE SIGNIFICANCE OF THE MEMBRANE PARAMETERS

The error analysis is reported in Appendix C. The values of the pure water permeability parameters, A, differ for the two tubes used in the experiments but remain practically constant (a maximum difference of 2 % was calculated) for the open and baffled tube experiments. Tube A was calculated to have a higher pure water permeability than tube B. This finding corresponded with the experimental results which showed higher permeate flows for tube A.

The values of the solute transport parameters, $\left(\frac{D_{AM}}{K\delta}\right)$, showed that tube A should have had a higher solute passage than tube B. This corresponded with the experimental findings. The values of this parameter increased (for both tubes) after the insertion of the baffles into the tubes, indicating that the insertion may have caused some damage to the membranes. Future work done in this field might well benefit from using the modelling technique alongside the experimental work to determine such potential damage immediately.

7.2 THE SIGNIFICANCE OF THE MASS TRANSFER COEFFICIENT

The mass transfer coefficient was calculated for each feed flow condition. Since the value of this coefficient is dependant only on the hydrodynamic conditions in the tube, it facilitated comparison of the effectiveness of each of the techniques used to alter the flow patterns within the tubes. A higher k value implied better fluid mixing within the tube and hence reduced concentration polarisation. This lead to enhanced TRO performance in terms of decreased salt passages and increased permeate flows.

The degree to which the salt passages decreased and the permeate flows increased with increased mass transfer coefficients differed according to magnitude of A and $\left(\frac{D_{AM}}{K\delta}\right)$ for each of the tubes. The mass transfer coefficient was shown to be relatively insensitive to permeate flow. Thus, an error analysis conducted on the mass transfer coefficient (using its variation with salt passage as a basis) revealed that the magnitude of the error in k varied according to the nature of the feed flow : the maximum error range (for a statistical 90 % significance) for the steady flow experiments (baffled and open tube) was 36 to 34 % while the error range for the pulsed flow experiments (baffled and open tube) was 55 to 125 %.

The error analysis implied that the magnitude of the mass transfer coefficient became less significant as its value increased, leading to progressively smaller decreases in salt passage for larger increases in k at its higher values. In other words, the improvement in the feed mixing for the water-sodium nitrate system caused by pulsing the feed flow became less significant as the intensity of the mixing increased. To minimise this error, the concentration polarisation at the tube wall would need to be greater than that experienced for this system. The feed solution should have a higher viscosity, the solute concentration should be higher, the feed flow Reynolds numbers should be lower and the system pressures should be greater than those investigated.

The results of the error analysis posed a problem for the explanation of the findings. Since the aim of the work was to compare the effectiveness of different techniques for enhancing mass transfer in TRO systems, it was necessary that the results associated with a particular technique indicate a categorical improvement compared to another (i.e. pulsing the feed flow in an open tube should improve the mass transfer in the tube, compared to that for open tube, steady flow, to the extent that the possible values of the mass transfer coefficients for the pulsed flow are consistently higher than the steady flow values for the same mean feed flow Reynolds numbers). The magnitude of the error in k dictates the magnitude of the range of the possible k values.

In most instances comparisons of relative performance for variations in the application of a technique (e.g. comparing the performance of one pulsing amplitude with another for the same feed flow in an open tube) became impossible if the implications of the error analysis had been strictly applied. In such instances the conclusions drawn were based on broad trends but should be considered in the light of the error analysis argument.

7.3 OPEN TUBE STEADY FLOW TUBULAR REVERSE OSMOSIS

The results of the open tube, steady flow TRO experiments were used as a set of mass transfer coefficients against which those for the other enhancement techniques could be compared. The results are reported in full in Appendix D.1 and discussed in Chapter 3. The values of k were used to predict salt passages and the permeate flows and good agreement with the experimental values was shown. The value of k increased exponentially with flow rate in the experimental range of feed flows. The values of k in the two tubes for the same feed flows showed little disagreement indicating similar hydrodynamic conditions in the tubes. The results indicated that k provided a convenient measurement of TRO performance since the difference in values of salt passage and permeate flow for each of the tubes for the same feed conditions (as a result of their different membrane parameters, A and $\left(\frac{D_{AM}}{K\delta}\right)$) became inconsequential.

7.4 PULSED FLOW OPEN TUBULAR REVERSE OSMOSIS

The results of this set of experiments are shown in Appendices D.2 and D.3 and are discussed in Chapter 4.

Pulsing the feed to a TRO membrane lead to gains in the mass transfer coefficient of up to 800 %. Increasing both the frequency and amplitude of the pulse lead to increases in the mass transfer coefficient.

A theory (based on an exponential relationship of mass transfer coefficient with the absolute value of the linear feed flow) under-predicted the gains in mass transfer coefficient for pulsed flow. This was attributed to the fact that the theory neglects the effects of natural convection and the mixing effects of eddies generated by the rapid acceleration at the beginning and ends of each of the pulse cycles.

Apparent differences in the hydrodynamic conditions in tubes A and B (on the basis of mass transfer coefficient) for the same feed conditions could be ascribed to experimental error. As stated previously, it would be useful during any future work of this nature to use the model concurrently with the experiments to update the fundamental membrane coeficients and parameters.

7.5 STEADY FLOW IN BAFFLED TUBULAR REVERSE OSMOSIS

The results of this set of experiments are detailed in Appendix D.4 and discussed in Chapter 5. The gains in mass transfer coefficient for the elliptical baffles are higher than those for the doughnut baffles (but this may be due to experimental error). The gains are highest at the lowest flow rates.

7.6 PULSED FLOW IN BAFFLED TUBULAR REVERSE OSMOSIS

The results of this set of experiments are detailed in Appendices D.5 and D.6 and are discussed in Chapter 6. The elliptical baffles appear to perform better than the doughnut baffles for the same feed conditions but this may be a result of experimental error. Increasing the frequency of the pulse increased the mass transfer coefficients but his was not necessarily so for increasing amplitude. This might correspond with the findings of Mackley et al. (1990) who stated that there would be no improvement for amplitudes greater than half the baffle spacing. Further experiments for amplitudes in this region (with systems with lower error characteristics) would be required to confirm this finding.

7.7 COMPARISON OF THE EFFECTIVENESS OF THE THREE TECHNIQUES FOR MASS TRANSFER ENHANCEMENT IN TUBULAR REVERSE OSMOSIS

On the basis of the gains in mass transfer coefficient over open tube, steady flow TRO, the effectiveness of the enhancement techniques may be rated as follows : pulsed, baffled TRO was most effective, followed by pulsed flow, open TRO and then steady flow baffled TRO. All techniques were effective but the gains for both pulsed flow techniques were markedly higher than for the steady baffled flow experiments.

NOMENCLATURE

A	pure water permeabilty constant [kg-mol H_2O/m^2.s.Pa]
a	mean to peak amplitude of oscillation in the tube [m]
C	solute concentration [g/ℓ]
c	molar density of the solution [kg-mol/m^3]
d	diameter [mm]
$\frac{D_{AM}}{Kb}$	solute transport parameter [m/s]
f	frequency [Hz]
f	Fanning friction factor
h	Sobey's (1980) expression for the channel depth in a Bellhouse oxygenator [m]
K	constant
k	mass transfer coefficient [m/s]
$\frac{\Delta l}{d}$	ratio of interbaffle spacing to tube diameter
M	molecular mass
N	flow through the membrane [k-mol/m^2s]
n	a number of objects (e.g. number of baffles)
PWP	pure water permeation rate through a given membrane area [kg/s]
P	operating pressure [Pa]
Pu	Pulsing number $\left(\frac{fa}{\bar{u}}\right)$
R	universal gas constant [Pa m^3/g-mol K]

r	radius [mm]
Re	Reynolds number ($\frac{\rho u d}{\mu}$)
S	operational membrane area [m^2]
or	standard polpulation variance
s	distance of a particle from the the tube inlet [m]
T	temperature [K]
T	period [s]
t	time [s]
$t_{0.05}$	90 % statistical certainty factor
t^*	time since beginning of each cycle [s]
u	velocity [m/s]
$V^*\overline{A}$	molar volme of pure solute [g-mol/m^3]
V_3	volume of permeate [m^3]
X	mole fraction
Z	gain ratio

Greek Symbols

μ	viscosity [Pa s]
π	osmotic pressure [Pa]
ρ	density [m^3/s]
τ	period of a cycle [s]
ω	frequency of oscillation [rad/s]

Subscripts and Superscripts

A	refers to the solute (in this case $NaNO_3$)
B	refers to the solvent (in this case H_2O)
b	refers to the baffled condition
c	critical condition (normally critical frequency)
e	enhanced (baffled, pulsed or both) fluid mixing condition
n	exponent defined by the situation
o	average or corresponding open tube condition
p	refers to the pulsed condition
1	refers to the condition at the center of the tube
2	refers to the condition adjacent to the tube wall
3	refers the condition of the permeate
$-$	average or mean

REFERENCES

Alani, S. (1992), Research and Development Manager, Biwater, Heywood, Lancs., Great Britain. Private Communication.

Alston, D.L. (1990), Electronics Consultant, Dept of Chemical Engineering, University of Natal. Private Communication.

Baird, M.H.I., Duncan, G.J., Smith, J.I. and Taylor, J. (1966). *Chem Eng Sci*, **21** p. 197.

Bauser, H., Chimiel, H., Stroh, N. and Walitza, E. (1986). *J Membrane Sci*, **27**, pp. 195-202.

Bellhouse, B.J., Bellhouse, F.H., Curl, C.M., MacMillan, T.I., Gunning, A.J., Spratt, E.H., MacMurray, S.B. and Nelems, J.M. (1973). *Trans Amer Soc Artif Int Organs*, **19**, pp. 77-79.

Brouckaert, C.J. (1991), Researcher, Department of Chemical Engineering, University of Natal, Durban. Private Communication.

Colman, D.A. and Mitchell W.S. (1990). *I. Chem. E. Symposium Series No. 118*, pp. 9.1-9.15, ISBN 0 85295 253 8.

Finnigan, S.M. and Howell, J.A. (1989). *Chem Eng Res Des*, **67**, pp. 278-282.

Finnigan, S.M. sand Howell, J.A. (1990). *Desalination*, **79**, pp. 181-202.

Gupta, B.B., Blanpain, P. and Jaffrin, M.Y. (1992). *J. Membrane Science*, **70**, pp. 257-266.

Hadingham, P.T. and Buhr, H.O. (1970). **Simulation of the Heart and Arterial Blood Flow**, First National Meeting of the South African Institution of Chemical Engineers, Durban.

Herrmann, Cal. C. (1982). *Desalination*. **42**, pp. 329-338.

Howes, T., Mackley, M.R. and Roberts, E.P.L. (1991). *Chem Engng Sci*, **46**(7), pp. 1669-1677.

Ilias, S. and Govind, R. (1990). *Sep Sci and Tech*, **25**(13-15), pp. 1307-1324.

Keil, R.H. and Baird, M.H.I. (1971). *Ind Eng Chem Process Des Dev*, **10**, p. 473.

Kennedy, T.J., Merson, R.L. and McCoy, B.J. (1974). *Chem Engng Sci*, **29**, pp. 1927-1931.

Lora, J. and Arnal, J.M. (1990). *Desalination*, **79**, pp. 261-269.

Mackley, M.R., Tweddle, G.M. and Wyatt, I.D. (1990). *Chem Engng Sci*, **45**(5), pp. 1237-1242.

Muldowney, G.P. and Punzi, V.L. (1988). *Ind. Eng. Chem. Process Res. Des.*, **27**, p. 2341.

Pitera, E.W. and Middleman, S. (1973). *Ind Eng Chem Process Des Dev*, **12**(1), p. 52.

Rautenbach, R. and Albrecht, R. (1989). **Membrane Processes**, Chichester : John Wiley and Sons.

Rudisill, E.N. and Levan, M.D. (1990). *Chem Eng Sci*, **45**(9), pp, 2991-2994.

Shen, J.J.S. and Probstein, R.F. (1979). *Ind Eng Chem Process Des Dev*, **18**(3), p. 547.

Sinha, D. and Douthart, Bob. (1991). *Ultrapure Water*, **8**(5), pp. 30-36.

Smith, F.T. (1976). *Quart J Mech Appl Math*, **29**, pp. 343-364.

Sobey, I.J. (1980). *J Fluid Mech*, **96**(1), pp. 1-26.

Sourirajan, S. and Matsuura, T. (1985). **Reverse Osmosis/Ultrafiltration Process Principles**, Ottawa : National Research Council, Canada.

Sourirajan, S. and Matsuura, T. (1986). *Encyclopedia of Fluid Mechanics*, pp. 1029-1143, Gulf Publishing Co.

Thomas, D.G. and Watson, J.S. (1968). *Ind Eng Chem Process Des Dev*, 7(3), pp. 397-401.

Weissman, M.H. and Mockros, L.F. (1968). *J Eng. Mech Div Amer Soc Civ Eng*, **94**, p. 857.

Appendix A
PERFORMANCE VARIABLES

Salt passage (%)

can be calculated by :

$$\frac{C_3}{C_1} \times 100$$

where

C_3 = permeate solute concentration, [g/ℓ]
C_1 = feed solute concentration [g/ℓ]

Retention (%)

can be calculated by :

$$1 - \frac{C_3}{C_1} \times 100$$

where

C_3 = permeate solute concentration, [g/ℓ]
C_1 = feed solute concentration [g/ℓ]

Permeate flow

can be calculated by :

$$\frac{V_3}{S\,t}$$

where

V_3 = the volume of permeate, [ℓ]
S = the operational membrane area, [m^2]
t = the elapsed time, [d]

Osmotic pressure

for an ideally dilute solution is defined by :

$$\pi = \frac{RT}{\overline{V}^{\bullet}_A} X_B$$

(*van't Hoff's law*)

$$\approx c_B R T$$

where

$\overline{V}^{\bullet}_A$ = the molar volume of pure A [g-mol/ℓ]
T = absolute temperature [K]
X_B = the mole fraction of B
c_B = the molar concentration of B
R = the universal gas constant [..]

Gain in k can be calculated by :

$$Z = \frac{k_e}{k_o}$$

where

k_e = the enhanced mass transfer coefficient [m/s]

k_o = the open tube, steady flow mass transfer coefficient at the corresponding feed flow rate [m/s]

Appendix B

EXPERIMENTAL PROCEDURE

B.1 MEMBRANE STORAGE AND SELECTION

The tubular membranes were obtained from **MEMBRATEK** as 12,5 mm diameter cellulose acetate reverse osmosis membranes. They were stored under glycerol with formaldehyde as the preservative at a pH just above 5.

The membranes had all been manufactured in the same batch and then cut in half and trimmed to lengths of 500mm. They had been marked to identify which ends had formed the *tops* and the *bottoms* of the original tubular membranes. This was necessary to select matched pairs of membranes to be used in the experiments. Previous experimental work (Pitera and Middleman, 1973) had shown significant differences in the behaviour of membrane pairs. It was suspected that this might have been caused by variance in the manufacturing process.

The membranes were washed at low pressure and high flows to remove traces of the glycerol and formaldehyde. The feed water was changed regularly and the conductivity of the retentate was monitored. RO permeate water was used as feed water for all the experiments.

Sections of the tubular membranes that had undergone similar manufacturing conditions were cut to lengths of 0,5 m and inserted in the membranes holders. The holders were stainless steel tubes of diameter 13 mm, with four sets of regularly spaced drainage holes. (Details of the rest of the equipment follows in the next section).

B.1.1 High-flow Pre-testing

B.1.1.1 Apparatus

TABLE B.1	
Device	**Specifications**
Positive displacement pumps	Two Hydracell D10 operating in parallel
Accumulator	1 m of stainless steel 0,05 m diameter pipe charged with air @ 0,1 MPa
Back-pressure valve	Carp 13 mm needle valve
Rotameter	Krohne G51.14
Pressure gauge	Wika Pneumatic : 0 to 10 MPa range
Feed tank	200 ℓ
Temperature controller	CGS Eurotherm analog
Conductivity meter	Radiometer CDM 83
	Type CDC 304 probe with temp. control
Note : All wetted parts were 316 stainless steel	

B.1.1.2 Diagram of apparatus

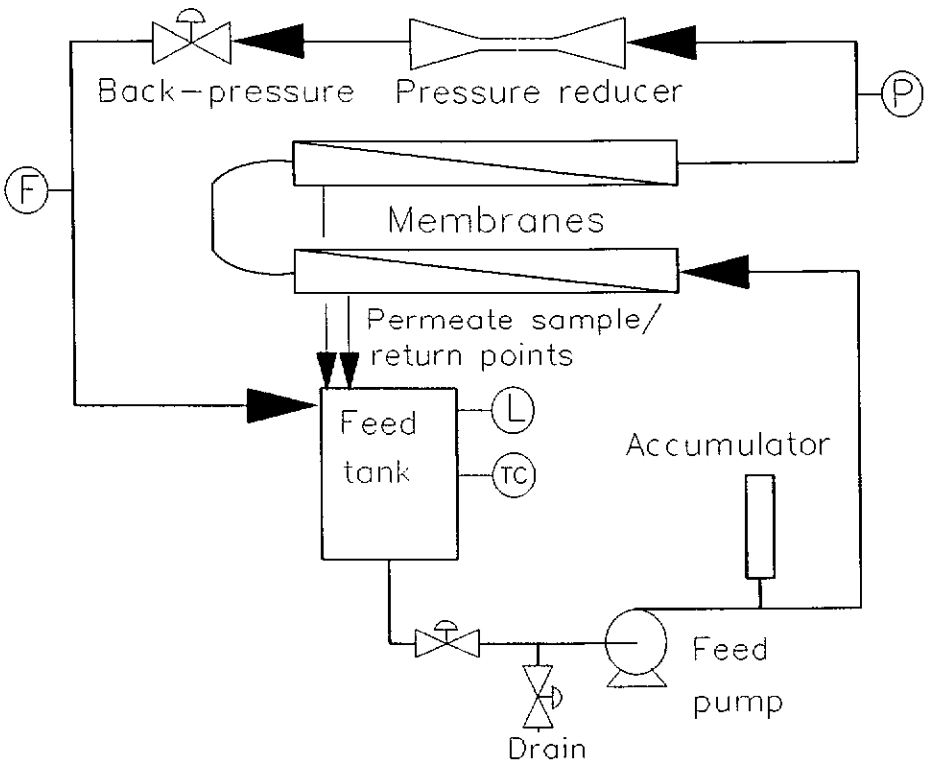

FIGURE B.1 : *Schematic diagram of the RO equipment used for membrane compaction*

B.1.1.3 Specification tests

The following operating specifications are supplied by **MEMBRATEK** for the performance of their tubular cellulose acetate RO membranes :

Factor	Variable
Linear velocity	1,5 m/s
Temperature	25 °C
Salt concentration	2000 g/ℓ of NaCl
pH	6,5
Pressure	4 MPa

The system was set at these conditions and the membrane performance was checked against the specifications :

Factor	Variable
Permeate flux	970 ℓ/m^2d
Salt passage	16,2 %

If the performance of the membrane matched or bettered the specifications they were considered suitable for experimental work. If not, the membranes were discarded. The system was flushed and cleaned via the same procedure as described above to remove the sodium chloride and thereby arrest any corrosion of the stainless steel.

B.1.1.4 <u>Compaction tests</u>

The compaction tests involved running the system at a constant pressure and monitoring the system performance until the permeate flows and the salt passages were essentially constant. (Normally the initial compaction is most severe although the phenomenon, associated with plastic deformation, continues over the useful lifetime of the membrane, and the intention was to reduce experimental errors that might be caused by the initial rapid permeate flow decline due to compaction). The feed concentration of the solute, sodium nitrate, was set at about 2 000 mg/ℓ, the system pressure at 4 MPa and the flow rate at 2,1 m/s (to minimise fouling which would interfere with the tests).

The intention was to run the system continuously but this was not always possible. An hour meter connected to the pump motor was used to monitor the time that the system had been in operation. The permeate fluxes and the salt passages of the membranes were monitored until an acceptable equilibrium was reached with respect to the permeate fluxes and salt passages.

B.1.1.5 <u>Pure-water permeation tests</u>

When satisfied that adequate compaction had been achieved, pure-water permeation tests were conducted to characterise the membranes. As the feed flow rate should have no effect on the outcome of these tests, they were conducted at the highest achievable flow at each of the four pressures : 2, 3, 4 and 5 MPa to minimise fouling. As with the other tests, RO permeate was used for the feed. Experimental technique was the same as for other readings (*cf* Appendix B.2.3.2

Experimental technique) except that sampling periods were reduced because of increased permeate flow and conductivity readings were not required. The results of these tests were to form the basis of the membrane characterisation for the mathematical modelling of the their performance, however, the value of the pure water permeation rate calculated by regression after the completion of the experimental work did vary after insertion of the baffles. It was decided to use the regressed value rather than that obtained experimentally as this allow a better fit of the regressed data and accounted for the change in experimental conditions.

B.1.2 Low-flow Tests

B.1.2.1 Apparatus

Device	Specifications
Speed controller	Thyridyne convertor Series 2 000
Variable speed d.c. Drive	Femco (max 1 780 rpm)
Positive displacement pump	Hydracell D10
Accumulator	1 m of stainless steel 5 cm diameter pipe charged with air @ 0,1 MPa
Pulsing pump	Maximum capacity of 25 mℓ Variable stroke
Pneumatic pulse generator	Electromatic SC 149 220 recycling timer
Membrane holders	Two 0,5 m perforated stainless steel, porous tubes
Pressure reducer	Various lengths of 1,5 mm tubing
Back pressure valve	6 mm needle valve
Ball rotameter	0 to 120 ℓ/h (0 to 2 ℓ/min) range
Pressure gauge	0 to 10 MPa range
Feed tank	7 ℓ (with level and temperature indicators, cooling coils)
Temperature controller	Eurotherm analog
Baffles	Teflon: elliptical and doughnut
Note : All wetted parts were 316 stainless steel (unless otherwise stated)	

Device	Specifications
Conductivity meter	Radiometer CDM 83
	Type CDC 304 probe with temperature control
Baffle supports	1,5 mm diameter rods of length 48 cm
Grommets	PCI rubber grommets of length 15 mm
Baffle spacers	3 mm OD tubing cut to lengths of 28; 49 and 78 mm
Baffle support holders	Teflon cylinders placed in grommets Length : 10 mm Two holes (3 mm deep) for baffle support insertion
Gutters	10 cm diameter polyurethane piping cut lengthwise (60 cm) in half. Ends and an outlet tube were cemented into position
Note : All wetted parts were 316 stainless steel (unless otherwise stated)	

B.1.2.2 Diagram of apparatus

Not all the apparatus was used for each of the sets of experiments and this is discussed, along with an idealised representation of the equipment used in each section, in the relevant chapter. Figure B.2 is a representation of the equipment as arranged for all the experiments.

B.1.2.3 Experimental procedure

B.1.2.3.1 Sodium nitrate and its concentration measurement

Analar grade sodium nitrate was chosen as the solute for these experiments because nitrate ions would not corrode the stainless steel to the same extent as the chloride ions of sodium chloride. Membrane performance tests are specified in terms of sodium chloride and no suitable conversion could be found for these solutes. Performance tests were therefore conducted with sodium chloride but the experimental work was performed using analar grade sodium nitrate.

A conductivity calibration curve was drawn up for a solution of sodium nitrate in RO permeate so that concentrations could be easily established. However, it was found that since the experimental concentration range (feed and permeate) was relatively large, two curves had to be used: one for the permeate and another for the feed.

These curves were translated into the empirical correlations :

$$C\ [g/l] = conductivity\ [S/m] \times 0{,}0892 - 0{,}252$$

and

$$C\ [g/l] = conductivity\ [S/m] \times 0{,}081044$$

to ascertain the salt concentration directly from the conductivity reading.

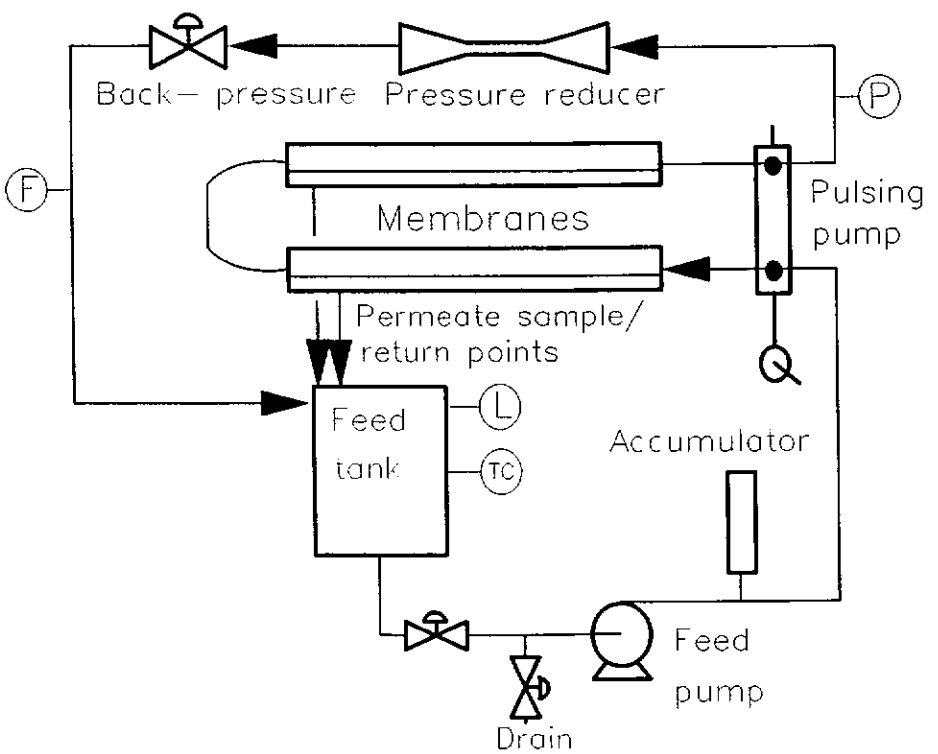

FIGURE B.2 : *Diagram of the apparatus used in the experiments. Different sections of the work used various combinations of the equipment and the relevant sections should be consulted as to the exact nature of each set-up.*

B.1.2.3.2 Membrane area

The membrane area used in the calculations was calculated during the standard membrane tests. The length of the membrane minus the region covered by the grommets was considered to be the membrane length and the diameter of the membrane was measured after the compaction tests. This area was calculated to be 0,00183 m^2 for each of the tubes.

This area was used for the open tube baffled tube calculations. There were two reasons for this. The baffles had a slightly smaller diameter than the tube and so the area around the baffle should be exposed. Also, the tests are of a comparative nature. If the baffles are to increase permeate flow, they should do so over the same membrane length (ie. the tube's effective area need not necessarily be kept the same for the baffled and open-tube experiments).

B.1.2.3.3 Operational variables

Membranes were tested at four pressures : 2; 3; 4 and 5 MPa. The system pressure was controlled by means of the pump speed and a back-pressure valve placed between the membrane/pulsing-pump outlet (and the pressure gauge) and the rotameter. The control proved to be highly unstable and lengths of fine bore (1,5 mm) tubing were used to provide a further pressure drop before the valve. These performed satisfactorily and could be changed relatively quickly for the different flow volumes. The back-pressure valve was then merely required for *fine tuning*.

Four flow rates were used that correspond to Reynolds numbers of 805; 1 611; 2 416 and 3 222 (linear velocities of 0,061; 0,12; 0,18 and 0,25 m/s respectively). The possibly obscure choice of numbers is a function of the tube diameters and the most convenient rotameter markings across the desired range of flow volumes. This provides a spread of laminar and transition region flows that are convenient to measure on the apparatus. The pressure and flow rate were controlled by varying the pump speed and adjusting the back pressure valve. This arrangement was preferable to a by-pass system in which the control was found to be more difficult.

Together, these flow and pressure readings provided a matrix of results that were repeated in the baffled and base-case investigations. In the pulsed and baffled-pulsed experiments, only some variables were tested to indicate trends across a range of pressures and the flow rates.

The temperature was set at 25 °C for the runs. This was controlled by a temperature controller that passed chilled tap water (at about 10 °C) through cooling coils placed in the feed tank.

The pulsing frequency was varied by setting the cycle period of the pulse on an electronic pulse generator. The unit was powered by 400 kPa compressed air. The pulse amplitude could be adjusted by setting the stroke distance with a lock-nut and then varying the travel distance with teflon spacers.

B.1.2.3.4 Experimental method

The system was run continuously, with the permeate returned directly to the feed tank when readings were not being taken.

The pump speed and the back pressure were varied to achieve the desired flow rate and pressure. The system was allowed to stabilise for fifteen minutes between readings to account for any hold up in the system. (This time span was arrived at by observing the variation in permeate quality with time from the setting of one of the variables. Fifteen minutes proved to be a good adjustment time span for all of the conditions).

B.1.2.3.5 Permeate flux calculation

The permeate flows for Tubes A and B were determined by timing the volumetric flow of the permeate from the gutters. Depending on the pressure of the run, the collection time varied between five and ten minutes. The permeate was collected in measuring cylinders and the volume collected was kept between 30 and 50 mℓ. This permeate flux was then calculated in ℓ/m^2d by including the membrane area.

B.1.2.3.6 Salt passage calculation

During the permeate sampling, a sample of the feed was taken and its conductivity measured. Once the permeate flows had been determined, their conductivities were gauged by placing the conductivity and temperature probes directly into the measuring cylinders. The permeate samples were returned to the feed tank. The salt passage was calculated on the basis of concentration since the conductivities were not a linear function of salt concentration over the entire range of the experimental work.

B.1.2.4 Experimental difficulties

The greatest difficulty was to obtain reproducible permeate flux readings. The permeate flow from the gutters was intermittent. For this reason, the monitoring time had to be as long as possible. The gutters were angled to improve run-off. Where readings were suspected of being erroneous, they were repeated. The standard test gave a good indication of the experimental scatter.

While the salt passage results were more consistent, the tests showed a gradual increase in feed salt concentration with time. This can be ascribed to the small feed tank to some extent. With the removal of permeate for readings, some would invariably be lost. While the tank was covered, it was clear that water was evaporating from it- noticeable in the condensation that occurred on the tank cover. Also evaporation of permeate in the gutters cannot be discounted. A combination of all these factors would have been exaggerated with the small feed tank volume. Fresh RO water (pH adjusted) was added to the feed to constrain the salt concentration within a narrow range.

Despite all efforts to the contrary, some fouling did occur. An old accumulator was changed because it was suspected that corrosion inside it was the cause of the rust in the system. This considerably alleviated the problem. The standard test was invaluable as an early indicator of fouling and was responsible for the identification of fouling. The baffle supports were removed and sponge balls were used to clean the membranes.

The pulsing pump could also have been a source of fouling. When the pump was removed for maintenance, it was noticed that the plunger had scored the walls of the pump. This might have lead to steel particles being passed into the feed. Added to this was the fact that the o-ring seals around the piston rod failed often due to the frictionally generated heat and this could have lead to rubber particles entering the feed stream.

The feed pump was also problematic because it began to pulse the feed flow. While it was noted that this was the purpose of building the secondary pump and as such should have been a welcome phenomenon, it would have adversely affected the readings, particularly so for the base case. The problem was resolved by replacing a leaking accumulator and overhauling the pump.

B.1.2.4.1 Vibration effects

Vibrations caused by the pulsing and the feed pump were initially considered as a possible source of performance enhancement. This was discounted because of the independent findings of Herrmann (1982) and Oesterle (*cf* 4.1.3). Furthermore, the membrane holders were mounted independent of, and thus largely isolated from, the feed pump, which was the main source of vibration in the equipment. During the pulsing experiments, the vibrations of the pulsing pump would have been transmitted to the membranes but it is felt that the intense mixing of the fluid would have had more effect on membrane performance than the entire membranes' vibration.

B.1.2.4.2 Entrance effects

In an experiment where one is attempting to measure differences induced by effects such as the onset of unsteady-laminar or turbulent flow, entrance effects may create vorticity within the tube. Kennedy et al. (1974) attempted to negate this by including a 1,2 m long calming pipe before the membrane. However, they conceded that this in itself was insufficient since the grommet that necessarily holds the membrane in place and prevents feed solution passing directly to the permeate side will generate some turbulence and constrict flow.

The problem was further complicated in this instance by the design of the detached baffle holders. These were themselves similar to baffles. One possible solution to these difficulties would have been to build much longer membrane holders and use longer membranes. The outer extremities of the membrane could be coated with an impermeable material and thus the ends of the membrane could act as calming channels.

In a practical sense this does not appear worthwhile. If the aim of the work is to show that alternative operating strategies deliver better results than traditional TRO use, then the *traditional* TRO configurations should be considered. TRO modules use 180° bends to channel the flow back into the tube array. Entrance to the modules is not designed to deliver *calm* flow. If one of the means attempted in this project is to be effected (particularly in the retentate end of a large plant where flows are low) it must deliver appreciably better results than the base condition. It must therefore perform better, despite the *assistance* of the entrance effects. This rationale, coupled with the constraints imposed by the membrane modification, led to the decision to disregard these effects.

Appendix C

MATHEMATICAL MODELLING AND ERROR ANALYSIS

C.1 COMPUTER MODELLING

A computer program was used to regress on the experimental data to calculate the Sourirajan (1985) constants and to predict the membranes' behaviour from these. The programme was written by Brouckaert (1992).

The experimental results were divided into four groups that corresponded to the groups of experiments : tubes A and B were treated separately as were the unbaffled tube and baffled tube results. The pulsed flow results were handled in their respective groups. For example, the results of pulsing the flow through open tube A were treated under the open tube A results along with those for normal flow. The four groups of experiments are hereafter referred to as the open tube A, open tube B, baffled tube A and baffled tube B experiments.

The rationale was that the two tubes did behave differently with respect to permeate flow and salt passage. The insertion of baffles into the tubes could have resulted in damage to the delicate membrane surfaces, further exacerbating this difference. Both of these ideas were shown to be possibilities by the results of mathematical modelling.

C.2 MODELLING METHODOLOGY

The model contains three parameters : the pure water permeation parameter (A); the solute transport parameter $\left(\frac{D_{AM}}{Kb}\right)$; and the mass transfer coefficient for diffusive mass transport of the fluid within the tube (k). The first of these is a property of the membrane, the second of the solute and the membrane and the third a function of the hydrodynamic conditions within the tube and should be independent of the membrane.

With this theoretical basis (that of the three parameters), the four groups of experimental results were analysed individually. Each run was considered as a single data set within the group. The program regressed over the entire group (i.e. all the data sets for each of the tube conditions) for the RO parameters A and $\left(\frac{D_{AM}}{K\delta}\right)$.

The value of k was determined from data sets with the same feed flow conditions (e.g. All the data sets with feed flow of $Re = 805$ and no pulsing were considered together but each of the pulsed flow cases for the same Reynolds number were treated independently). The regression used the Sourirajan equations 2.1 to 2.4. The regression is represented in Figure C.1.

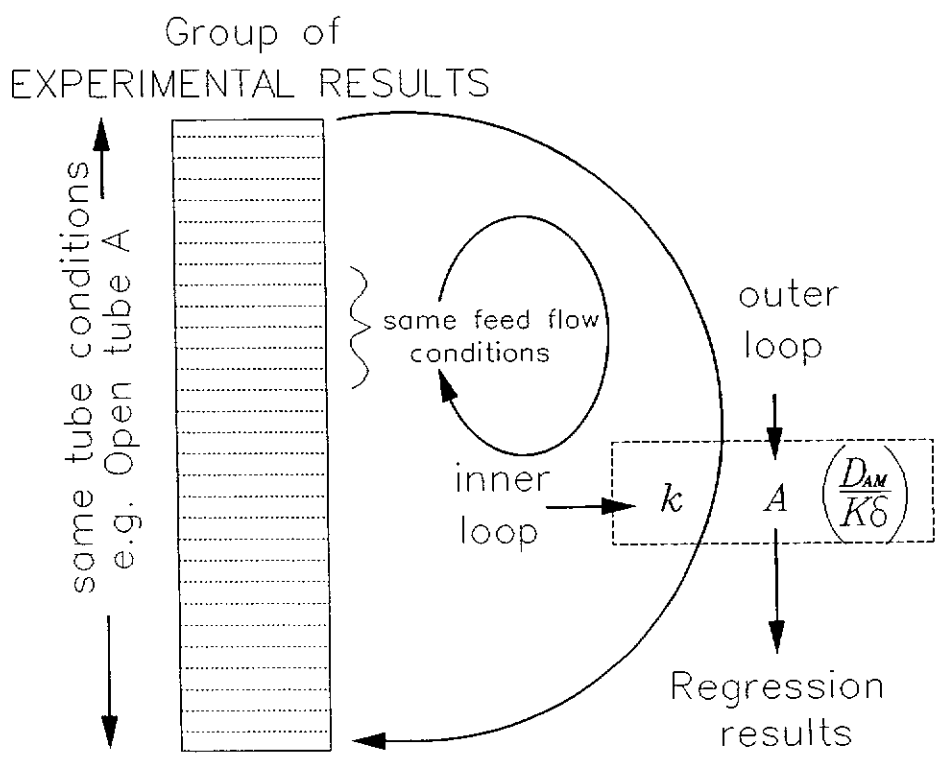

FIGURE C.1 : *Pictorial representation of the regression procedure used showing the data from which each of the three parameters was calculated*

The reason for regressing for A and $\left(\frac{D_{AM}}{K\delta}\right)$ over each group of data was that these values are functions of the membrane and solute which should, theoretically, be constant for each of the experimental groups.

The mass transfer coefficient, k, was established for each sub-set of data having the same hydrodynamic feed conditions. For the unpulsed flow experiments this was not problematic since each hydrodynamic condition had been examined at least three (and in the case of the base experiment, about fifteen) times. However, for each of the pulsed flow experiments, each run was under different hydrodynamic conditions. In turn each run consisted of four values on which the regression could act : feed concentration, feed flow condition, permeate concentration and permeate flow.

Regressing over the entire group for the first two constants meant that a larger domain was available to the regression for A and $\left(\frac{D_{AM}}{K\delta}\right)$. Furthermore, one could expect more accurate values for the mass transfer coefficients if the program had four data points for each run from which to infer a single (as opposed to three) parameter.

C.3 PURE WATER PERMEABILITY CONSTANT

The calculated pure water permeability constants, A, showed that tube A had a higher permeability than tube B.

Tube	Condition	A kgmol $H_20/m^2.s.Pa \times 10^{14}$
A	Open	6,64
B	Open	6,28
A	Baffled	6,52
B	Baffled	6,25

This corresponds to the experimental findings since tube A produced consistently higher permeate flows than tube B. These constants were only marginally lower for the baffled experiments, a reduction of 1,9 and 0,5 % for tubes A and B respectively. The decision not to make allowances for any decrease in membrane area caused by baffles sitting on the membrane surface therefore seems vindicated.

One would expect membranes to have different pure water permeabilities and it was fortunate that this pair of membranes had such similar constants. (Pitera and Middleman (1973) reported the A's for their tube pairs and these showed differences of up to 40 %).

The pure water permeability coefficients were established by regression and not experimentally because of the difficulty of running such experiments for each group of experiment's configuration.

C.4 SOLUTE TRANSPORT PARAMETER

The calculated solute transport parameters, $\left(\frac{D_{AM}}{K\delta}\right)$, revealed a higher value for Tube A, corresponding to the higher salt passages found in this tube experimentally. Both these values increased significantly for the experiments conducted after baffle insertion, lending credence to the belief that membrane damage occurred on insertion. However, membrane damage should also be associated with an increase in the permeability coefficient. There is only a marginal decrease in permeability coefficient (probably associated with the blocking of some of the membrane area by the baffles) and so the reason for the significant increase in solute transport coefficient between the experimental sets remains unresolved.

Tube	Condition	$\left(\frac{D_{AM}}{K\delta}\right)$ m/s x 10^7
A	Open	4,09
B	Open	3,58
A	Baffled	6,52
B	Baffled	4,65

What is significant about these findings is that the mathematical results coincide with the intuitive expectations for each of the experimental sets.

C.4.1 The Significance of the Mass Transfer Coefficient

The advantage of determining a mass transfer coefficient for each run is that it is theoretically reliant only on the hydrodynamic conditions within the tube. In this instance, where the tube rendered different performances for the same independent variables, probably through differences in their manufacture, the single coefficient provided a comparative performance measure.

The mass transfer coefficient provides an indication of the magnitude of the concentration gradients within the tube. A higher value of k implies a lower concentration gradient associated with better fluid mixing.

Hence, comparing the coefficients for each flow condition provides a measure of the effectiveness of each strategy in reducing concentration polarisation, theoretically independent of the RO membranes characteristics.

The value of k represents the essence of each of the data sets. It can used with the membrane parameters to generate the salt passages and permeate flows for given experimental conditions. It is therefore a good measure of the error that can be expected for the experiments.

C.4.2 Difficulties with the Mass Transfer Coefficient

The main difficulty with this measurement can best be described by Figures C.2 and C.3. They show the coefficient as a function of salt passage and permeate flow for each of the experimental groups respectively. It should be noted that the apparent discrepancy in performance for a set of coefficients is due to the different values of the pure water permeability constants and solute transport parameters for each experimental group.

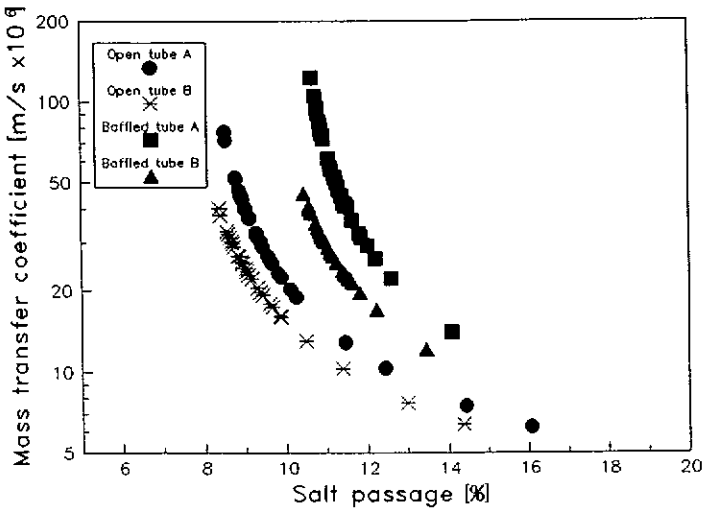

FIGURE C.2 : *Graph of regressed mass transfer coefficients vs predicted salt passages for all of the experimental work. Each experimental group is represented by a separate set of data points. The coefficients are plotted on a logarithmic scale to emphasise the small range of coefficients where no enhancement is used (ie. open tube experiments).*

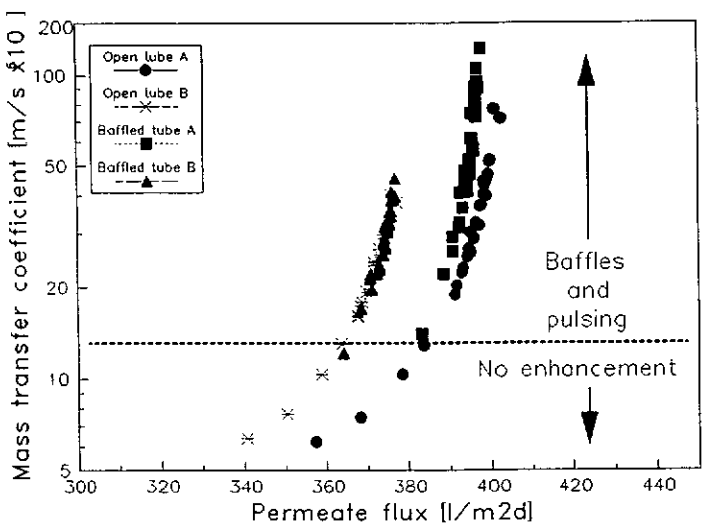

FIGURE C.3 : *Graph of regressed mass transfer coefficients vs predicted permeate flows for all of the experimental work. Each experimental group is represented by a separate set of data points. The coefficients are plotted on a logarithmic scale to emphasise the small range of coefficients where no enhancement is used (ie. open tube experiments).*

The increase in mass transfer coefficient relative to the increase in the corresponding variable is great. Thus a small improvement in performance, that might be the result of experimental error, is magnified considerably in the final result.

The graphs show that, for the experimental domain chosen, mass transfer enhancement was so successful as to make the comparison of the techniques used very difficult. To rectify this one would have to use high viscosity fluids, high pressures, lower flow rates and higher feed concentrations. All these alterations would ensure lower coefficients over a wider domain but would place the results of the work outside the range of normal RO operation.

However, the net result is that it is difficult to draw comparative conclusions from this work. The stated findings of each chapter might seem inconclusive or scant but they are necessarily conservative.

C.4.3 Error Analysis

The mass transfer coefficients were determined by regression from the experimental values of permeate flow and salt passage. The regressed values were therefore subject to errors arising from experimental errors in the primary data.

The ultimate test of the acceptability of the mathematically derived value of k and the two membrane parameters would be to check how well the experimental data fitted their predictions. However, Figures C.2 and C.3 show that at the higher values of k, the exercise would be meaningless. After a number of attempts at obtaining a suitable estimate of the error, the following methodology was settled on.

Figures C.2 and C.3 (and the calculation procedure) show that the mass transfer coefficient is relatively more sensitive to permeate flow than to salt passage. Consequently the salt passage value would be more influential in setting the value of k via the regression procedure. Using the base tests, standard population variances (S) and means ($\bar{k}$) were calculated for the experimental salt passage values. Assuming that the experimental relative errors (i.e. relative to the magnitude of the true value) are normally distributed, the 90 % confidence limits for the measurements were taken as :

$$k \pm \frac{S \quad t_{0.05}}{\bar{k}} \quad k$$

This provided a standard error for each of the open and baffled tubes. Since the values of k fall into two distinct categories (normal and pulsed flow), eight graphs of mass transfer coefficient versus salt passage were generated. For each range, a good fit was obtained via an exponential regression.

Using the standard error, the upper and lower experimental limits of the salt passages for each of the experimental domains was generated. By calculating the mass transfer coefficients for the upper and lower experimental values of salt passage, a standard error for k was arrived at :

Flow	Condition	Tube	Maximum standard error [%] $\frac{Err(k)}{\lvert k \rvert} \times 100$
Normal	Open	A	34
		B	30
	Baffled	A	26
		B	30
Pulsed	Open	A	125
		B	70
	Baffled	A	73
		B	55

As expected, the errors for the steady flow tests are comparatively low. Consider, also, that the values of the mass transfer coefficients in this region are also lower, implying that the error range is also significantly lower. The high error in the pulsed-flow, open tube A results is a combination of a large variance in experimental error for open tube A and a near infinite increase in mass transfer coefficient with salt passage for those experiments.

While the errors in the mass transfer coefficients may seem large, they are of the same order as those found by Colman and Mitchell (1991). Their errors are not reported, but analysis of their graphs leads to this conclusion.

Appendix D

RAW DATA

Standard Experimental Conditions:

Feed temperature : 25 °C
Solute concentration : 13 500 mg/ℓ

TABLE D.1 : *Base case results*

Feed		Permeate					
		A			B		
Pressure MPa	Flow rate Re	Salt pass %	Flux ℓ/m²d	k x10⁶ m/s	Salt pass %	Flux ℓ/m²d	k x10⁶ m/s
5	3 222	9,9	483	12,89	9,4	452	13,05
5	2 416	10,9	475	10,36	10,0	452	10,33
5	1 611	13,4	491	7,52	11,8	470	7,69
5	805	15,6	460	6,24	13,8	445	6,40
4	3 222	12,0	394	12,89	10,9	368	13,05
4	2 416	12,8	391	10,36	11,7	370	10,33
4	1 611	14,3	368	7,52	12,7	353	7,69
4	805	16,0	358	6,24	14,2	343	6,40
3	3 222	13,4	266	12,89	12,2	251	13,05
3	2 416	15,6	261	10,36	14,2	251	10,33
3	1 611	16,6	256	7,52	15,4	245	7,69
3	805	16,8	251	6,24	15,4	235	6,40
2	3 222	20,2	164	12,89	18,2	146	13,05
2	2 416	21,1	161	10,36	19,2	142	10,33
2	1 611	21,4	164	7,52	20,0	143	7,69
2	805	22,7	153	6,24	21,3	146	6,40

TABLE D.2 : *Open tube : Pulsing versus frequency results*

Feed		Pulse variables		Permeate					
				A			B		
Pressure MPa	Flow rate Re	Frequency Hz	Amplitude mm	Salt pass %	Flux ℓ/m^2d	k x10^6 m/s	Salt pass %	Flux ℓ/m^2d	k x10^6 m/s
4	3 222	2,50	93	9,0	409	44,64	8,7	383	29,71
4	3 222	1,25	93	9,1	404	36,98	8,9	388	26,64
4	3 222	0,50	93	9,6	399	26,81	9,3	378	20,46
4	3 222	0,25	93	9,9	394	22,39	9,6	378	17,84
4	3 222	0,00	0	12,0	394	12,89	10,9	368	13,05
4	2 416	2,50	93	8,9	414	46,93	8,7	383	30,27
4	2 416	1,25	93	9,5	406	29,03	9,2	391	21,35
4	2 416	0,50	93	9,8	414	25,26	9,5	391	19,31
4	2 416	0,25	93	10,1	399	20,25	9,9	376	16,11
4	2 416	0,00	0	12,8	392	10,36	11,7	370	10,33
4	1 611	2,50	93	9,0	404	40,04	8,8	378	26,87
4	1 611	1,25	93	9,3	399	31,87	9,1	373	22,85
4	1 611	0,50	93	9,6	399	25,95	9,4	373	19,73
4	1 611	0,25	93	10,3	394	18,94	9,9	368	15,95
4	1 611	0,00	0	14,3	368	7,52	12,7	353	7,69
4	805	2,50	93	8,8	408	51,62	8,6	383	32,96
4	805	1,25	93	8,9	408	44,86	8,8	383	29,01
4	805	0,50	93	9,3	406	32,59	9,1	383	23,59
4	805	0,25	93	9,8	396	23,19	9,7	368	17,35
4	805	0,00	0	16,0	358	6,24	14,2	343	6,40

TABLE D.3 : *Open tube : Pulsing versus amplitude*

Feed		Pulse variables		Permeate					
				A			B		
Pressure MPa	Flow rate Re	Frequency Hz	Amplitude mm	Salt pass %	Flux ℓ/m^2d	k $x10^6$ m/s	Salt pass %	Flux ℓ/m^2d	k $x10^6$ m/s
4	2 416	1,25	167	8,5	394	71,90	8,4	368	37,91
4	2 416	1,25	130	8,5	394	77,09	8,4	368	40,12
4	2 416	1,25	93	8,7	379	52,20	8,6	368	31,26
4	2 416	1,25	56	9,0	379	37,12	8,9	359	25,11
4	2 416	0,00	0	12,8	391	10,36	11,7	370	10,33
4	805	1,25	167	9,0	399	43,24	9,0	377	25,56
4	805	1,25	130	9,0	396	40,38	8,6	377	32,40
4	805	1,25	93	8,9	396	44,79	8,8	372	28,93
4	805	1,25	56	9,4	386	28,42	9,0	363	23,68
4	805	0,00	0	16,0	358	6,24	14,2	343	6,40

TABLE D.4 : *Baffled flow results*

Feed		Permeate					
		A			B		
Pressure MPa	Flow rate Re	Salt pass %	Flux ℓ/m^2d	k $x10^6$ m/s	Salt pass %	Flux ℓ/m^2d	k $x10^6$ m/s
5	3 222	10,0	525	31,44	9,9	497	22,17
5	2 416	10,1	531	29,27	10,1	492	21,52
5	1 611	10,5	506	22,15	10,1	483	17,02
5	805	12,3	505	14,02	12,2	472	12,14
4	3 222	11,6	403	31,44	11,3	386	22,17
4	2 416	11,9	389	29,27	11,5	368	21,52
4	1 611	13,0	383	22,15	12,5	366	17,02
4	805	13,8	383	14,02	13,7	366	12,14
3	3 222	15,2	271	31,44	14,8	256	22,17
3	2 416	15,6	273	29,27	15,0	261	21,52
3	1 611	15,6	276	22,15	15,3	268	17,02
3	805	17,8	261	14,02	17,1	257	12,14
2	2 819	20,0	173	31,44	19,4	153	22,17
2	2 416	22,5	157	29,27	21,8	150	21,52
2	1 611	22,0	173	22,15	21,6	153	17,02
2	805	23,2	155	14,02	22,9	146	12,14

TABLE D.5 : *Baffled tube : Pulsing versus fequency*

Feed		Pulse variables		Permeate					
				A			B		
Pressure MPa	Flow rate Re	Frequency Hz	Amplitude mm	Salt pass %	Flux ℓ/m^2d	k $x10^6$ m/s	Salt pass %	Flux ℓ/m^2d	k $x10^6$ m/s
4	3 222	2,50	93	10,9	407	72,57	10,6	387	39,98
4	3 222	1,25	93	11,1	409	57,03	10,9	383	32,17
4	3 222	0,50	93	11,3	405	49,90	11,0	389	30,38
4	3 222	0,25	93	11,5	404	41,96	11,1	383	29,02
4	3 222	0,00	0	12,0	394	12,89	10,9	368	13,05
4	2 416	2,50	93	10,7	399	105,25	10,5	386	45,54
4	2 416	1,25	93	10,8	403	92,11	10,8	386	35,42
4	2 416	0,50	93	11,1	399	61,32	10,8	378	33,30
4	2 416	0,25	93	11,4	399	44,66	11,1	373	28,12
4	2 416	0,00	0	12,8	391	10,36	11,7	370	10,33
4	1 611	2,50	93	11,3	395	47,02	11,1	373	26,81
4	1 611	1,25	93	11,4	393	41,15	11,2	370	25,64
4	1 611	0,50	93	11,8	396	32,47	11,5	376	22,76
4	1 611	0,25	93	12,2	388	26,29	11,8	368	19,69
4	1 611	0,00	0	14,3	368	7,52	12,7	353	7,69
4	805	2,50	93	10,7	404	123,48	10,7	383	38,80
4	805	1,25	93	10,8	399	90,35	10,8	378	34,16
4	805	0,50	93	11,1	399	55,82	11,1	378	27,47
4	805	0,25	93	11,4	394	41,99	11,4	372	23,17
4	805	0,00	0	16,0	358	6,24	14,2	343	6,40

TABLE D.6 : *Baffled tube : Pulsing versus amplitude*

Feed		Pulse variables		Permeate					
				A			B		
Pressure MPa	Flow rate Re	Frequency Hz	Amplitude mm	Salt pass %	Flux ℓ/m^2d	k x10^6 m/s	Salt pass %	Flux ℓ/m^2d	k x10^6 m/s
4	3 222	1,25	167	11,2	406	52,15	11,0	391	31,45
4	3 222	1,25	130	11,2	410	52,45	10,9	391	33,05
4	3 222	1,25	93	11,1	409	57,03	10,9	383	32,17
4	3 222	1,25	56	11,5	399	40,92	11,7	383	22,11
4	3 222	0,00	0	12,0	394	12,89	10,9	368	13,05
4	2 416	1,25	167	10,9	395	74,61	10,5	374	41,19
4	2 416	1,25	130	10,9	404	82,55	10,6	378	38,71
4	2 416	1,25	93	10,8	403	92,13	10,8	386	35,42
4	2 416	1,25	56	10,9	399	76,63	10,7	378	35,47
4	2 416	0,00	0	12,8	391	10,36	11,7	370	10,33
4	1 611	1,25	167	11,3	394	48,17	10,9	378	31,80
4	1 611	1,25	130	11,4	395	44,77	11,1	369	27,85
4	1 611	1,25	93	11,4	393	41,15	11,2	370	25,46
4	1 611	1,25	56	11,6	393	36,48	11,4	373	23,71
4	1 611	0,00	0	14,3	368	7,52	12,7	353	7,69
4	805	1,25	167	10,8	404	84,49	10,8	378	33,06
4	805	1,25	130	10,8	404	94,97	10,9	383	31,87
4	805	1,25	93	10,8	399	90,57	10,8	378	34,16
4	805	1,25	56	10,9	399	68,22	10,9	378	30,81
4	805	0,00	0	16,0	358	6,24	14,2	343	6,40

Appendix E

PULSE WAVE FORM CHARACTERISATION

E.1 METHOD OF WAVE FORM CHARACTERISATION

The pulsing pump piston was connected to a spring loaded potentiometer by a length of cord. The position transducer was wired to a circuit that is shown in Figure E.1.

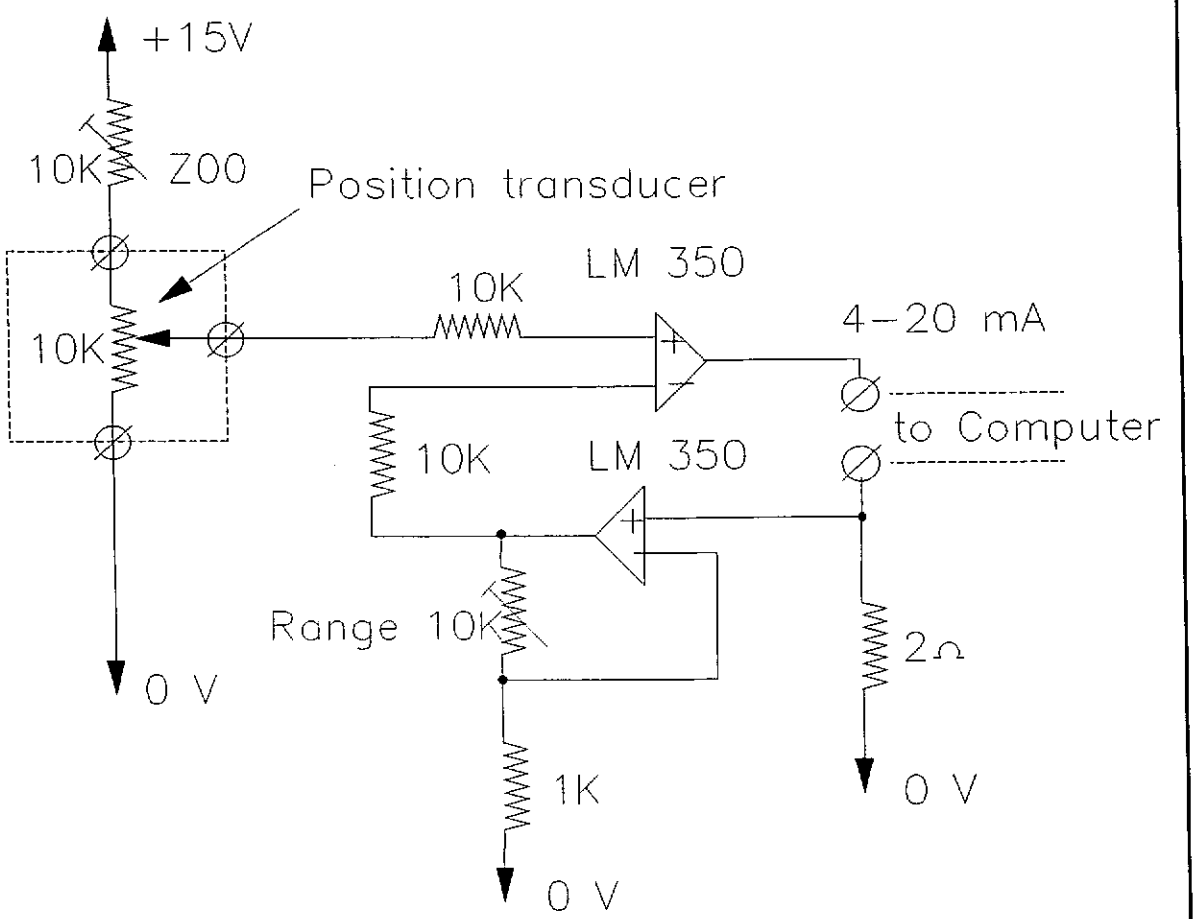

FIGURE E.1 : *Circuit diagram of the position measurement device used to link the position transducer to the computer*

The circuit delivered a continuous 4-20 mA current to the computer. A programme written by Alston (1990) was used to read this current as often as possible (approximately every 15 ms). At each computer *clock tick* (every 50 ms) the current values in the buffer were averaged and this value was stored in an array. After 500 readings had been taken, the array was saved as an ASCII text file. The programme was run while the pump pulsed over a range of feed flows. The wave form was found to be independent of feed flows).

This file was imported into a spreadsheet. The time of each reading was calculated. The current value was converted into a distance value by finding the current limits and making a linear mathematical adjustment for the corresponding amplitude. The zero distance value was taken as the starting point at the reverse pulse. The discrepancy between the pump amplitude and the amplitude of fluid oscillation within the membrane was accounted for. All amplitudes reported in this thesis represent the fluid amplitude of oscillation within the membrane.

Plotting position as a function of time would have shown plots of the type shown in Figure E.2.

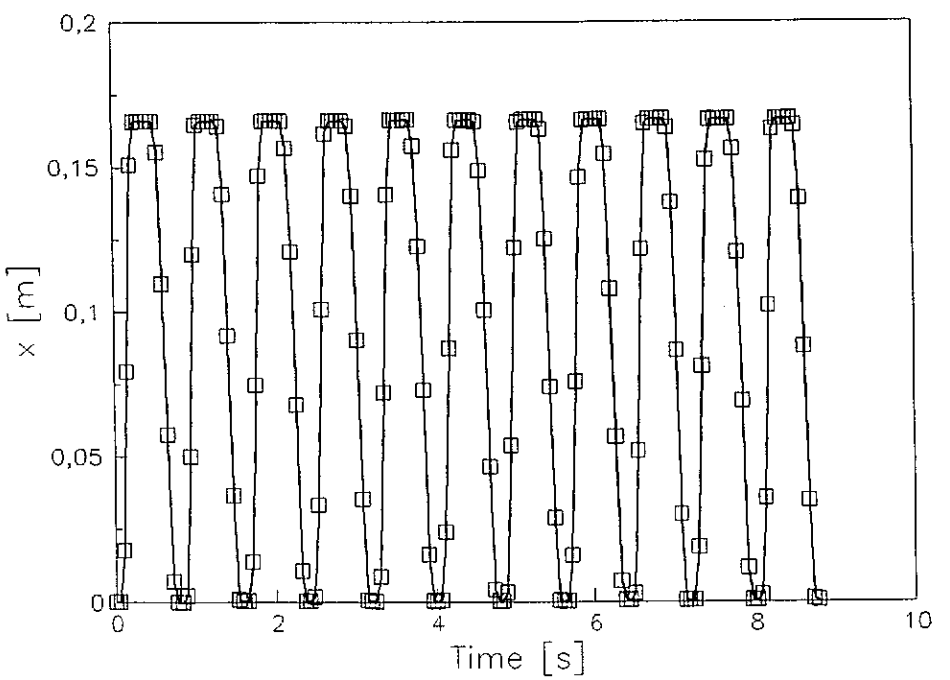

FIGURE E.2 : *Example of a plot of position with time for a particle in the tube under the influence of the pulsing pump at an amplitude of 167 mm and a frequencies of 1,25 Hz*

To consolidate the available data into a plot from which the velocity of the forward and backward pulses could be determined, the time was adjusted to represent the time from the beginning of each pulse cycle as follows :

$$t^* = t - n^{\tau}$$

where t^* = time since the inception of each pulse cycle, (s)
t = total time since inception of measurement (s)
n = number of cycles since the beginning of the run
τ = period of the pulse, (s)

Plotting position as a function of t^* produced a composite curve, an example of which is shown in Figure E.3

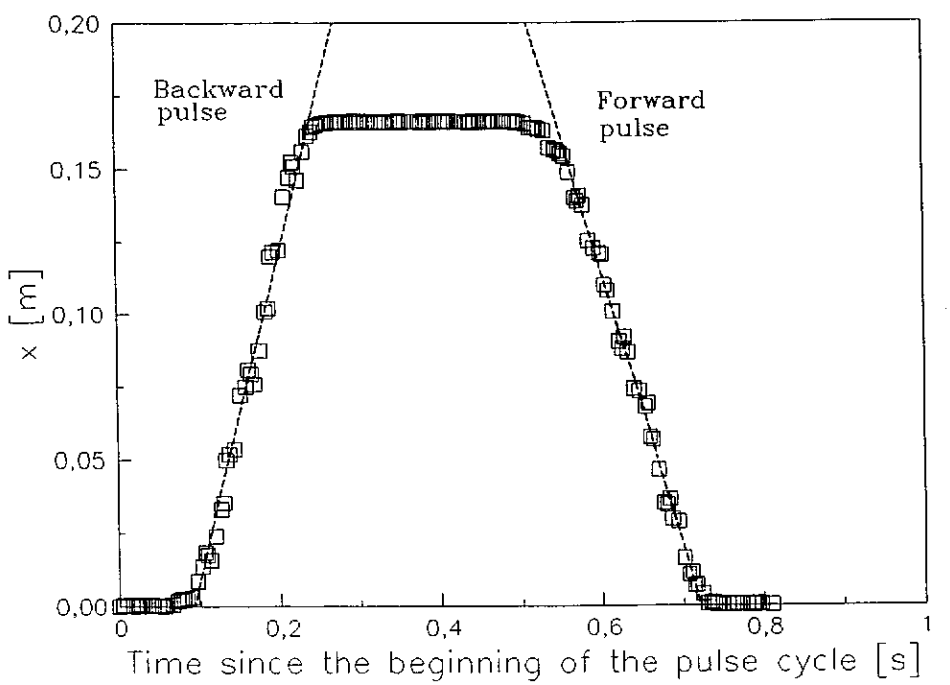

FIGURE E.3 : *An example of a composite plot of pulsed particle position as a function of the time since the beginning of the pulse cycle for an amplitude of 167 mm and a frequency of 1.25 Hz*

A linear regression of the slopes of composite pulse plot returned a value of each gradient. This gradient represents the velocity of each phase of the cycle. (The stationary phases were naturally ignored in this process).

This procedure was repeated at each of the amplitudes and frequencies used in the experiments.

E.2 VELOCITIES OF THE PHASES OF THE PULSES

The forward and backward velocities calculated for the range of pulse amplitudes and frequencies are shown in Table E.1

TABLE E.1 : *Table of forward and backward pulse velocities and duration of each pulse at given frequencies and amplitudes*

Frequency Hz	Amplitude (in tube) cm	Forward velocity m/s	Period of forward pulse s	Backward velocity m/s	Period of backward pulse s
1,25	16,7	0,94	0,18	-1,19	0,14
1,25	13,3	0,79	0,16	-1,20	0,12
1,25	9,3	0,69	0,14	-0,95	0,10
1,25	5,6	0,61	0,09	-0,71	0,08
2,50	9,3	0,69	0,13	-0,95	0,10
0,50	9,3	0,67	0,14	-0,96	0,10
0,25	9,3	0,66	0,14	-0,81	0,11

Using these values, the gains in mass transfer coefficient for pulsed flow predicted by the square wave theory discussed in Section 4.1.2.1 could be calculated using Eqn 4.9.